Crystalline assemblies of folded oligomers

Dissertation zur Erlangung des Grades
“Doktor der Naturwissenschaften”
am Fachbereich Chemie und Pharmazie der
Johannes-Gutenberg-Universität in Mainz

Kay Lederer
born in Gera, Germany

Mainz 1999

Tag der Prüfung: 14.12.1999

Table of contents

1. Introduction

Langmuir showed early in this century with a number of elegant experiments that amphiphilic molecules, molecules with a hydrophobic tail and a hydrophilic head, are capable to assemble in monomolecular layers at the air-water interface.[1] Since that time extensive research has been carried out in this field of two-dimensional (2-D) layers at the air-water interface, as they provide very useful information on molecular assemblies not accessible by other techniques. They may serve as models for the investigation of the structure and function of biological membranes and a great number of relevant compound classes, like lipids, steroids, sugars proteins and ions have been included in the research on monolayers.[2] It is also possible to induce epitaxial growth of three-dimensional (3-D) crystals within the subphase, if the monolayer above this subphase is appropriately designed.[3-5] Furthermore, monolayers may be used as models for biomineralization processes assuming them as a template for mineral crystallization.[6,7] Monolayer films can usually be transferred onto solid supports to obtain multilayers,[8] which opens another wide spectrum of possible applications.[9-14]

Self-assembled monolayers are a special type of monolayers and of general interest for the understanding of early stages of molecular self-organization and crystallization because they can be considered as a spontaneously formed crystalline state. In a process similar to 3-D crystallization from the gaseous phase, the molecules at the air-water interface can, after solvent evaporation, move freely on the water surface and orient themselves in a way to maximize the attractive interaction between them and to minimize the overall energy of the system. Thus, they fix their conformation and orientation with respect to each other. If this process happens spontaneously, it is called a self-assembly. The advantage of this 2-D self-assembled state is, that it is less rigid than an assembly in a 3-D crystal and therefore also „premature“ stages of a final crystalline structure may exist in such a layer and give useful information on the mechanism of the crystallization process of a given type of compound. It is therefore of great importance to get an insight into the molecular, or even atomic, structure of such monolayers.

Compared to a 3-D structure, a monolayer consists of a very low number of molecules and direct structure determination is difficult using conventional methods due to very weak response signal intensities. Therefore, the main requirement for a method to determine the structure of a monolayer is a very intense, highly focussed incident signal and an exactly calibrated set-up geometry. Laser has been successfully used to determine the molecular orientation and symmetry within monolayers by surface second harmonic generation.[15-19] However, it is not possible to obtain direct information on the molecular structure from such measurements. Fluorescense spectroscopy does furnish some information on crystallinity and morphology on the micrometer scale[20-23] but little information on the molecular level can be extracted from such measurements. A useful tool for the determination of the local arrangements of molecules is Fourier transform IR spectroscopy which has become applicable to monolayers at the air-water interface.[24-30] The determination of the structure of a crystalline, or periodically ordered, monolayer close to atomic resolution has become possible during the last decade by a newly developed surface sensitive X-ray method that utilizes highly focussed, monochromatic synchrotron X-ray radiation. This grazing incidence X-ray diffraction (GIXD) allows the determination of the structure of a crystalline monolayer in situ, as the monolayer is formed at the interface.

1.1. Surface sensitive X-ray methods[31]

Grazing incidence X-ray diffraction (GIXD). In X-ray scattering the measured intensity is proportional to the number of scatterers, i.e. the sample volume exposed to the X-ray beam. This irradiated volume is proportional to the penetration depth of the radiation into the sample. X-rays of about 1 Å wavelength penetrate into the medium from a few micrometers (for a highly absorbing material) up to some millimeters (for weakly absorbing materials). Surface effects do usually not extend more than 100 Å into the medium. Therefore scattering signals arising from this surface region are overlayed by the strong bulk signals are usually not observed. In order to utilize X-ray scattering for surface analysis this problem can be elegantly overcome by shining the incident X-ray radiation at a grazing angle α_i onto the surface which leads to total external reflection of the radiation.

The reason, why total reflection of X-rays can occur at the air-water interface is the anomalous dispersion of water under such conditions. Electrons in atoms can be considered to act like oscillators having resonance frequencies determined by their binding forces, that is, depending on whether they are in the *K*, *L* etc., shells of an atom. When the frequency of the incident radiation is far away from these characteristic frequencies, the presence of such oscillators simply causes a change in the velocity of the transmitted wave which is usually related to the refractive index *n* of the medium. Is, however, the frequency of the incident radiation close to the characteristic frequencies of the oscillators, resonance absorption occurs and a phase shift takes place. This is called anomalous dispersion of a medium. Experimentally it was found, that *n* for X-rays normally used in diffraction experiments is less than unity by a few parts per million in most materials. The refractive index *n* of matter for X-rays of a wavelength around 1 Å is given by[32]

$$n = 1 - \delta - i\beta \quad , \tag{1}$$

with $\delta = 2\pi\rho r_0/k^2$ where $k = 2\pi/\lambda$ is the X-ray wave number and λ the wavelength. ρ is the electron density and $r_0 = 2.82 \times 10^{-13}$ cm is the classical electron radius. Usually δ is in the order of 10^{-5}. The term β is equal to $-\mu/2k$ where μ is the linear absorption coefficient. For $\lambda \approx 1$ Å the value of μ is very small and therefore $\beta << \delta$. Figure X shows a plane wave with wavevector $\boldsymbol{k}_i$ incident at an angle α_i on a planar interface separating a homogeneous medium with refractive index *n* from the vacuum. The wave will be partially reflected into the vacuum in the direction given by $\alpha_r = \alpha_i$ and partially refracted into the medium in the direction given by α'_r. Snell's law for this case is therefore

$$n\cos\alpha'_r = \cos\alpha_i \, . \tag{2}$$

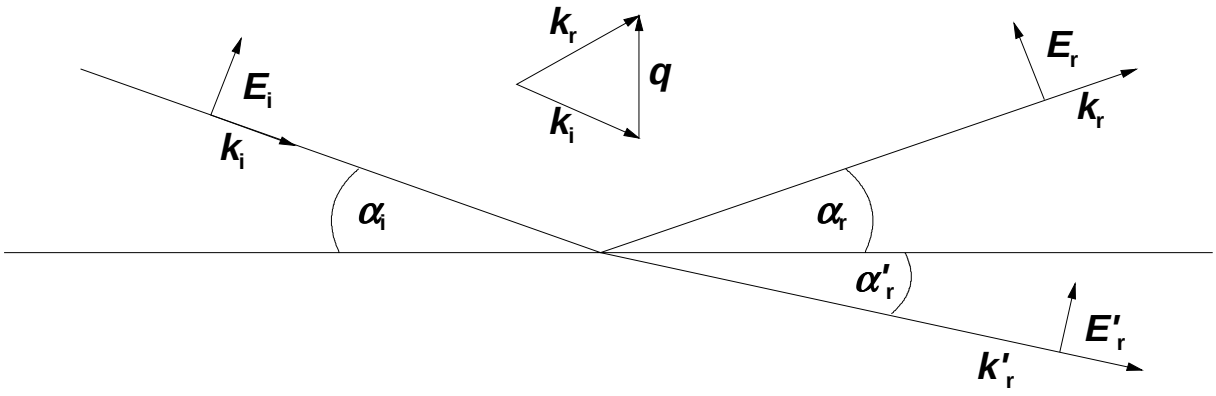

Figure 1. Refracted ($\boldsymbol{E'}_r$) and reflected ($\boldsymbol{E}_r$) waves resulting from an incident plane wave with amplitude $|\boldsymbol{E}_i|$ at an interface between vacuum and a medium with the refractive index n on the example of p-polarized electromagnetic waves. Electric fields are illustrated for one polarization only. $\boldsymbol{q}$ is the scattering vector, $\boldsymbol{k}_i$ and $\boldsymbol{k}_r$ are the incident and reflected wave vectors respectively of magnitude $2\pi/\lambda$. As for X-rays $\alpha'_r < \alpha_i = \alpha_r$ (as $n < 1$) total external reflection occur if $\alpha_i \leq \alpha_c$, where α_c is the critical angle for total external reflection. $|\boldsymbol{q}| = |\boldsymbol{k}_r - \boldsymbol{k}_i| = (4\pi/\lambda)\sin\alpha_r$ is the magnitude of the scattering vector $\boldsymbol{q}$.

As for X-rays $n < 1$, for incidence angles less or equal to a critical angle α_c, defined as $\alpha_c = \cos^{-1}(n) = (2\delta)^{1/2}$, the phenomenon of total reflection occurs:[33] the incident wave is totally reflected, while the refracted wave becomes evanescent traveling along the interface. The amplitude of the evanescent wave decays exponentially with depth of penetration. The penetration depth lies in the range of 50 to 100 Å for $\alpha_i < 0.5\alpha_c$.[31] Periodicity in positions of the molecules in a film of that thickness gives rise to a peak of diffracted intensity and thus provides crystallographic information on the 2-D structure. Such diffraction is called grazing incidence X-ray diffraction (GIXD).[34,35]

In 3-D crystals diffraction from a set of periodically arranged lattice planes with an interplanar spacing d occurs only when the Bragg law is obeyed. This is when the length of the scattering vector $|\boldsymbol{q}|$ (given by $|\boldsymbol{k}_f - \boldsymbol{k}_i| = 4\pi\sin\theta/\lambda$) is equal to $2\pi d^*$, with d^* being the reciprocal of the interplanar spacing d and the normal to the planes bisects the angle between the incident and diffracted beam. Mathematically expressed in terms of the reciprocal lattice vectors this means $\boldsymbol{d}^* = h\boldsymbol{a}^* + k\boldsymbol{b}^* + l\boldsymbol{c}^*$, where $\boldsymbol{a}^*$, $\boldsymbol{b}^*$ and $\boldsymbol{c}^*$ are the reciprocal vectors of the unit cell vectors $\boldsymbol{a}$, $\boldsymbol{b}$ and $\boldsymbol{c}$

respectively. *h*, *k* and *l* are integers that represent the Miller indices of planes with a spacing d_{hkl}. Diffraction in 3-D crystals is observed if the scattering vector $\boldsymbol{q}$ coincides with (*h*,*k*,*l*) points of the reciprocal 3-D lattice (Figure 2).

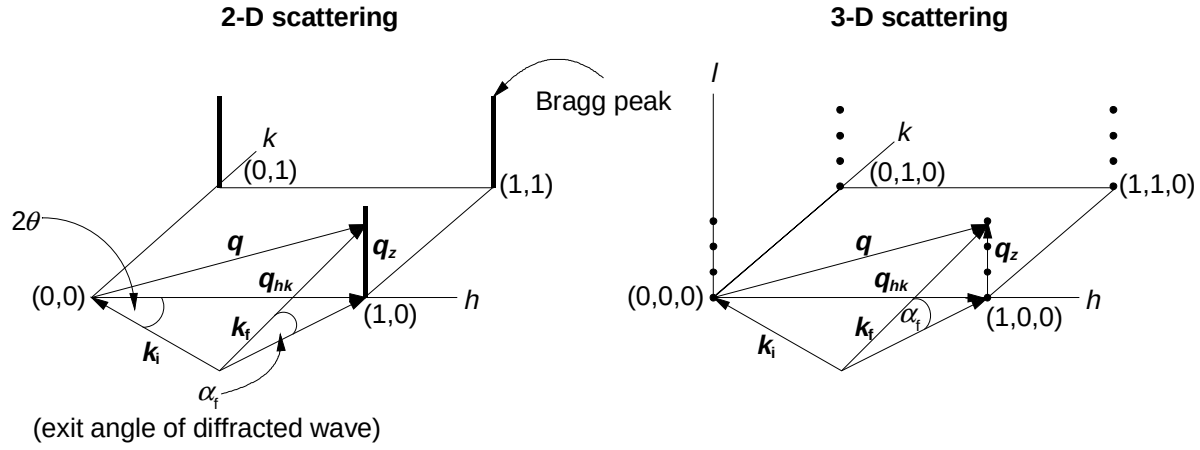

Figure 2. General 2-D and 3-D scattering geometry. $\boldsymbol{k}_i$ and $\boldsymbol{k}_f$ are the wave vectors of the incident and diffracted beams respectively. The scattering vector $\boldsymbol{q} = \boldsymbol{k}_f - \boldsymbol{k}_i$ is composed of $\boldsymbol{q}_{xy}$, which is parallel to the monolayer plane, and $\boldsymbol{q}_z$, which is perpendicular to it. In two dimensions the horizontal component of the scattering vector, $\boldsymbol{q}_{xy}$, must coincide with a reciprocal lattice vector $\boldsymbol{q}_{hk}$ with integer coordinates (*h*,*k*) and length $|\boldsymbol{q}_{hk}| = (4\pi/\lambda)\sin\theta_{hk}$ for diffraction to occur. The scattering from a 2-D crystallite in reciprocal space appears in the form of rods (Bragg rods) in the $\boldsymbol{q}_z$ direction, perpendicular to the plane of the monolayer and its reciprocal net. For comparison, the scattering from a 3-D crystal in a given orientation lies in reciprocal (or $\boldsymbol{q}$-) space on the reciprocal lattice points (*h*,*k*,*l*). The Bragg law is obeyed if the length of the scattering vector, $|\boldsymbol{q}|$ (given by $|\boldsymbol{k}_r - \boldsymbol{k}_i| = (4\pi/\lambda)\sin\alpha_f$, where k_f is the wave vector of the diffracted wave), is equal to $2\pi d^*$, with d^* being the reciprocal of the interplanar spacing *d*.

For a 2-D crystal lying in the *xy* - plane the diffraction condition is that the horizontal component of the scattering vector, $\boldsymbol{q}_{xy}$, coincides with a reciprocal lattice vector $\boldsymbol{q}_{hk}$, with $\boldsymbol{q}_{hk} = 2\pi\boldsymbol{d}^* = 2\pi(h\boldsymbol{a}^* + k\boldsymbol{b}^*)$. There is no selection rule or restriction on the vertical component of the scattering vector, $\boldsymbol{q}_z$, and therefore the Bragg scattering appears as continuous rods on the 2-D reciprocal lattice points[36,37] (Figure 2). The finite thickness of the 2-D crystal causes these rods to extend over finite $\boldsymbol{q}_z$ intervals. The intensity distribution along these intervals is determined by the vertical electron density distribution in the molecules and is expressed as a Fourier transform of the resulting electron density along the film normal. The intensity modulation contains information on the direction and magnitude of the molecular tilt in the 2-D crystalline

assembly.[38,39] Additional information on the electron density distribution in the vertical direction, laterally averaged over both the ordered and disordered parts of the monolayer can be obtained from the deviation of the measured X-ray reflectivity.

Specular X-ray reflectivity. Specular reflectivity is sensitive to the interference between X-rays reflected at various depths in the monolayer. By fitting the measured data to model electron density distributions the mean density distribution in the direction of the normal of the monolayer plane can be obtained. This results in the thickness of the layer. Specular reflection, in general, means that the measured reflected wave vector lies in the plane spanned by $\boldsymbol{k}_i$ and the normal to the surface and, that $\alpha_i = \alpha_f$ (Figure 1). The specular reflectivity of an ideal surface is given by the well-known Fresnel law of optics.[33] In general for reflection at an interface this Fresnel equation results in equation (3).

$$R_F(q_z) = \left| \frac{q_z - \left[q_z^2 - q_c^2 + i(4\pi\mu/\lambda)\right]^{1/2}}{q_z + \left[q_z^2 - q_c^2 + i(4\pi\mu/\lambda)\right]^{1/2}} \right|^2 . \qquad (3)$$

$q_z = (4\pi/\lambda)\sin\alpha_i$ is the magnitude of the z vector of the momentum transfer and $q_c = (4\pi/\lambda)\sin\alpha_c$ is the critical value of q_z for total external reflection. The complex term arises from absorption effects (cf. above). Neglecting absorption and for $q_z < q_c$, equation (3) gives $R_F = 1$, i.e. total reflection. As q_z increases beyond q_c, R_F decreases and, for $q_z \geq 4q_c$, approaches $R_F(q_z) \approx (q_c/2q_z)^4$. As the range of interest may extend to $q_z/q_c \approx 30$ or more,[38,40-42] reflectivities of as low as 10^{-8} have to be measured. It becomes clear that for such measurements a high-intensity radiation source like synchrotron radiation is required. Equation (3) is valid only for an ideally flat surface across which the electron density $\rho(z)$ varies stepwise between two constant values. If $\rho(z)$ is not a step function but varies continuously in the surface region, the reflectivity is modified[38,40-42] leading to equation 4, where ρ_∞ is the constant electron density in the bulk of the subphase.

$$R(q_z) = R_F(q_z)\left|\Phi(q_z)\right|^2 \qquad (4)$$

$$\Phi(q_z) = \frac{1}{\rho_\infty}\int \frac{d\rho(z)}{dz} e^{iq_z z} dz \qquad (5)$$

By measuring $R(q_z)$ it is therefore in principle possible to determine the variation of the electron density normal to the surface, and hence of a monolayer floating on it. The function Φ is complex and only its modulus can be derived from the measured reflectivity but not its phase. Here one is left with a phase problem known from X-ray crystallography. Therefore to date virtually all specular reflectivity data were analyzed by fitting a parametrized model density $\rho(z)$ to the measured data applying equations (3), (4) and (5). The simplest strategy for that is to create a model of a monolayer consisting of a stack of slabs,[43] or boxes, each corresponding to an abstract part of the monolayer of constant electron density ρ_i and thickness l_i. For example, two such slabs, or boxes, would be needed to describe the two different parts of a monolayer of an aliphatic alcohol.[44] The refining of such a model, i.e. the fitting to the measured reflectivity curve, is carried out by fitting parameters like the electron densities ρ_i and the thickness l_i of the boxes. The constant electron density of the semi-infinite subphase has to be added below the interface. Finally, the model density must be smeared out in the z-direction to account for the vertical roughness of the interface. The root-mean-square-roughness, σ, is around 3 Å and caused mainly by thermally excited capillary waves on the surface.[38,41,42]

1.2. General packing characteristics of aliphatic chain molecules in Langmuir monolayers on water and interpretation of the GIXD patterns

The basic assumption for a description of how unit cell dimensions and molecular orientations of simple aliphatic molecules may be deduced from GIXD data is that the molecules have freely rotating alkane chains, i.e. a cylindrical symmetry. In a monolayer such cylinders may pack in three different 2-D cell types: hexagonal ($a_h = b_h$, $\gamma_h = 120°$), distorted hexagonal ($a_h = b_h$, $\gamma_h < 120°$)[#] and oblique ($a \neq b$, $\gamma \neq 90°$), as shown in Figure 3. The molecules in a hexagonal cell are always aligned perpendicular to the surface normal (untilted molecules). In the rectangular packing the molecules may be tilted along a symmetry direction (either a or b) and in the oblique packing they are tilted in a direction slightly off a symmetry direction.

[#] The distorted hexagonal packing may be more appropriately described as centered rectangular, the most common packing arrangement for monolayers of aliphatic chain amphiphiles investigated so far. The resulting unit cell parameters are obtained by vector addition as $a = |\boldsymbol{a}_h + \boldsymbol{b}_h|$, $b = |\boldsymbol{a}_h - \boldsymbol{b}_h|$, $\gamma = 90°$.

All Langmuir monolayers studied so far by GIXD can be described as mosaics of randomly ordered 2-D crystallites on the water surface. There is as yet no way of controlling this mosaicity of crystalline monolayers, i.e. in other words the monolayers are powders within the plane. The diffraction is always averaged over all domain orientations in the monolayer plane (powder averaging).

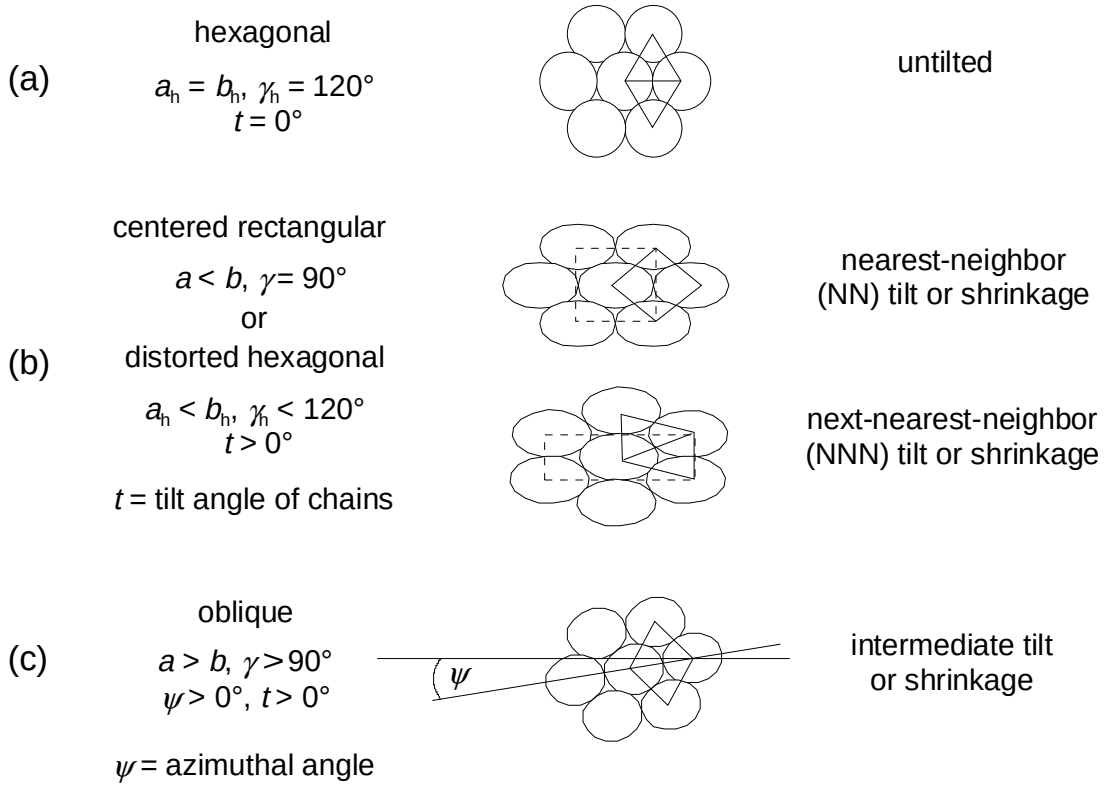

Figure 3. Geometrically three general types of packing are possible for cylinder-like molecules in a monolayer: hexagonal, rectangular and oblique. The hexagonal packing consists of untilted molecules. All nearest neighbor distances are equal. In the rectangular packing this arrangement is distorted. The unit cell shrinks in a symmetry direction and a tilt in one of the two symmetry directions is possible. The oblique packing consists of molecules tilted in an intermediate direction.

As a consequence, of the three vectors $\boldsymbol{q_x}$, $\boldsymbol{q_y}$ and $\boldsymbol{q_z}$ of the momentum transfer only the magnitude of the vertical vector $\boldsymbol{q_z}$ can be separately measured. It is not possible to determine the in-plane components individually, but only the combination $q_{xy} = (q_x^2 + q_y^2)^{1/2}$. Because lattice fluctuations and lattice defects cause the peak intensities to decay rapidly with decreasing momentum transfer, the first order peaks, which

correspond to the distances between neighboring molecules, are the most intense and, frequently, the only ones observed (Figure 4). First order peaks with common q_{xy} indicate a hexagonal packing with equal distances between the molecules. Two distinct values of q_{xy} point towards a rectangular unit cell, three peaks are due to an oblique unit cell. Obviously, the available diffraction data is not sufficient to perform structural analysis in a classical crystallographic sense. Knowledge of the possible packings of aliphatic chains in bulk crystals and lattice energy calculations are additionally employed to complete the interpretation of the GIXD data.[31,45,46] Usually the structures within monolayers are rather simple and can, with certain approximations, be determined to near atomic resolution.

The simplest approach towards structure determination by GIXD is to treat a crystalline domain of the monolayer as a 2-D crystal consisting of uniformly oriented rigid molecules.[47,48] The scattering pattern in reciprocal space is then given by the product of two factors: the structure factor (reflecting translational order of the molecular centers in the plane of the monolayer) and the form factor of the individual molecule. The structure factor of a 2-D lattice consists of a set of delta-function discontinuities along lines (the Bragg rods) normal to the monolayer plane. The form factor along a cylinder-like molecule is large only on a plane normal to its long axis, which is called the „reciprocal disc“ of the molecule. The intersections of the first order Bragg rods with the reciprocal disc give rise to six diffraction maxima (Figure 4a-d). If the molecules are not tilted, the reciprocal disc, and hence all the peaks, lie in the plane of the monolayer (Figure 4a). All six first order wave vectors $\boldsymbol{q}$ have the same length and all the peaks overlap (complete degeneracy). This degeneracy is lifted when the lattice is distorted from purely hexagonal. This may arise for instance as a result of ordering of the backbone planes of the molecules. Distinct peaks at different values of $\boldsymbol{q}$ are observed (Figure 4b-d). The tilt angle t is the angle between the reciprocal disc and the monolayer plane. For a distortion in which the unit cell stretches or shrinks in the direction of the nearest-neighbor (NN) molecule, a symmetry plane normal to the plane of the monolayer is preserved and the resulting unit cell is centered rectangular. This gives rise to two distinct first-order wave vectors on powder averaging: one pair with $\pm \boldsymbol{q}_{\mathbf{n}}$, the other two with $\boldsymbol{q}_{\mathbf{d}}$ (the subscripts n and d stand for non-degenerate and degenerate peaks respectively). $|\boldsymbol{q}_{\mathbf{n}}| > |\boldsymbol{q}_{\mathbf{d}}|$ indicates

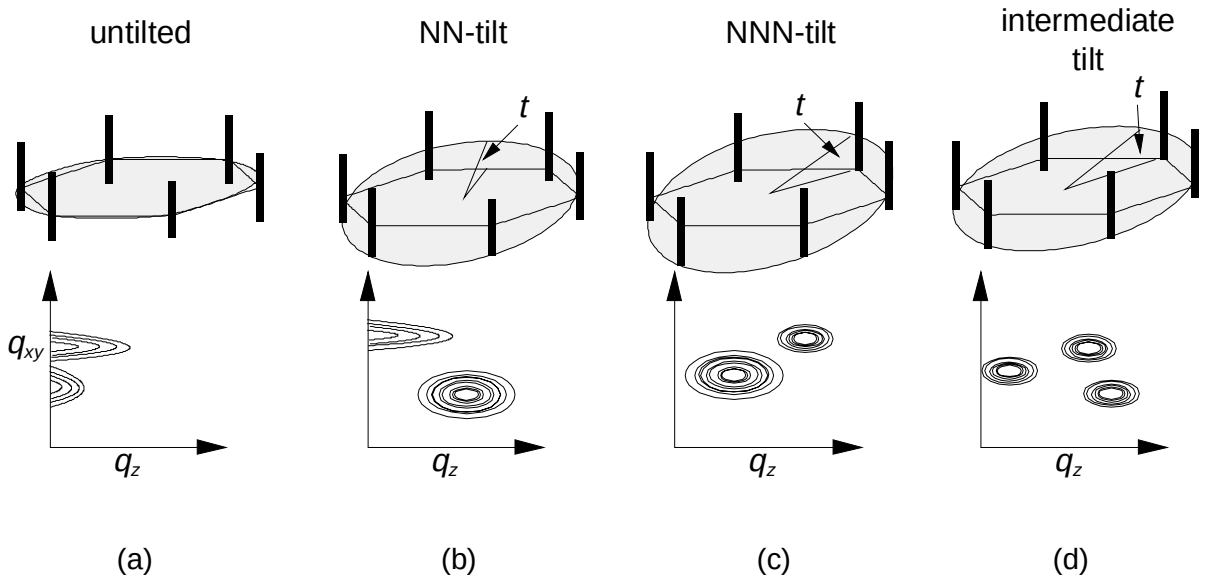

Figure 4. (top) Reciprocal discs of a cylinder-like molecule in a crystalline monolayer domain with: (a) untilted, (b) nearest-neighbor (NN) tilted, (c) next-nearest-neighbor (NNN) tilted and (d) intermediately tilted molecules. (bottom): First order GIXD signals schematically. Due to lattice fluctuations and lattice defects the peak intensities decay rapidly with increasing momentum transfer. Therefore, these first order peaks, which correspond to the distances between neighboring molecules, are the most intense and, in many cases, the only observed ones. They are equivalent to the strong subcell reflections in a 3-D crystal.

that the unit cell is stretched in the direction of the NN molecule. The opposite inequality means a shrinkage of the unit cell in that direction. The degeneracy of the peaks is also lifted if the molecules are tilted with respect to the surface normal. The distance q_z, by which the peaks are moved out of the monolayer plane, depends on the molecular tilt angle as well as on its azimuth or direction. The only peaks on the reciprocal disc that remain in the monolayer plane are those on the line perpendicular to the tilt direction. This occurs for one pair of peaks if the molecules are NN-tilted. The other four peaks move out of this plane: two upwards and two downwards (the two peaks below the water surface can naturally not be measured, cf. Figure 4b). The wave vectors of the two visible out-of-plane peaks have equal q_z components and are therefore degenerate in the diffraction pattern. The tilt angle is given by $\tan t = q_{z,d}/[q_{xy,d}^2 - (q_{xy,n}/2)^2]^{1/2}$. When the molecules are NNN tilted all the wave vectors move out of the plane. The two distinct values of q_z are in the ratio $q_{z,n} : q_{z,d} = 2:1$ and the molecular tilt angle is given by $\tan t = q_{z,n}/q_{xy,n}$ (Figure 4c). In these phases, in

which the molecules are tilted in a symmetry direction, the distinction between degenerate (d) and non-degenerate (n) peaks is unambiguous. The ratio $q_{z,n}$:$q_{z,d}$ can only be 0:1 or 2:0. In an untilted phase (Figure 4a) the distinction is more complicated. In the idealized model of cylinder-like molecules the integrated intensity of the degenerate peak should be twice as large as that of the non-degenerate peak. However, in praxis there are often significant deviations from this ideal 2:1 ratio.[49] This observation was explained by calculating the molecular structure factors and intensity ratios from atomic scattering factors, assuming an all-trans conformation of the molecules and ideal (zero temperature) packing. It was found that the intensity ratio depends on the orientation of the backbone planes of the molecules and symmetry constraints.[49]

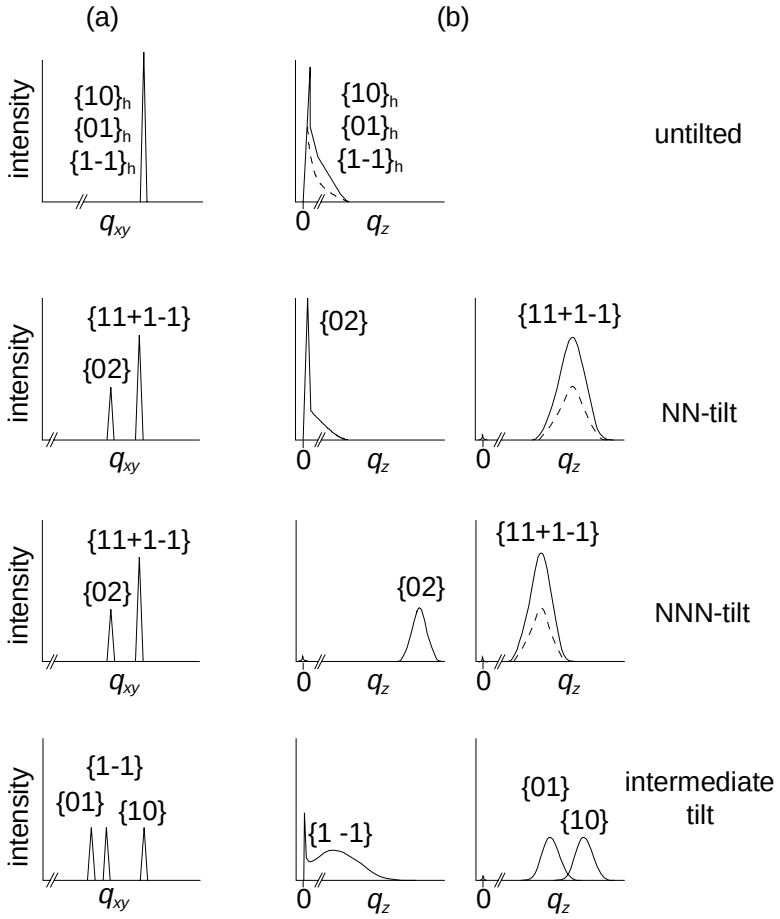

Figure 5. Possible assignment of GIXD peaks arising from a monolayer of cylinder-like molecules. Column (a): reflections shown as $I(q_{xy})$; the intensity distributions are called „Bragg peaks“. The analysis of their full width at half maximum (FWHM) yields information on the crystalline coherence length in the chosen direction. Column (b): reflections shown as $I(q_z)$; the intensity distributions are called „Bragg rods“. The analysis of their full width at half maximum (FWHM) yields information on the crystalline film thickness. Molecular models can be fitted to these $I(q_z)$ shapes and as a result give a ‘real’ picture of the crystalline packing of the molecules.

If the tilt azimuth is intermediate between NN and NNN (Figure 4d), or if the distortion of the unit cell is asymmetrical, there are three distinct first order peaks. Each peak is described by two components of the momentum transfer, which is six measured values in total. Since the monolayer model is completely described by five parameters (three for the in-plane lattice and two for the tilt magnitude and direction), the measured values cannot be completely independent. The relationship between them is readily shown to be $q_{z,1} + q_{z,2} = q_{z,3}$, where peak 3 is the one with the largest q_z. The two q_z ratios 0:1 and 2:1 for the symmetric tilts follow from this more general relationship as particular cases in which one of the q_z values is repeated, and result in 0 + 1 = 1 and 1 + 1 = 2, respectively. Once the three first-order peaks have been assigned, the shape of the subcell in reciprocal space is completely determined.

The peaks can be assigned in crystallographic notation in terms of either a hexagonal or a centered rectangular unit cell (Figure 5).[31] The latter is more common. Denoting the basic translations of the centered rectangular unit cell containing two molecules by [1,0] and [0,1] (when the lattice is hexagonal the length of the vector [0,1] is $\sqrt{3}$ times larger than [1,0]) one finds that, if the two molecules in the rectangular cell are equivalent, the reflections {01} and {10} are forbidden as are all {*hk*} reflections where $h + k$ is odd. The lowest-order reflections are {02} (non-degenerate) and the two reflections {11} + {1-1} (which have equal length and are degenerate). When the two molecules in the unit cell are not equivalent due to packing of the molecular backbones, the structure factors of the odd $h + k$ reflections may become non-zero. However, the {10} and {01} intensities were considered too weak to be measured.[50]

Determining a structure of a Langmuir monolayer by an X-ray method differs from the classical three-dimensional crystallography in two essential ways: Firstly, the available diffraction data are extremely limited and, in most cases, consist of first order diffraction peaks only. This lack of data can be partially compensated for by utilizing the knowledge of the packings of long aliphatic chain molecules, mainly n-alkanes, in bulk crystals. Secondly, the local packing determined for a mesophase cannot be extended to the long order, as it is routinely done in crystallography. The range of positional correlation in these crystallites is finite. The symmetry of the local packing describing the relative positions of the molecules within some tens of

intermolecular distances need not to coincide with the long-range symmetry governing the thermodynamics of the monolayer.

Concentrating on the local packing only it is possible to relate the structures of cylinder-like molecules in monolayers quite well to the packing arrangements n-alkanes exhibit in 3-D crystals.[51,52] In this case the packing of the chains should be characterized by the dimensions $a_{\perp}$ x $b_{\perp}$ of a rectangular cell projected onto a plane perpendicular to the axis of the molecular chains (in the following text appearing as a_p and b_p). A distribution of cell dimensions were extracted from GIXD data of monolayers of non-chiral substances. It became obvious that orientational disorder,

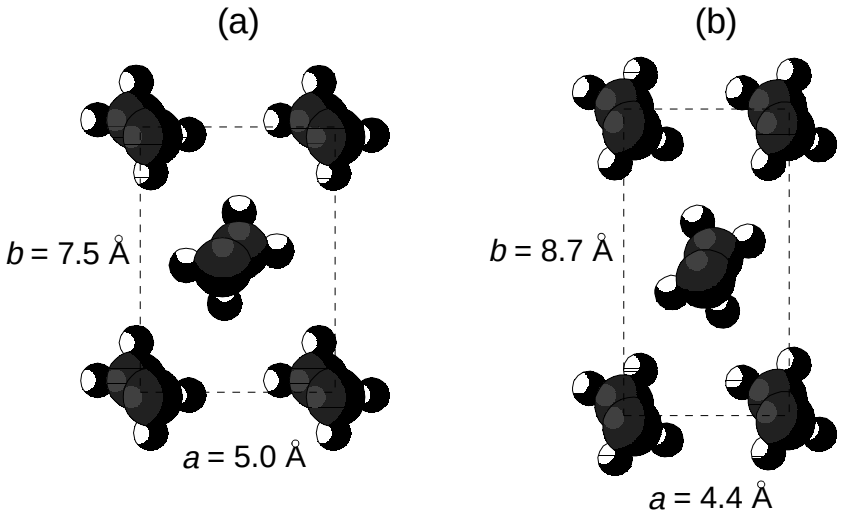

Figure 6. (a) Herringbone (HB) and (b) pseudoherringbone (PHB) packings of hydrocarbon chains.[54]

i.e. hexagonal local packing of the molecules, requires a relatively large area per chain (20 - 21 Å^2) and occurs at temperatures of about, or higher than, room temperature. Lowering the temperature causes a reduction of the area per chain and a concominant distortion of the unit cell to yield a rectangular cell. This transition between a mesophase and a crystalline phase is reversible. The rectangular distortion was observed to result in two different, relatively dense packings of the chains of dimensions $a_{\perp}$ x $b_{\perp}$ = 5.0 x 7.5 and 4.4 x 8.8 Å^2 respectively (areas per chain = 18.5 and 19.0 Å^2 respectively). The dimensions of the former one (5.0 x 7.5 Å^2) are fingerprint evidence for the well-known herring-bone (HB) arrangement, a common packing mode of hydrocarbon chains in 3-D crystals.[51] The unit cell

dimensions 4.4 x 8.8 Å^2 of the second packing arrangement are noticably different from those of the standard HB packing. A search for a possible packing mode that satisfies the 4.4 x 8.8 Å^2 cell is a mode considered as implausible by Kitaigorodskii[53] because of its lower packing density compared to the HB packing. This, in 3-D crystals rather unusual packing, is now commonly labeled pseudo-herring-bone (PHB) packing. The unit cells for the HB and PHB packings are scetched in Figure 6. The PHB motif was characterized by Kitaigorodskii on the basis of the van der Waals radii of the carbon and the hydrogen atoms. According to this the angle between the backbone planes of the chains, ϕ, should be 40°. The projected unit cell parameters of this arrangement are, according to Kitaigorodskii, 4.2 x 9.0 Å^2. The values shown in Figure 6 differ slightly from this and follow from lattice energy calculations.[54] The majority of densely packed NN-tilted monolayer phases have projected unit cell dimensions very close to those of the PHB motif. The PHB packing is common in 2-D amphiphilic systems.

A third possible packing arrangement arises from a minimum in the lattice energy calculations.[54] This packing motif is characterized by an angle ϕ = 180° and corresponds to a packing which is constrained by an *a*-glide symmetry. If the a-glide constraint is released, the structure relaxes to a triclinic or monoclinic packing in which all the chains have their backbone planes parallel to each other. The two molecules in the unit cell are related by translation. Although this packing motif of the chains has rarely been encountered for Langmuir monolayers composed of non-chiral molecules,[55] it was found for some compounds investigated in this work and is probably imposed by their unusual molecular structure.

Concluding this, according to the minima in the energy of a two-dimensional lattice of alkane molecules with their chains axis aligned normal to the interface three packings in a rectangular cell are possible: The two molecules in the unit cell are related by an *a*-glide, by a *b*-glide or purely by translation. The structure of a large number of monolayer could be successfully solved utilizing GIXD, mainly at the air-water interface. Most of the studies have been carried out on partially ordered[56-68] and crystalline[69-75] Langmuir layers of simple fatty acids, phospholipids, aliphatic alcohols and *n*-alkanes and of derivatives of these compounds. Most of these ordered monolayers pack in a rectangular unit cell containing two chains related by

glide symmetry, although also translation symmetry occurs. Structures of low-temperature crystalline phases (T ≈ 5°C) in Langmuir layers usually correspond well to the structures of the dense packing modes of hydrocarbon chains in 3-D crystals. Higher-temperature phases are mesophases which possess partial orientational and translational disorder and are discussed very detailed elsewhere.[76]

1.3. The concept of this work

Chain folding in natural[77] and synthetic[78] oligomers and polymers has been intensively studied under many aspects. Experiments[79] and molecular dynamics simulations[80-82] on ethylene oligomers have been carried out to show that chain folding is a function of chain length. The required length for folding to occur in such oligomers is about 150 carbon atoms depending mainly on the crystallization conditions.[83-86] Recently, the control of the conformation of polymers by appropriately designing the folding regions within the polymer has become a topic of interest.[87-89] One problem is that, even if the folds can be distributed evenly along the polymer chain, one can neither control nor predict their precise location.

This work will show that it is possible to design and readily synthesize molecules containing alkyl chains that are able to pack into 2-D crystals at the air-water interface[90-93] and into 3-D crystals in bulk by folding into a predetermined pattern. As the alkyl chains in these molecules have a chain length much shorter than the above mentioned 150 carbon atoms the crystalline arrangements of these folded molecules are an example for supramolecular design. The van-der-Waals interaction between hydrocarbon chains serves as a tool to fix a supramolecular structure of the molecules and their functional groups. The monolayers of such molecules could be of interest as model systems to study early stages of molecular self-organization and crystallization and as model systems for biological membranes. The molecular design in this work is a general approach and could be utilized for related systems in order to bring about a folded conformation.

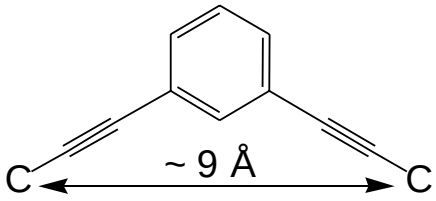

Figure 7. The 1,3-bis(ethynylene)benzene unit. It acts as a rigid spacer separating the two attached alkyl chains by approximately 9 Å.

The strategy is to obtain linear oligomers by linking linear, aliphatic chains of similar or equal length by evenly spaced, rigid structural units. The type of rigid spacer unit, that was chosen for this purpose, is the 1,3-bis(ethynylene)benzene unit (Figure 7). Its dimensions, corresponding to a 9 Å intramolecular separation of the attached chains, would preclude van der Waals contacts between the chains.

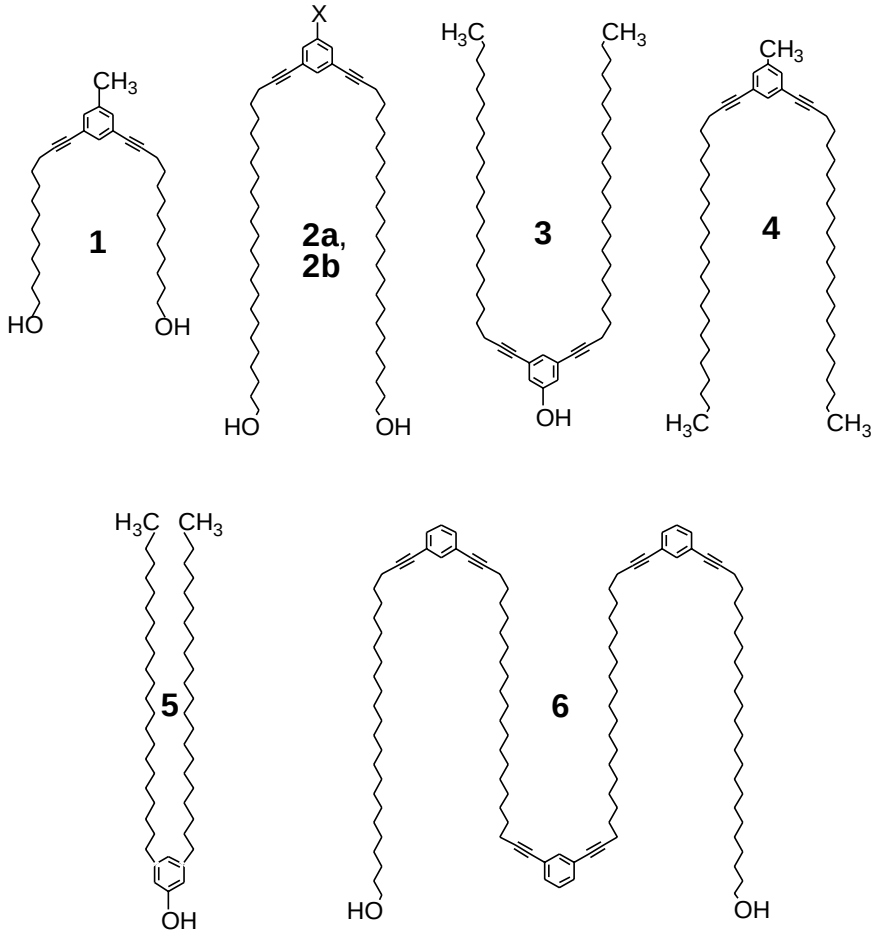

Figure 8. The seven molecules synthesized and investigated in this work. A modification of molecule **2a** (X = OTHP) is molecule **2b** (X = H) which addresses the question of the influence of a bulky substituent at the rigid spacer unit on the crystallization behavior of **2a**.

By choosing the intramolecular chain-to-chain separation to be 9 Å, being approximately twice the normal van der Waals distance between aliphatic chains in crystals, the definition of a molecular fold in this work is given: The folded conformation should not be stabilized by intramolecular chain-to-chain interaction, as in conventional two-chain amphiphiles, but rather by intermolecular contacts leading to the formation of a close-packed crystalline monolayer containing folded molecules. In other words: If the concept is correct, the molecules designed in this way should self-assemble into crystalline monolayers at the air-water interface and in bulk by adopting a kind of U-shape.

A variety of structurally related molecules has been synthesized for this purpose (Figure 8). The molecular design involved a variation of the chain length, of the type, number and position of functional groups and, finally, of the number of spacer units in the oligomer. Apart from molecule **5**, all molecules have a common strucural feature: the 1,3-bis(ethynylene)benzene unit. Molecule **5** differs markedly in its structure as it contains a smaller spacer unit. It was synthesized and investigated as an example for a conventional two-chain amphiphile. Conventional, in this case, means an intramolecular chain-chain separation of 5 Å. This should allow for intramolecular chain-chain interaction during crystalline assembly and should result in one of the classical packing arrangements known from alkane crystallography.[51]

The packing arrangements of the Langmuir monolayers were determined by GIXD using synchrotron radiation. This work presents the first example of a structural prove for folded molecular conformations of oligomers at the air-water interface.[94,95] Additional information on the average thickness of some of the monolayer systems was obtained either by specular X-ray reflectivity measurements or from topography images of the films transferred onto solid support using scanning force microscopy (SFM).

Finally, the crystalline packing and supramolecular arrangement imposed by the 1,3-bis(ethynylene)benzene unit of a molecule in a monolayer is compared to the single crystal structure of the same molecule in bulk.

2. Results and Discussion

2.1. Synthesis

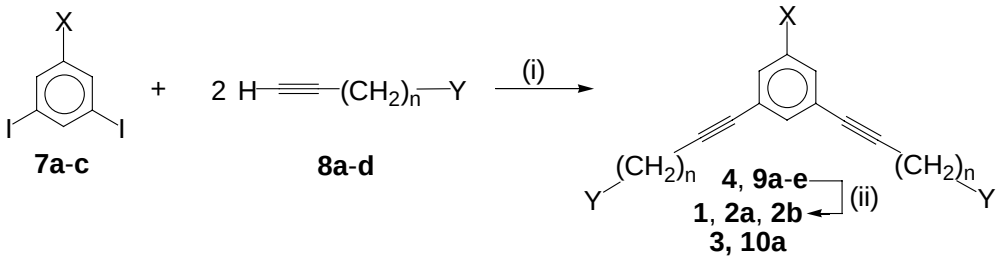

7a-c **8a-d**

7	X
a	H
b	CH_3
c	OTHP

8	Y	n
a	OTBDMS	19
b	OTMS	11
c	OTBDMS	23
d	CH_3	21

	X	Y	n
9a	H	OTBDMS	19
9b	CH_3	OTMS	11
9c	OTHP	OTBDMS	23
9d	H	OTBDMS	23
9e	OTHP	CH_3	21

Compounds **1**-**4** and the precursor compound **10a** for the synthesis of **6** were obtained by deprotection.

		X	Y	n
9a →	**10a**	H	OH	19
9b →	**1**	CH_3	OH	11
9c →	**2a**	OTHP	OH	23
9d →	**2b**	H	OH	23
9e →	**3**	OH	CH_3	21
	4	CH_3	CH_3	21

Scheme 1. Key: (i) $Pd(PPh_3)_2Cl_2$, CuI, THF, piperidine, rt, 16 h; (ii) for **9a**-**d**: *n*-$BuNF_4$, THF, rt, 1 h for **9e**: dioxane, MeOH, TosOH, rt, 1 h.

The key step in the synthesis of compounds **1**-**4**, **6** and **10** is an aryl-alkynyl coupling catalyzed by $Pd(PPh_3)_2Cl_2$ and CuI. Compounds **4** and **9a**-**e** (Scheme 1) were obtained by coupling 1,3-diiodobenzenes **7** with 1-alkynes **8**. Subsequent deprotection of the OH-groups of products **9a**-**e** yielded the compounds **1**, **2a**, **2b**, **3** and **10a**. Compound **10a** is one of the starting materials for the synthesis of molecule **6** (Scheme 2). The α,ω-diol **10a** was transformed into the α,ω-diyne **10c** via the α,ω-dibromide **10b** synthetic intermediate. The α,ω-diyne **10c** was coupled with the 3-alkynyliodobenzene **11** (Scheme 2) to give, after desilylation, the molecule **6**. Coupling partner **11** was obtained as the main product by the reaction of 1,3-diiodobenzene **7a** with one equivalent of the O-protected alkynol **8c** and was easily isolated by column chromatography.

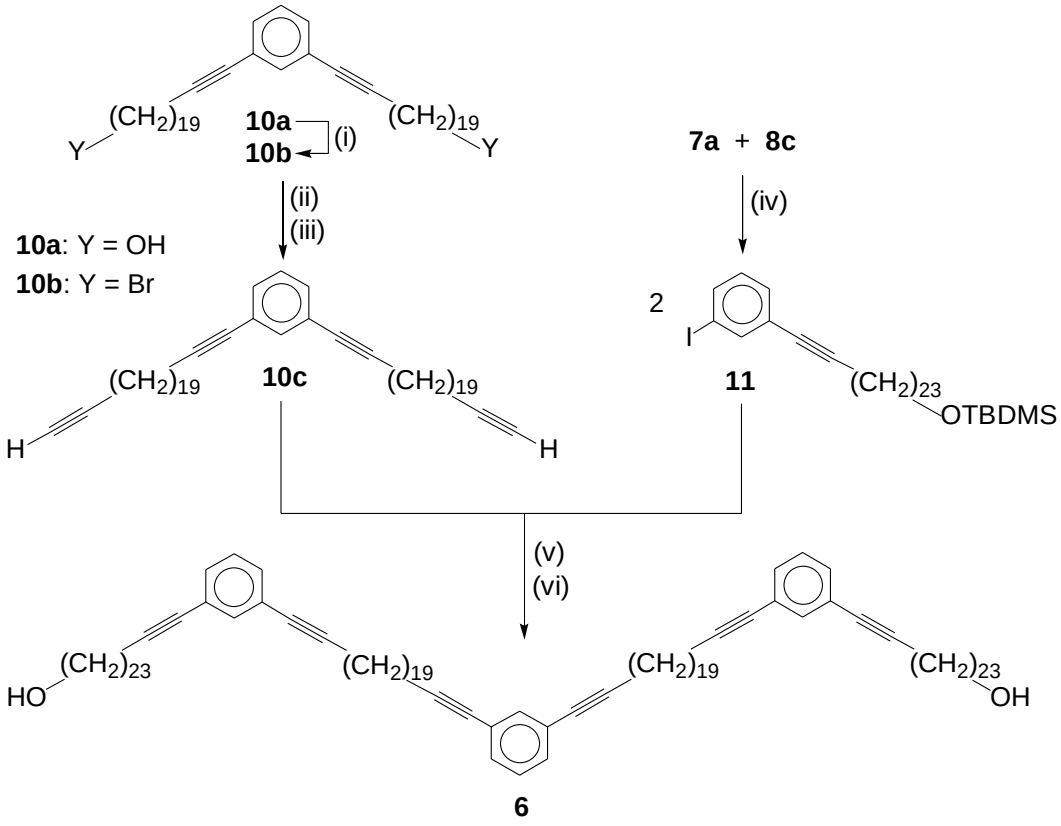

Scheme 2. Key: (i) PPh_3, Br_2, imidazole, CH_2Cl_2, rt, 8 h; (ii) LiC≡C-TMS, THF, 1,3-dimethyl-3,4,5,6-tetrahydro-2(1H)-pyrimidone, rt, 16 h; (iii) *n*-$BuNF_4$, THF, 1 h, rt; (iv) $Pd(PPh_3)_2Cl_2$, CuI, THF, piperidine, rt, 16 h; (v) $Pd(PPh_3)_2Cl_2$, CuI, THF, piperidine, rt, 16 h; (vi) *n*-$BuNF_4$, THF, 1 h, rt.

Compound **5** was synthesized by a coupling reaction catalyzed by $Ni(dppp)Cl_2$ of the alkyl Grignard **13** with the protected 3,5-dichlorophenol **12** followed by desilylation of the coupling product (Scheme 3).

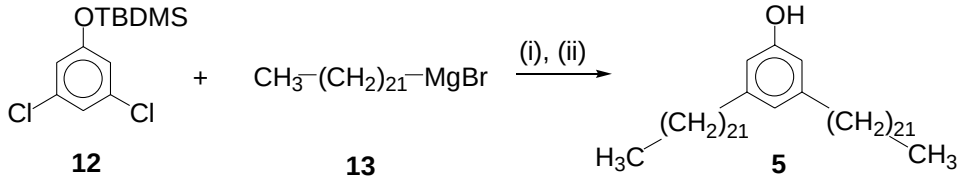

Scheme 3. Key: (i) $Ni(dppp)Cl_2$, diethyl ether, reflux, 5 d; (ii) *n*-$BuNF_4$, THF, 1 h, rt.

Although several possibilities have been tried to synthesize functionalized long, aliphatic carbon chains during this work,[96-98] an halide-alkyne exchange followed by alkyne isomerization was found to be the most reliable and effective source to get monodisperse aliphatic chains of sufficient purity (Scheme 4).

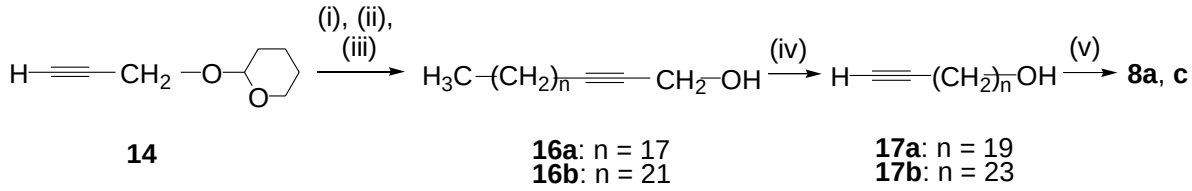

Scheme 4. Key: (i) *n*-BuLi, THF, -80 °C, 30 min; (ii) CH_3-$(CH_2)_n$-Br (**15a**: n = 17, **15b**: n = 21), 1,3-dimethyl-3,4,5,6-tetrahydro-2(1H)-pyrimidone, rt, 16 h; (iii) dioxane, MeOH, TosOH, rt, 1 h; (iv) Li, H_2N-$(CH_2)_3$-NH_2, KO^{t}Bu, 45 °C, 16 h; (v) TBDMS-chloride, imidazole, DMF, rt, 3 h.

The THP-protected propynol **14** was deprotonated using n-BuLi at low temperatures to prevent simultaneous deprotonation of the CH_2 group. This lithium acetylide was subsequently reacted with the alkyl halides **15**.[99] After deprotection the resulting alkynols **16** were isomerized under strongly basic conditions in analogy to a procedure given by Shaw.[100] Purification by column chromatography yielded the α,ω-alphatic alkynols **17** which were subsequently silylated[101] to give **8a** and **8c** (Scheme 1). The long n-alkyne **8d** was directly obtained by reacting docosyl bromide **15b** with lithium trimethylsilyl-acetylide. Deprotection yielded **8d**. The short chain **8b** was synthesized by J. Thiel[102] using the commercially available HO-$(CH_2)_{11}$-Br, which was O-protected prior to the substitution reaction.

The 1,3-bis(ethynylene)benzene unit in the final oligomer is produced by a catalytic alkynyl-aryl coupling (Scheme 1). Only one of the three different diiodobenzene derivatives used in this work, the 1,3-diiodobenzene itself, was commercially available. The 3,5-diiodotoluene **7b**[103] was kindly supplied by S. Höger. The THP- (tetrahydropyran-2-yl-) protected diiodophenol **7c** was synthesized using a procedure developed by Sigurd Höger (Scheme 5).[104] The starting material of this synthesis was the 2-amino-3,5-diiodo-nitrobenzene (**19**) obtained from *o*-nitroaniline (**18**). The amino group of **19** was converted to a diazonium group which was reduced by boiling ethanol to yield **20**. **21** was then obtained by the reduction of

the nitro group of **20** and was the starting material for the final conversion to the 3,5-diiodophenol **22**. The crude diiodophenol **22** was protected to give **7c**.

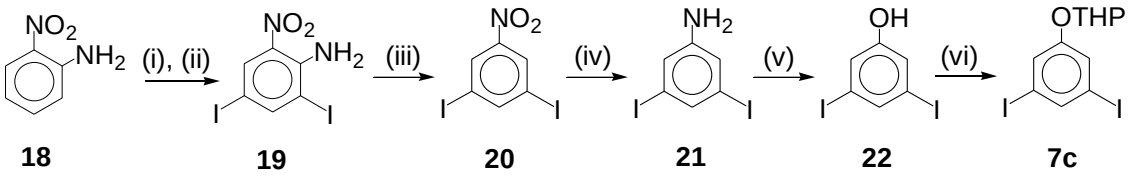

18 **19** **20** **21** **22** **7c**

Scheme 5. Key: (i) iodine monochloride, dichloro ethane, reflux, 3 h; (ii) $NaNO_2$, H_2SO_4, ethanol, 0 °C, 3h; (iii) ethanol, reflux, 16 h; (iv) $Na_2S_2O_4$, 1-methoxy-2-propanol, reflux, 3 h; (v) butyl nitrite, CH_3COOH, H_2SO_4, 105 °C, 30 min; (vi) DHP, TsOH, CH_2Cl_2, rt, 3 h.

2.2. Thermal characterization

The characterization of compounds by differential scanning calorimetry (DSC) gives useful information on characteristic parameters like the melting (T_m), crystallization (T_c) and glass transition (T_g) temperature of a compound, heat of fusion (ΔH_m), heat of crystallization (ΔH_c), heat capacity (c_p) and others. Furthermore it allows an estimation of the crystal quality if reference data are available and also of the purity of a given compound. In this chapter generally the first heat-up curve of a DSC experiment refers to the heat-up scan of the compound crystallized from solution (CH_2Cl_2) on slow evaporation of the solvent. It was a reproducible result that this scan in all cases revealed the higher values for the melting temperature, T_m, and for the melting enthalpies, ΔH_m, in comparison to the corresponding values obtained for the same compound crystallized from the melt. This indicates that on crystallization from solution a higher crystal perfection is achieved.

A purity analysis by DSC[105] could not be carried out as data of the pure compounds were not available. In principle, one may consider to extrapolate the width at half maximum of the melting peaks as a function of the square root of the heating rate to zero heating rate and use this as a criterion of purity. This method, however, is prone to falsification as all DSC melting peaks are broadened due to the time it takes to conduct the heat of fusion. Even substances which are known to melt within 0.005 K can easily give a melting peak of 3 to 5 K width.[106] Furthermore, an X-ray diffraction experiment, as described in chapter 2.3.2. (not shown), on a crystalline monolayer of compound **4** containing detectable amounts (HPLC: ~3 mol%) of a single chain impurity revealed that there is no difference in the crystalline self-assembly between this compound **4** and compound **4** without any detectable impurity.

Compound **1** was characterized by DSC at different rates of heating and cooling (Figure 9). The highest degree of crystallinity is, as just mentioned, achieved on crystallization from solution. The scans at different heating rates reveal an interesting behavior of compound **1**: Even at slow cooling rates **1** does not crystallize from the melt. It has a T_g at around -48°C. For comparison, the T_g of poly(ethylene) is at about -33 °C.[105] Above T_g there are two crystallization processes. The latter one

forms the stable, crystalline phase which also formed on crystallization from solution. It is most likely this phase that has been obtained as a single crystal and is discussed in chapter 2.4.

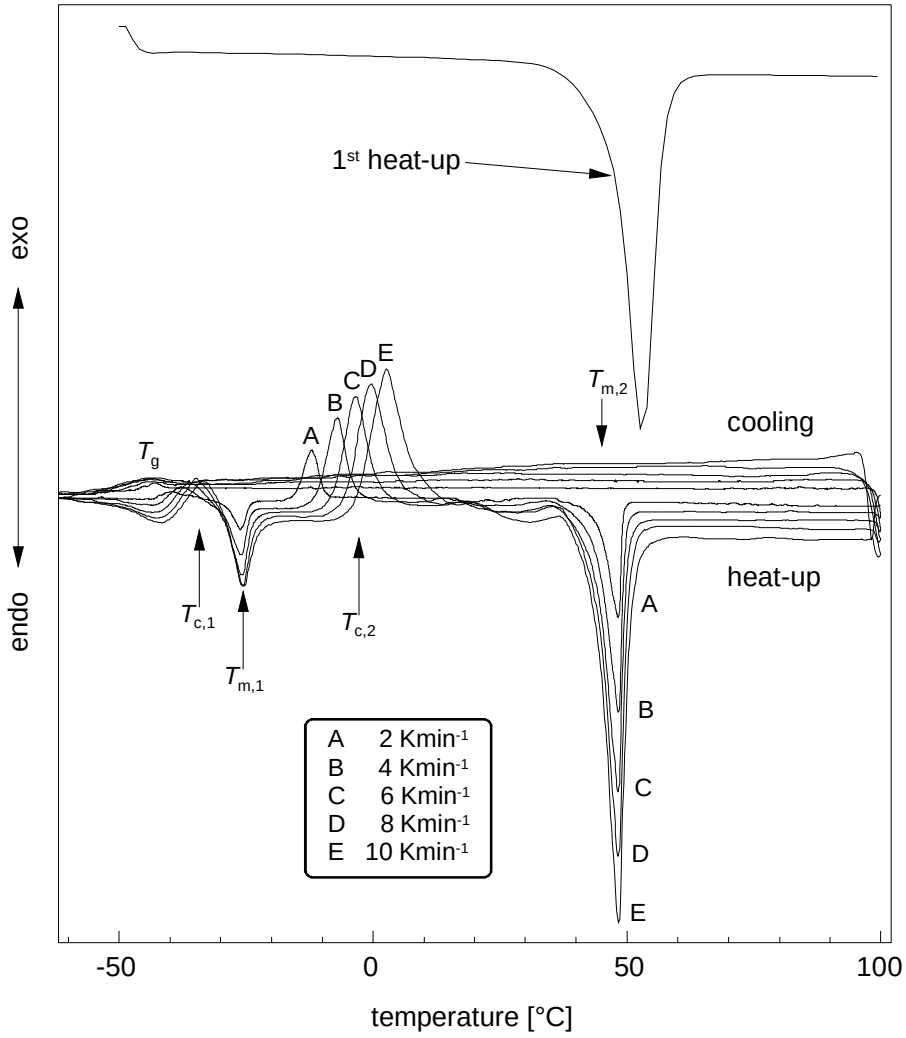

Figure 9. DSC scans of compound **1** at several heating and cooling rates. The 1st heat-up scan was carried out on **1** crystallized from CH_2Cl_2 solution at 10K/min.

	$T_{g,midpoint}$ [°C]	$T_{g,midpoint\ DIN}$ [°C]	$T_{c,1}$	$T_{m,1}$	$T_{c,2}$	$T_{m,2}$
1st heat up	-	-	-	-	-	50.38
A	n.a.	n.a.	-39.44	-26.11	-12.01	48.22
B	-49.10	-49.06	-37.77	-26.04	-7.04	48.17
C	-47.52	-47.72	-36.17	-25.86	-3.39	47.97
D	-47.74	-48.00	-34.76	-25.67	-0.28	47.98
E	-46.45	-47.16	-33.63	-25.57	2.80	47.99

Table 1. Characteristic temperatures for compound **1**. $T_{m,2}$ of the first heat-up scan is T_m of **1** crystallized from CH_2Cl_2 solution.

	Δc_p [kJmol^{-1}K^{-1}]	$\Delta H_{c,1}$ [kJmol^{-1}K^{-1}]	$\Delta H_{m,1}$ [kJmol^{-1}K^{-1}]	$\Delta H_{c,2}$ [kJmol^{-1}K^{-1}]	$\Delta H_{m,2}$ [kJmol^{-1}K^{-1}]
1st heat up	-	-	-	-	66.67
A	n.a.	-6.01	9.97	-19.08	46.50
B	0.26	-8.81	8.40	-23.75	47.07
C	0.49	-7.72	8.62	-26.46	48.38
D	0.52	-8.36	6.86	-28.68	45.84
E	0.52	-7.62	5.34	-26.66	46.11

Table 2. Δc_p and ΔH values for **1** at different heating rates. $\Delta H_{m,2}$ of the first heat-up scan is ΔH_m of **1** crystallized from CH_2Cl_2 solution.

The question why compound **1** does not crystallize from the melt cannot unambiguously be answered. Most likely, though, this behavior indicates that, coming from the melt, severe conformational changes within the molecules **1** must occur in order to achieve a conformation that will allow close packing of **1** in a crystal. If the chains are too short the van-der-Waals interactions between them are not sufficiently strong to force the molecule into this conformation. Longer chains would increase the lattice energy of the molecular packing and would aid the molecules to adopt the required conformation. For this reason, molecules **2**-**6** (Figure 8) contain alkyl chains of approximately twice the length of the alkyl chains of **1** in order to increase the intermolecular chain-chain interactions.

1-tetracosyne (**8d**) is an integral part of molecules **3**, **4**, and **5**. Molecules **2a**, **2b**, and **6** contain pentacos-1-yn-25-ol (**17b**). Heneicos-1-yn-21-ol (**17a**), the shorter analogue to **17b**, is structurally related to the chains in the middle part of **6**. These three chains, **8d**, **17a**, and **17b**, are not simple *n*-alkanes and therefore the thermal data available for *n*-alkanes[107] cannot be used for comparison with the data obtained for compounds **2-6**. One could relate the ΔH_m values obtained for **2-6** to the ΔH_m value per CH_2-unit measured on fully extended and 100% crystalline poly(ethylene). This value is 4.1 kJmol^{-1} per CH_2-unit.[107] However, in order to get a measure for the crystallinity of molecules **2-6** their ΔH_m values are compared to the ΔH_m values of the corresponding chain crystallized from CH_2Cl_2 solution on slow evaporation of the solvent. Figure 10 shows the first heat-up scans of the three chains **8d**, **17a**, and **17b**.

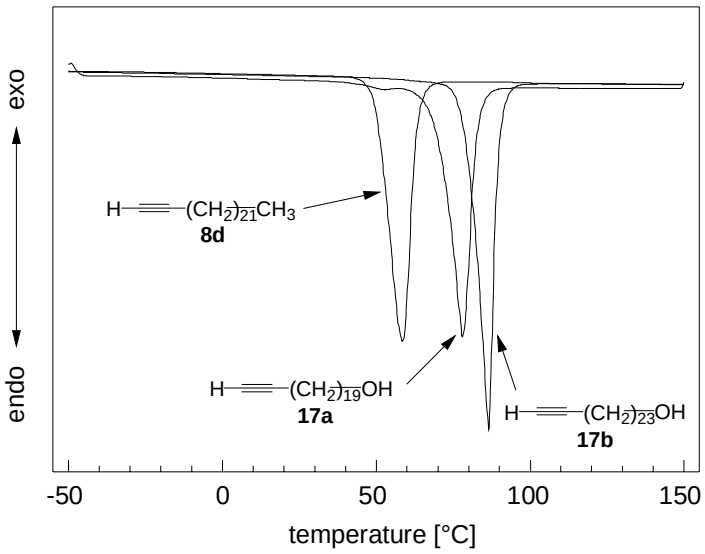

alkyl chain	T_m [°C] 1st heat-up	ΔH [kJmol^{-1}] 1st heat-up
8d	53.50	76.08
17a	72.08	66.24
17b	81.75	87.97

Figure 10. 1st heat-up scans of the alkyl chains **8d**, **17a**, and **17b** crystallized from CH_2Cl_2 solution.

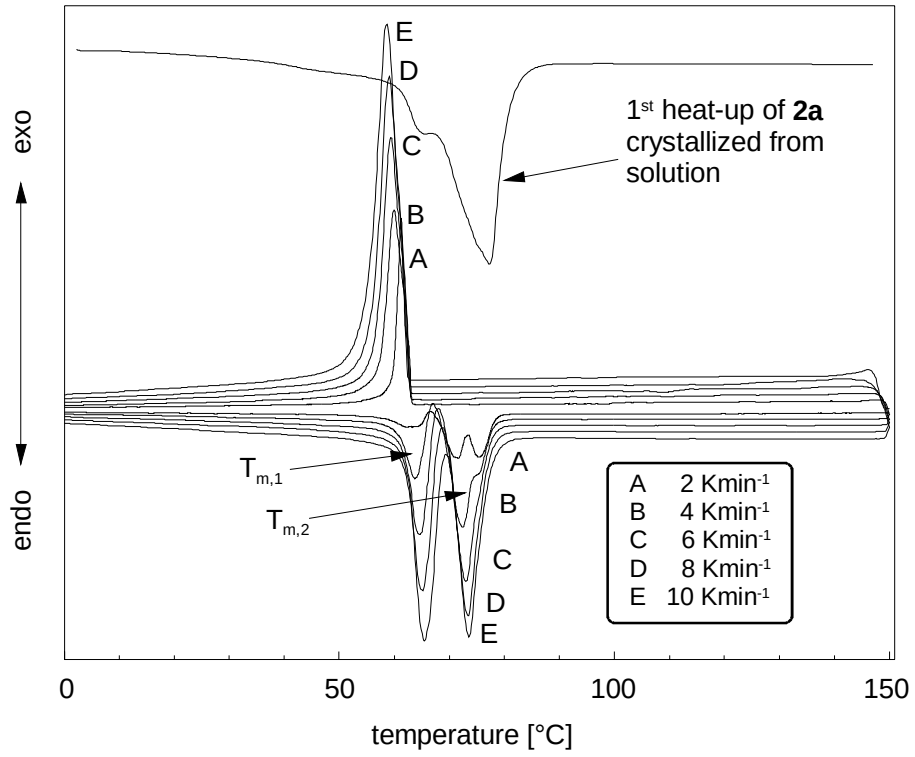

Figure 11. DSC scans of compound **2a** at several heating and cooling rates. The 1st heat-up was carried out on **2a** crystallized from solution at 10K/min.

	T_c [°C]	$T_{m,1}$ [°C]	$T_{m,2}$ [°C]	ΔH_c [kJmol^{-1}K^{-1}]	$\Delta H_{m,1}$ [kJmol^{-1}K^{-1}]	$\Delta H_{m,2}$ [kJmol^{-1}K^{-1}]	$\Delta H_{m,1} + \Delta H_{m,2}$ [kJmol^{-1}K^{-1}]
1st heat up	-	-	77.49	-	-	132.39	132.39
A	61.94	62.28	71.47	-91.27	22.69	75.93	98.62
B	60.74	63.56	72.05	-92.48	28.61	65.62	94.24
C	60.41	64.25	72.39	-91.74	36.98	56.35	93.33
D	60.30	72.60	64.55	-89.51	49.23	44.94	94.17
E	60.09	64.67	72.69	-90.29	47.59	43.84	91.43

Table 3. Characteristic temperatures and enthalpies for compound **2a**. T_c is the crystallization temperature on cooling, $T_{m,1}$ and $T_{m,2}$ are the melting temperatures of the two crystalline phases. The same indexing holds for the ΔH values. $T_{m,2}$ and $\Delta H_{m,2}$ for the first heat-up are T_m and ΔH_m, respectively, of **2a** crystallized from CH_2Cl_2 solution.

The 1st heat-up scan in Figure 11 shows that compound **2a** crystallizes from solution forming two phases. ΔH_m = 132.39 kJmol^{-1} (Table 3) of the first heat-up is considerably (about 44 kJmol^{-1}K^{-1}) lower than 2(ΔH_m) = 175.95 kJmol^{-1} of the single chain **17b** (Table in Figure 10). Scanning at different heating and cooling rates revealed that the higher temperature phase is favorably formed at lower cooling rates. The sum of the ΔH_m values of the two melting peaks is always equal to the ΔH_m value of the cooling peak (Table 4). At very low cooling rates a third crystalline phase appears. The TGA scan in Figure 12 shows that **2a** is stable up to 200 °C.

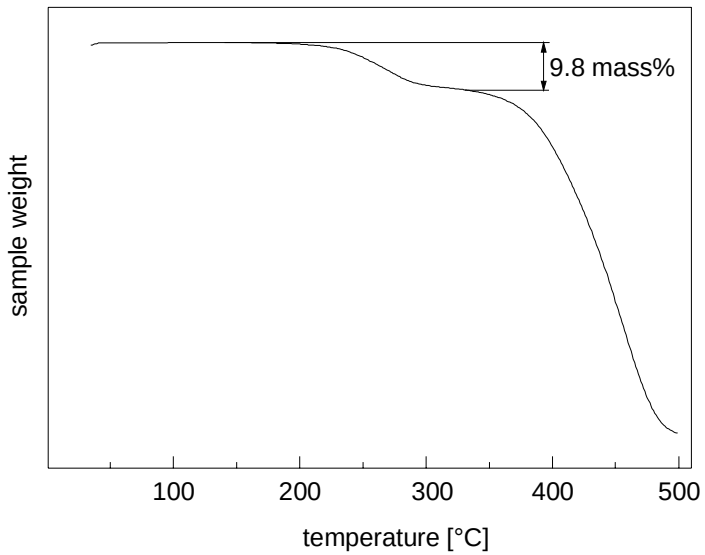

Figure 12. A TGA scan shows that compound **2a** is stable up to 200 °C. The weight loss above 200 °C corresponds to the weight of the THP-group.

The DSC scan of compound **2b** (Figure 13) shows that only one crystalline phase is formed on crystallization from solution as well as from the melt. As compound **2b** differs from compound **2a** only in that it lacks the bulky THPO-group at the 1,3-bis(ethynylene)benzene spacer unit (Figure 8) it is obvious that the THPO-group markedly obstructs the bulk crystallization of the above discussed **2a**.

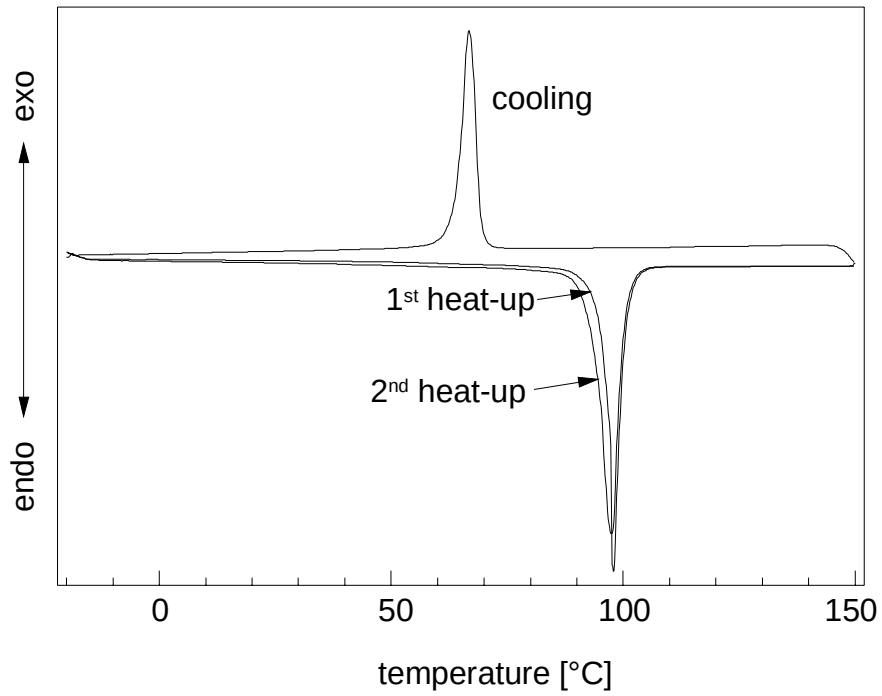

Figure 13. DSC scans of compound **2b** at 10 K/min. The 1st heat-up was carried out on **2b** crystallized from CH_2Cl_2 solution.

	T_m [°C] 1st heat-up	T_c [°C] cooling	T_m [°C] 2nd heat-up	ΔH_m [kJmol^{-1}] 1st heat-up	ΔH_c [kJmol^{-1}] cooling	ΔH_m [kJmol^{-1}] 2nd heat-up
2b	95.60	68.58	95.53	167.62	-153.11	152.56
3	70.43	54.04	58.93	146.14	-101.96	101.03
4	57.81	44.32	50.31	139.88	-104.06	101.32
5	64.28	57.40	61.03	30.44	-91.79	36.72
			68.48(T_c)			-10.80
	77.88		76.61	76.87		55.76
6	90.37	45.02	50.24	252.32	-136.51	100.22
			60.84 (T_c)			-168.44
			90.11			183.60

Table 4. Characteristic temperatures, heat of fusion and heat of crystallization for compounds **2b**, **3**, **4**, **5**, and **6**.

The melting temperatures (Table 4) are highest among all T_m measured in this work supposedly due to strong hydrogen bonding between the molecules in the crystal. The value of ΔH_m = 167.62 kJmol^{-1} (Table 4) of the first heat-up is very close to 2(ΔH_m) = 175.95 kJmol^{-1} of the single chain (**17b**) (Table in Figure 10) meaning that molecules **2b** form rather perfect crystals from solution.

Compound **3** is complementary to **2b** (Figure 8). Its two alkyl chains (**8d**) are hydrophobic whereas the spacer unit contains an OH-group. Figure 13 shows the DSC scans of compound **3** and again only one crystalline phase is formed at the standard cooling rate of 10 K/min. As for **2b**, the value of ΔH_m = 146.14 kJmol^{-1} (Table 4) of the first heat-up is very close to 2(ΔH_m) = 152.16 kJmol^{-1} of the single chain **8d** (Table in Figure 10). This indicates very good crystallinity of molecules **3** crystallized from solution.

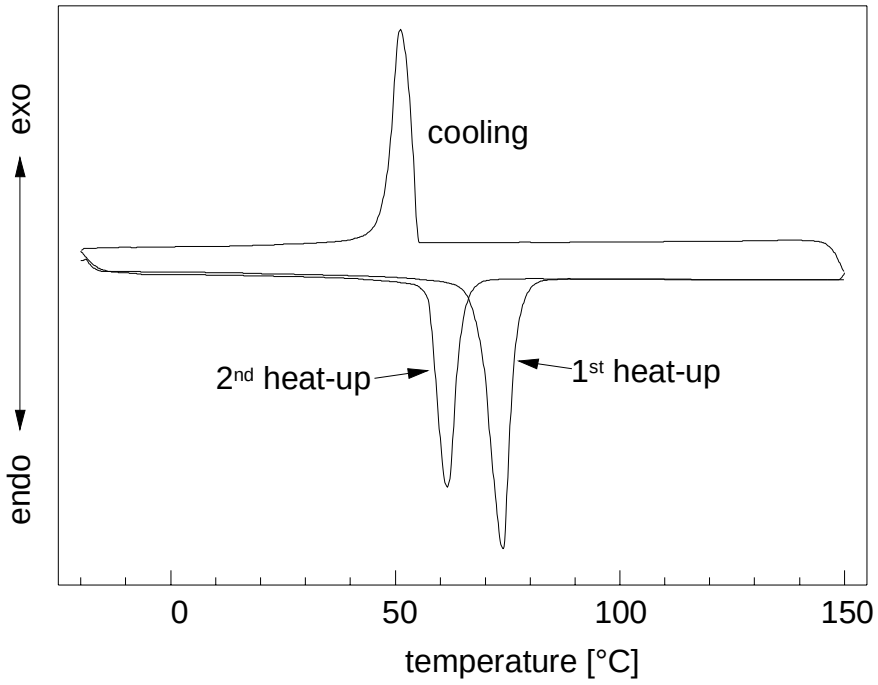

Figure 14. DSC scan of compound **3** at 10 K/min. The 1st heat-up was carried out on **3** crystallized from CH_2Cl_2 solution.

The DSC scans of compound **4** (Figure 15), which has no OH-group (Figure 8), shows a pretty similar behavior to **2b** and **3**. One crystalline phase is formed. The melting point is lower than in the case of **2b** and **3** probably due to the fact that no hydrogen bonding can occur. Again, the value of ΔH_m = 139.88 kJmol^{-1} (Table 4) of the first heat-up is very close to 2(ΔH_m) = 152.16 kJmol^{-1} of the single chain **8d** (Table in Figure 10).

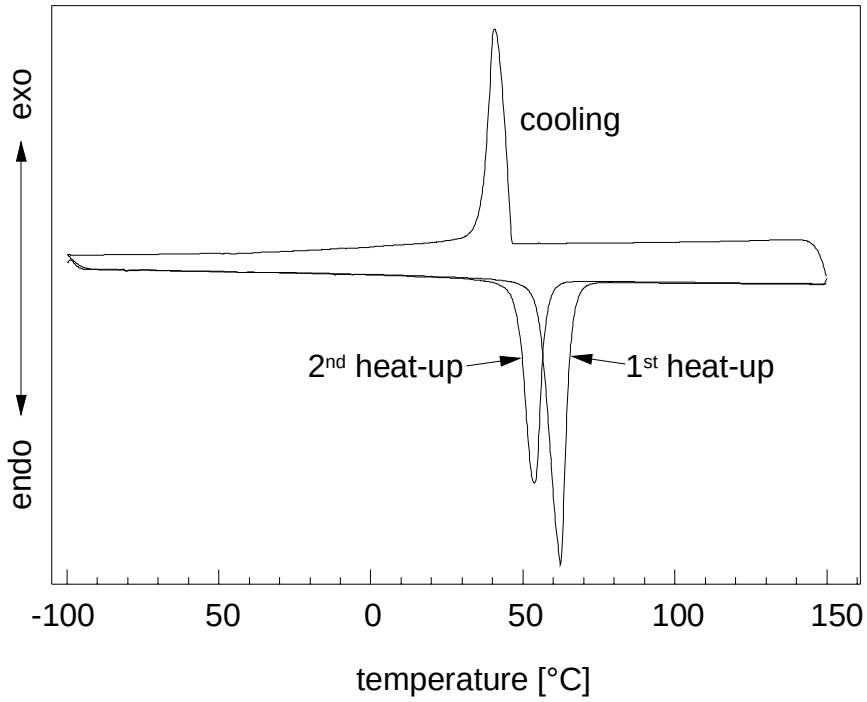

Figure 15. DSC scans of compound **4** at 10 K/min. The 1st heat-up was carried out on **4** crystallized from CH_2Cl_2 solution.

Because **1**-**4** belong to the same compound class, all being centered by the 1,3-bis(ethynylene)benzene unit, their thermal characterization is now briefly summarized. The chain length in **1** is not sufficient to achieve a molecular conformation of **1** that allows close packing of the molecules into a crystal in the time scale of the DSC measurement on cooling from the melt. Compound **2a** readily crystallizes from the melt forming two crystalline phases. The relatively low ΔH_m value in comparison to **2b** indicates that the bulky THPO-group at the spacer unit induces imperfections during bulk crystallization. Compounds **2b**, **3**, and **4** each form one, highly crystalline phase in bulk crystallization.

A somewhat different behavior was expected for compound **5**, an example for a classical two-chain amphiphile. Molecule **5** is similar to molecule **3** but lacks the two triple bonds at the spacer unit. As a consequence, the distance (~5 Å) between the stems of the alkyl chains of **5** is approximately half of the distance between the chain stems in all other molecules studied in this work (Figure 7). The DSC scans in Figure 16 show that there are initially two crystalline phases formed from solution. Although not visible in the cooling peak, the 2nd heat-up shows that those two phases also form on crystallization from the melt. The low temperature phase now appeared slightly stronger. Surprisingly, the sum of both melting enthalpies $\Sigma(\Delta H_m)$ = 107.31 kJmol^{-1} of the first heat-up scan is considerably lower than the value of ΔH_m = 146.14 kJmol^{-1} for compound **3** (Table 4) whose alkyl chains have exactly the same length.

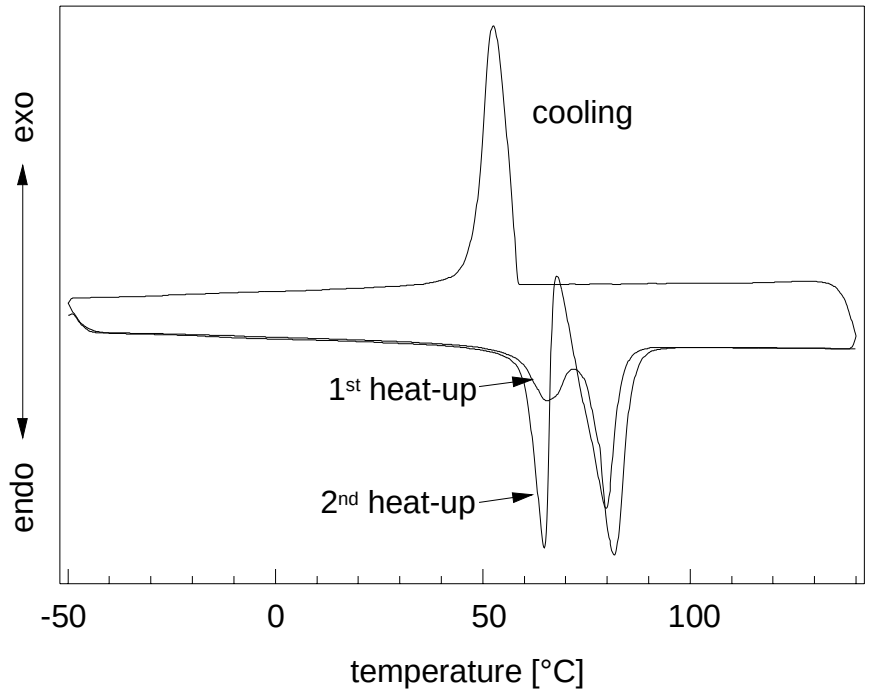

Figure 16. DSC scans of compound **5** at 10 K/min. The 1st heat-up was carried out on **5** crystallized from CH_2Cl_2 solution.

Finally, compound **6** was characterized by DSC. Looking at the molecule in Figure 8 one can imagine several conformations of **6** in a crystalline packing. Consequently, one can expect rather complex crystallization behavior.

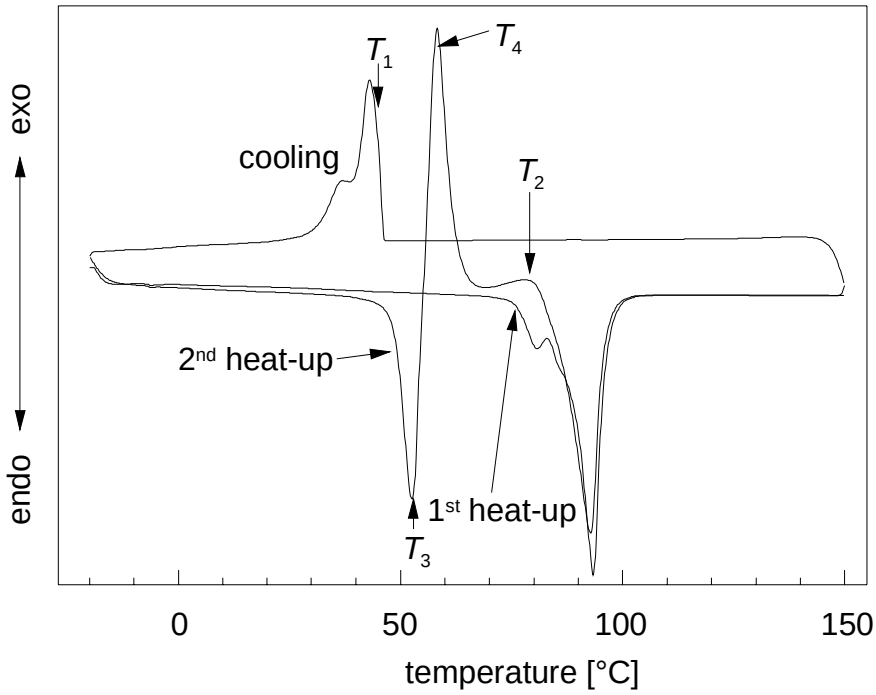

Figure 17. DSC scans of compound **6** at 10 K/min. The 1st heat-up was carried out on **6** crystallized from CH_2Cl_2 solution.

The first heat-up scan corresponds to **6** crystallized from CH_2Cl_2 solution. There is only one major melting peak just above 90 °C with some features prior to melting which are probably caused by the onsetting conformational mobility within the molecules. The ΔH_m value of this peak (ΔH_m = 252.32 kJmol^{-1}) is lower than expected. The expected value of ΔH_m = 311.6 kJmol^{-1} is in this case obtained by multiplying ΔH_m = 4.1 kJmol^{-1} per CH_2-unit of fully extended and 100% crystalline poly(ethylene)[107] with the number of CH_2 units in the shortest chain (nineteen in the middle part) and with the number of chains (four) in the molecule **6**. The fact, that ΔH_m is lower than expected indicates that the chains of **6** are not in their full length ideally packed in the bulk crystal. On cooling of **6** two overlapping crystallization peaks appear. Heating up the melt-crystallized **6** resulted in a sequence of melting-recrystallization-melting typically seen in this form only for flexible, linear macromolecules.[105]

Optical microscopy (not shown) revealed that on cooling at 10 K/min **6** forms a liquid crystalline mosaic texture which solidifies at about 46 °C (T_1 in Figure 17). One

could speculate, that in the melt molecules **6** exist in a fully stretched conformation giving rise to a main chain smectic liquid crystalline arrangement. On the other hand, cooling the melt very slowly just below the melting point (T_2 in Figure 17) resulted in the very slow growth of needle-like crystals. If the solidified, liquid-crystalline state is heated up from room temperature at a rate of 10 K/min one gets a clear melt at about 50 °C (T_3 in Figure 17). Holding the melt at 57 °C (T_4 in Figure 17) results in a rapid growth of spherulites surrounded by liquid crystalline mosaic texture. On further heating the liquid crystalline texture is converted into needle-like crystals. An isotropic melt is obtained just above 90 °C.

2.3. Self-assembled crystalline monolayers

2.3.1. (*Π-A*) isotherms

A first indication of the spreading properties of the seven compounds was obtained from the surface pressure-area (*Π-A*) isotherms, which are consistent with the formation of insoluble films at the water surface (Figure 18). The isotherms of compounds **1**-**5** each display a steep rise in surface pressure at a nominal molecular area of 30-50 Å^2. The nominal molecular area is defined as the Langmuir trough area devided by the number of spread molecules and given in Å^2. As all molecules **1**-**5** have two chains per molecule, this value of the molecular area indicates that in every case the two chains do not lie flat on the water surface and that the chains are parallel to each other. Two all-trans hydrocarbon chains typically require a molecular area of about 40 Å^2. For compound **6** the surface pressure rises steeply reaching an area per molecule of about 80 Å^2, already indicating that the molecules self-assemble by adopting a conformation in which their four chains are oriented almost perpendicular to the water surface.

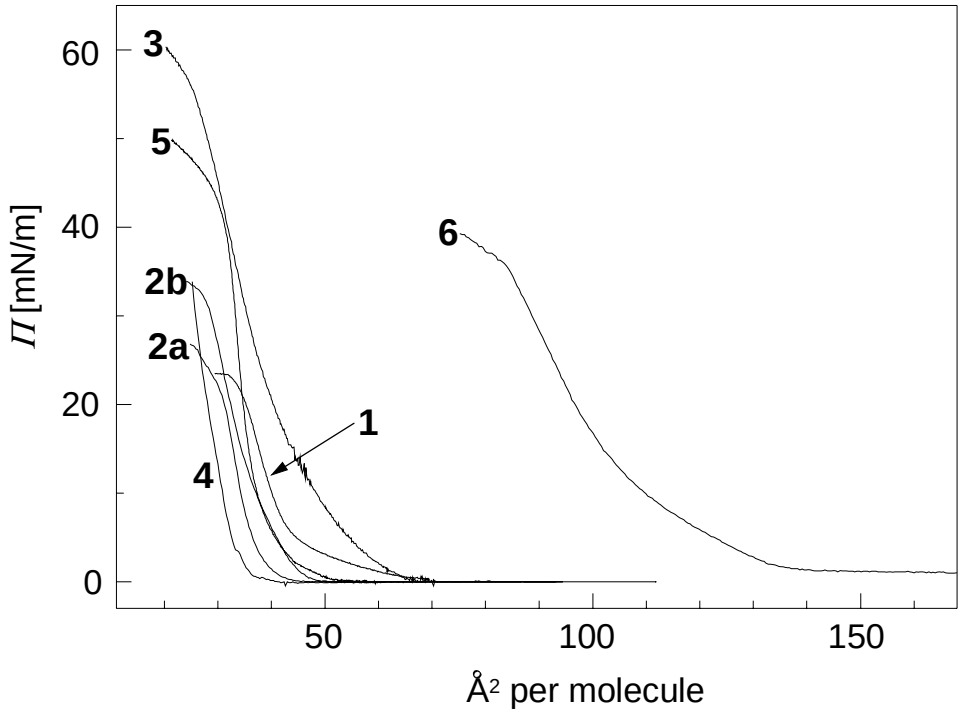

Figure 18. *Π-A* isotherms of compounds **1**-**6** at the air-water interface

The following structural charaterizations of films have been performed by GIXD in situ at the air-water interface at various points along the (Π-A) isotherms always starting from low nominal molecular areas.

2.3.2. Structural characterization of the self-assembled monolayers by GIXD

Compound **1**: For the film obtained on spreading a solution of **1** in dichloromethane for a molecular area of 70 Å^2 no diffraction signal was observed. This means that there is no crystalline self-assembly of **1** under these conditions. The film was then

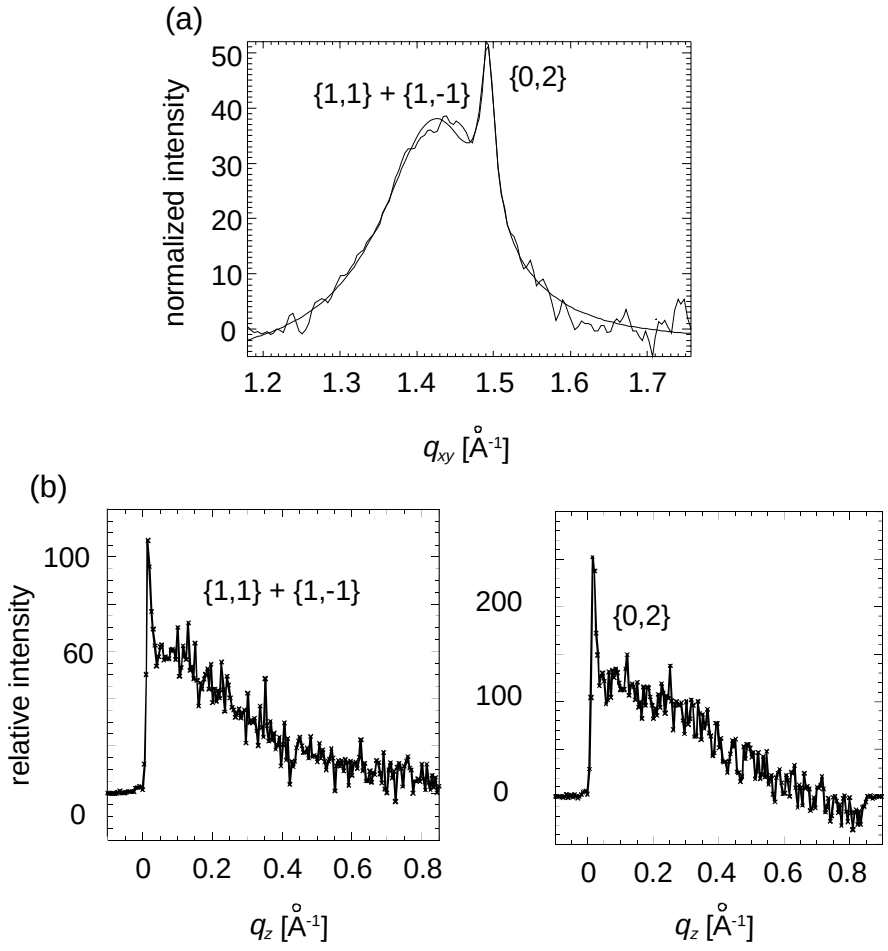

Figure 19. (a): Bragg peaks measured for the monolayer of **1** at 41 Å^2/molecule. (b): The two separate Bragg rods. The high noise level does not allow a Bragg rod fitting to obtain a representative model of **1** in the monolayer. The maximum of the {11} + {1-1} peak is at about 0.1 - 0.2 Å^{-1}.

compressed to 41 Å^2/molecule (21 mN/m) which corresponds to the cross-section of two hydrocarbon chains and, as the molecule **1** has two chains, to complete surface coverage. The weak diffraction signal measured from this film is shown in Figure 19a. This GIXD pattern displays two weak diffraction peaks at q_{xy} values of 1.42 Å^{-1} and 1.49 Å^{-1}. The peaks were assigned h_s and k_s subcell Miller indices {11} + {1-1} and {02} respectively and resulted in the dimensions of the rectangular subcell a_s = 5.2 Å and b_s = 8.4 Å. The tilt of the molecules with respect to the surface normal can only be estimated because the noise level in the Bragg signals is rather high. Assuming, that the $q_{z,max}$-position of the {11} + {1-1} peak lies in the range of 0.1 to 0.2 Å^{-1} gives $t \approx 10°$.[108] The thickness D of the crystalline part of the film is estimated from the full width at half maximum of the Bragg rod ($FWHM(q_z)$) as $D \approx 10$ Å. This value of D would, if the molecular tilt is taken into consideration, correspond to a monolayer of **1**. The dimensions of the projected subcell, i.e. the subcell viewed along the chain axis, are $a_p = a_s \cos t = 5.1$ Å and $b_p = b_s$, knowing that the molecules are tilted along the a direction. The $FWHM(q_{xy})$ allows an estimation of the crystalline coherence lengths L (extent of lateral order) within the monolayer. For the {11} and {02} direction one gets $L_{11} \approx 35$ Å and $L_{02} \approx 350$ Å. The length of the b_s axis, 8.4 Å, approximately corresponds to the intramolecular distance between two all-trans chains separated by the 1,3-bis(ethynylene)benzene unit.

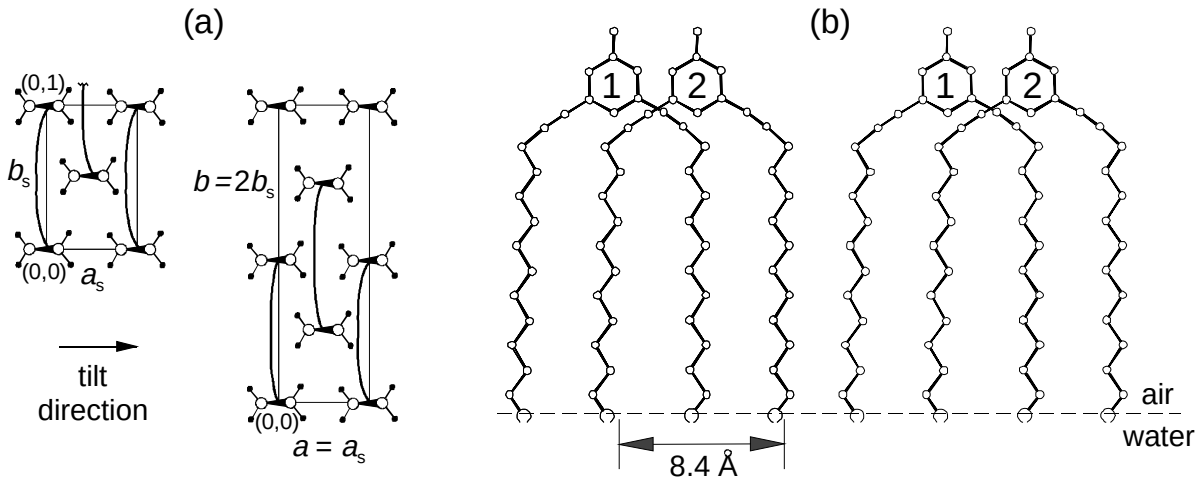

Figure 20. (a): The most plausible way to arrange molecule **1** in the subcell is to place its two chains at the lattice points (0,0) and (0,1). The unit cell contains two molecules and the molecules are arranged in molecular ribbons along the b axis and tilted along the a direction (as follows from the position of the $q_{z,max}$). (b): Scetch of the side view of this packing arrangement. The molecular ribbon 1 is adjacent to ribbon 2.

Thus a molecule must be arranged in the unit cell with the two chains aligned parallel to the b_s axis at (x,y) positions (0,0) and (0,1) and tilted along the a_s axis (Figure 20a, left). Furthermore, the b_s axis belongs to a subcell and must be doubled to give the true unit cell repeat as $b = 2b_s = 16.8$ Å (Figure 20a, right). Along the a_s axis the unit cell repeat remains unchanged, $a = a_s$. For this *ab* unit cell, which contains two molecules, the Miller indices of the {0,2} and {1,1} + {1,-1} Bragg peaks must be re-assigned to {0,4} and {1,2} + {1,-2} respectively. Consequently, molecules in adjacent ribbons are placed with their chains at positions (0,0.5) and (0.25,±0.75) as shown in Figure 20a, right. This arrangement yields intermolecular distances with favorable van-der-Waals contacts and close packing of molecules **1**.

The molecular packing within the monolayer cannot be represented by a molecular model, as a Bragg rod fitting is not possible due to the poor quality of the measured data (Figure 19b). One can suppose a structure for the monolayer of **1** following the conclusions shown in Figure 20a which leads to a molecular arrangement depicted schematically in Figure 20b. At this point it is important to note that Figure 20b is a schematic drawing, not a molecular model fitted to the measured $I(q_z)$ profiles. In order to prove this supposed structure, better quality GIXD data are required to obtain sensible molecular models describing the packing arrangements of such folded, or U-shaped, molecules within the monolayer. For this purpose compounds **2a** and **2b** were synthesized in which the length of the chains at the 1,3-bis(ethynylene)benzene unit was doubled to increase the van-der-Waals interaction between the chains. The poor crystallinity of the monolayer may also be due to the bulky CH_3-group at the 1,3-bis(ethynylene)benzene unit. This effect was studied by attaching an even bulkier substituent to the spacer unit in the case of **2a**, whereas compound **2b** does not have any bulky group at the spacer unit.

Compound **2a**: In contrast to the monolayer of **1**, that diffracted only in the compressed state, the monolayer of **2a** on water yielded diffraction peaks already in the uncompressed state at a molecular area of 50 $Å^2$ and no observed surface pressure. This means that the crystalline arrangement of molecules **2a** at the air-water interface is a result of a spontaneous self-assembly process.

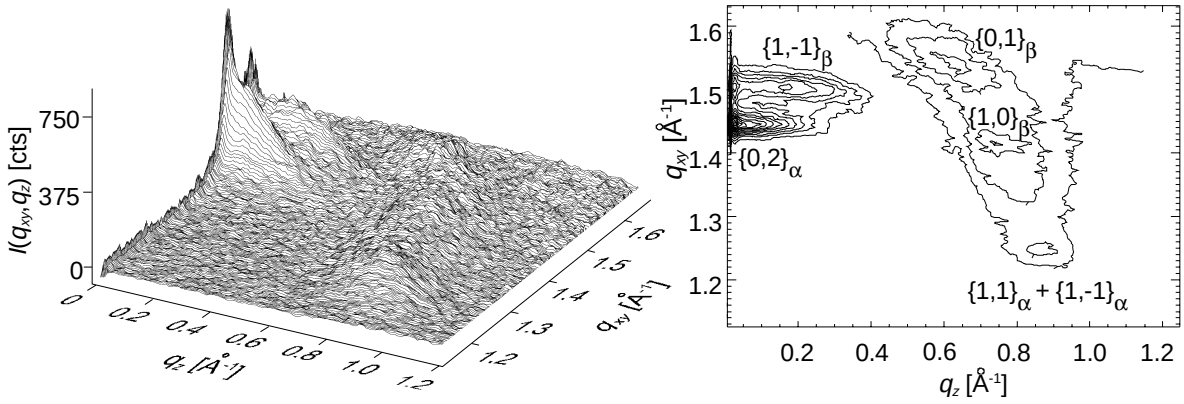

Figure 21. GIXD pattern $I(q_{xy}, q_z)$ measured for the monolayer of **2a** as surface plot (left) and contour plot (right, contours are lines of equal diffracted intensity) at a nominal molecular area of 50 Å^2.

Five peaks were discerned in the GIXD pattern, which is shown in Figure 21 as two-dimensional surface and contour plots of the scattered intensity $I(q_{xz}, q_z)$ as a function of the horizontal q_{xz} and the vertical q_z components of the scattering vector $\boldsymbol{q}$. These peaks were rationalized in terms of two crystalline phases, α and β (5.1., Table 1). The α-phase is described by a rectangular unit cell of dimensions a_s = 6.2 Å, b_s = 8.7 Å and area = $a_s b_s$ = 54 Å^2. The molecular tilt t = 41° is along the a direction. The projected cell dimension a_p is given by $a_p = a_s \cos t$ = 4.7 Å. The subcell of the α-phase is centered since the {0,1} and {1,0} reflections were not observed. Again, the value of 8.7 Å corresponds to the intramolecular distance between the all-trans chains linked by the 1,3-bis(ethynylene)benzene unit and therefore the true length of the cell b axis is $b = 2b_s$ = 17.4 Å fixing the structure along the b axis in the way depicted in Figure 20a for molecules **1**. Along the a_s axis the unit cell repeat remains unchanged, $a = a_s$. For this ab unit cell, which contains two molecules, the Miller indices of the {0,2} and {1,1} + {1,-1} Bragg peaks must be re-assigned to {0,4} and {1,2} + {1,-2}, respectively. Consequently, molecules in adjacent ribbons are placed with their chains at (x,y) positions (0,0 0,0.5) and (0.5,0.25 0.5,0.75) as shown in Figure 20a for molecules **1**. This arrangement yields intermolecular distances with favorable van-der-Waals contacts. Structural considerations allow positional disorder of adjacent ribbons which may be offset randomly along the b direction by ±0.5b. In this way, equidistant separation between chains along directions 0.5(a±0.5b) can be

obtained by virtue of symmetry, also resulting directly in the appearance of a rectangular unit cell.

The remaining three Bragg signals belong to the β-phase and describe an oblique unit cell (cf. Figure 4d, chapter 1.2.). The peaks were assigned Miller indices (5.1., Table 1) and yield the subcell dimensions a_s = 5.1 Å, b_s = 4.7 Å and γ_s = 119°. This cell has a repeat area of $a_s b_s \sin\gamma_s$ = 20.9 Å^2. As this area corresponds to the area occupied by a single alkyl chain the cell cannot contain a repeat of molecule **2a**. In order to be able to compare this cell to the unit cell of the α-phase, the subcell of the β-phase was converted into a pseudo-rectangular cell of dimensions $a = |\boldsymbol{a}_s + \boldsymbol{b}_s|$, $b = 2|\boldsymbol{a}_s - \boldsymbol{b}_s|$, γ = 95.5° and area = 82.3 Å^2. A detailed description of this conversion is given in 5.3. for the oblique phase in the monolayer of **2b**. The value of *b* is about twice the intramolecular distance between the two chains separated by the 1,3-bis(ethynylene)benzene unit. The unit cell contains two molecules related by translation along the unit cell diagonal at the positions *x*, *y*, *z* and ½ + *x*, ¼ + *y*, *z*. This agrees with our previous predictions for the unit cell of **1** (Figure 20a). The molecules are tilted in a direction approximately corresponding to the *a* direction by *t* = 30° from the surface normal. The exact tilt direction is calculated as explained in 5.3. and is about 5° off the unit cell *a* direction. The crystalline film thickness *D* = 23 Å is calculated from the *FWHM*(q_z). It corresponds to a monolayer of **2a**. Assuming the packing arrangement of the α-phase of **2a** to be the same as for molecules **1** (Figure 20a), calculations using in Cerius^2[109] yielded relatively strong {0,1} and {1,1}+{1,-1} Bragg rods, the latter being incompatible with observation.[110] These calculated intensities can arise only from the contribution of the 1,3-bis(ethynylene)benzene unit in an ordered arrangement.

X-ray structure factor calculations[49] using atomic coordinate models created in Cerius^2 with the help of the above derived unit cell parameters were performed for the two crystalline phases α and β. It was assumed that the OH-groups are in contact with the water surface.[111]

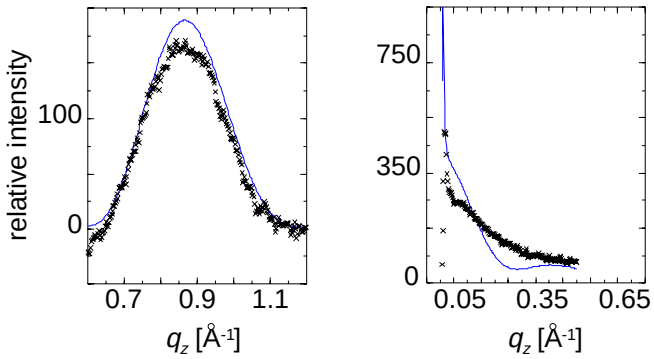

Figure 22a. Measured (crosses) and fitted (full lines) Bragg rod intensity profiles of the crystalline α-phase in the self-assembled monolayer of molecules **2a** at a nominal molecular area of 50 Å^2.

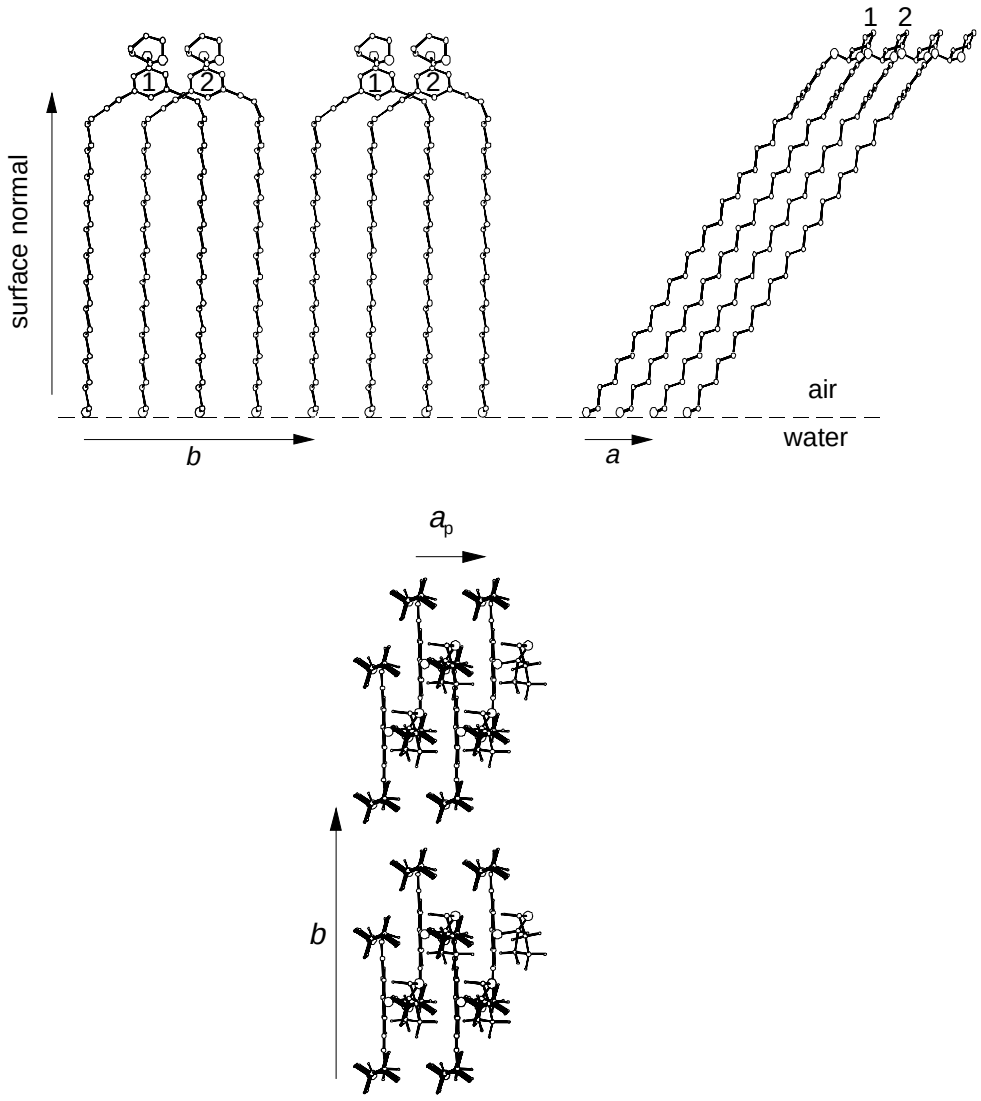

Figure 22b. Atomic coordinate molecular model of molecules **2a** in the crystalline α-phase in the view along: (top, left) the *a* axis, (top, right) the *b* axis and (bottom) the chain axis.

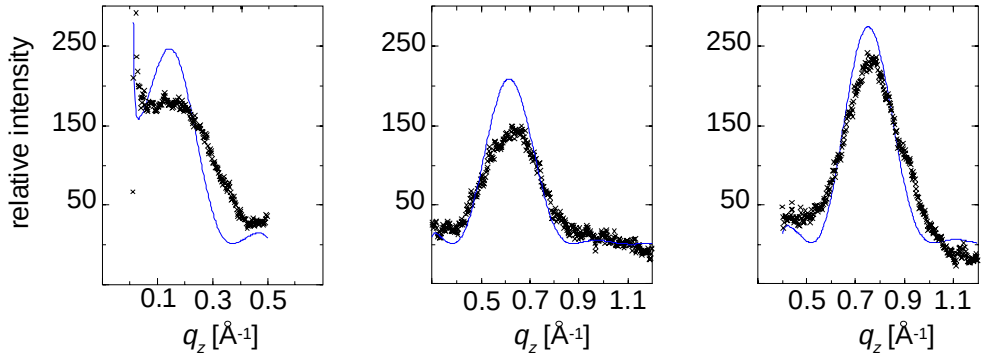

Figure 23a. Measured (crosses) and fitted (full lines) Bragg rod intensity profiles of the crystalline β-phase in the self-assembled monolayer of molecules **2a** at a nominal molecular area of 50 Å^2.

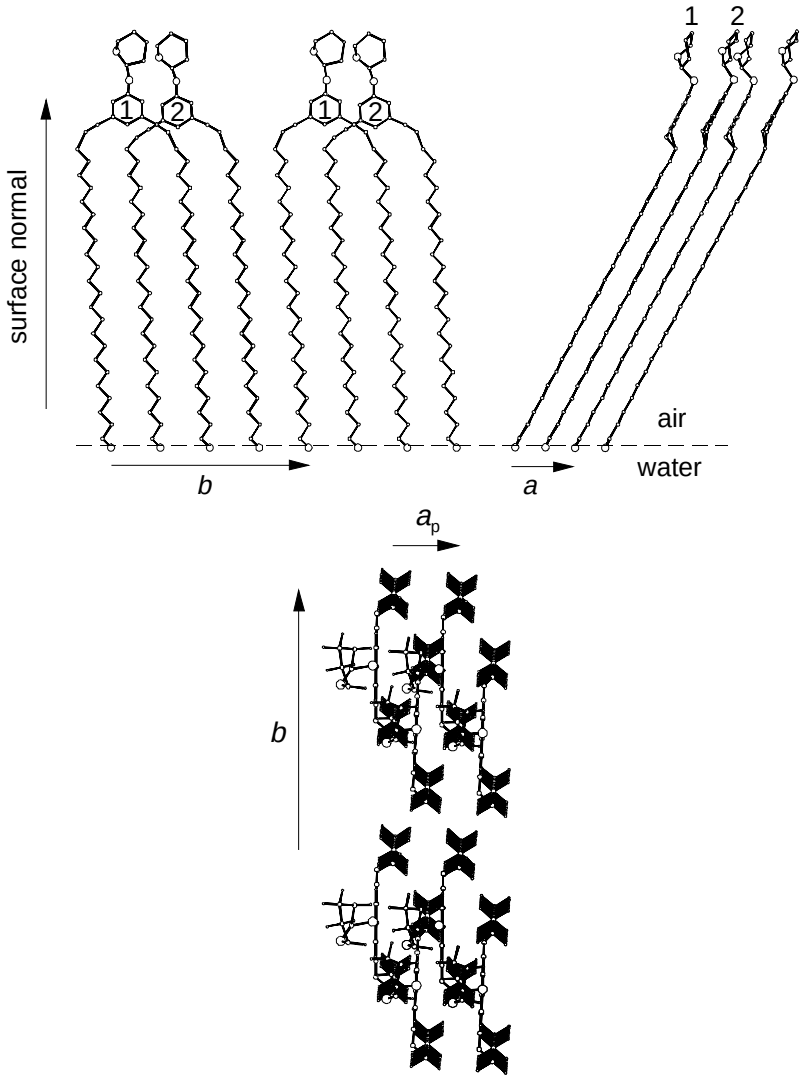

Figure 23b. Atomic coordinate molecular model of molecules **2a** in the crystalline β-phase in the view along: (top, left) the *a* axis, (top, right) the *b* axis and (bottom) the chain axis.

The calculated Bragg rod intensity profiles (full lines in Figure 22a and Figure 23a) are in reasonable agreement with the measured profiles and consistent with the thickness of a monolayer of **2a**. The corresponding 2-D packing arrangements of **2a** in the dimorphic crystalline monolayer is shown in the Figures 22b and 23b for the α and β phase respectively. One can clearly see the ribbon (or layer) structure of the crystalline arrangement. For clarity, only the ordered arrangement in the *ab* unit cell is presented. Note that the calculated Bragg rods of the {0,4} and {1,2}+{1,-2} reflections shown in Figure 22a and 23a would be the same for the ordered and disordered arrangements discussed above. The basis of the atomic coordinate models were $(CH_2)_{23}$-chains which were minimized in their energy in Cerius[2]. These chains were then arranged in the unit cell according to the conclusions summarized in Figure 20a. The symmetry operation relating the two molecules in the unit cell to each other (either glide symmetry or pure translation) was chosen on the basis of the best fit of the calculated data to the measured data. An insight into this procedure of achieving the best fit is given for molecule **6** in 5.4.2. The procedure involves the optimization of the three Eularian angles of the system. Once the intensity profile of the chain model fitted the measured data well the 1,3-bis(ethynylene)benzene unit was added to the model. In the case of the two crystalline phases in the monolayer of **2a** the final fits displayed in Figures 22a and 23a are calculated for the complete molecule **2a**. However, the fits obtained for the chains without the 1,3-bis(ethynylene)benzene unit were indistinguishable from the fits that included the 1,3-bis(ethynylene)benzene unit. This means that the spacer units do not have a marked contribution to the measured $I(q_z)$ profiles. The origin of the measured $I(q_z)$ profiles is the scattering at the periodic array of the alkyl chains. Although their arrangement limits the number of possible orientations of the spacer groups (the one shown in Figures 22b and 23b being the most likely) the question of their absolute orientation in the packing arrangement cannot be answered on the grounds of the GIXD data. In view of the equality of intermolecular and intramolecular distances in this packing arrangement one may again, as for molecules **1**, envisage crystalline disorder since, in going from one molecular ribbon to the next, each ribbon can adopt an alternative position being shifted by a value of $\pm\frac{1}{4}b$.

Upon compression of the monolayer of molecules **2a** to a molecular area of 23 $Å^2$ the dimorphic, self-assembled system underwent a transition to a packing

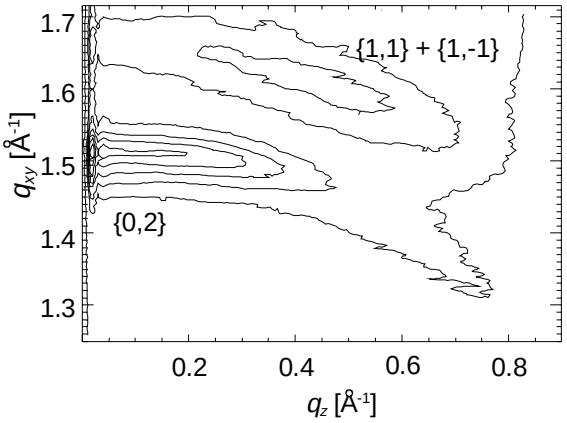

Figure 24. Contour plot of the diffracted intensity $I(q_{xy}, q_z)$ measured for the monolayer of **2a** at a nominal molecular area of 23 Å^2.

arrangement which contains a single crystalline phase. The five Bragg signals coalesced into two signals (Figure 24). These two signals describe a rectangular unit cell of dimensions a = 4.4 Å, b = 2(8.31 Å) and area = 2(36.6 Å^2) which contains two molecules. The molecular tilt is t = 16° from the surface normal in the a direction. The two Bragg peaks are skewed along Scherrer lines $q_{total} = (q_{xy}^2 + q_z^2)^{1/2}$ = constant indicating that the monolayer is bent due to the severe compression (23 Å^2 is about half of the area required for complete surface coverage). A shape analysis[112] of the contours of scattered intensity, $I(q_{xy}, q_z)$, yields a measure of the monolayer bending with an angular distribution of ~18° between the monolayer and the plane of the water surface. The average crystalline film thickness is 30 Å, which corresponds to a monolayer of **2a**, and the crystalline coherence lengths are in the range of 100 to 150 Å.

Compound **2b**: The effect of the bulky head group (the THPO-group) at the spacer unit of **2a** was studied by investigating the self-assembly behavior of molecule **2a**. Molecule **2b** is equivalent to the molecule **2a**, but lacks the bulky group OTHP at the spacer unit (Figure 8). The GIXD pattern measured for **2b** spread on water at a nominal molecular area of 100 Å^2 which corresponds to 40% surface coverage (Figure 25) is very similar to the pattern observed for molecule **2a** (Figure 21). In agreement with the results for **2a** one finds the same dimorphism, i.e. a coexistence of a rectangular (α-phase) and an oblique (β-phase) two-dimensional subcell (5.1., Table 2) although the β-phase is less oblique than in the monolayer of **2a**.

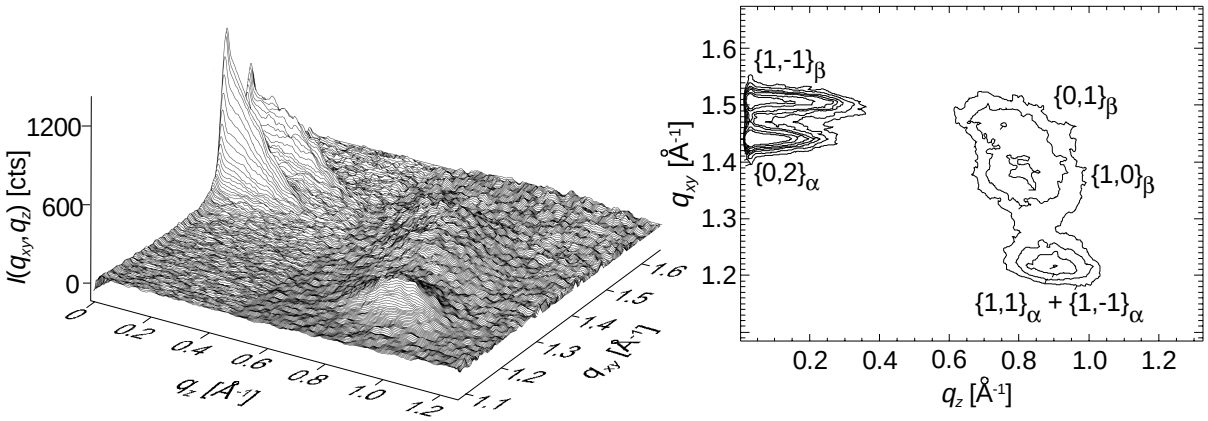

Figure 25. GIXD pattern $I(q_{xy}, q_z)$ measured for the monolayer of **2b** as surface plot (left) and contour plot (right, contours are lines of equal diffracted intensity) at a nominal molecular area of 100 Å^2.

The subcell dimensions and the molecular chain tilt of the two crystalline phases of **2b** are very similar to the corresponding phases found for molecule **2a** as are, by consequence, their two-dimensionally crystalline packing arrangements. These results demonstrate: (a) the negligible effect of the bulky THPO-group at the spacer unit on the self-assembly of inverted U-shape molecules at the air-water interface and (b) the reproducibility of the self-assembly of this general type of molecule. Looking back at the results obtained in chapter 2.2. it is interesting to note that the THPO-group at the spacer unit did have a marked influence on the bulk crystallization of **2a**.

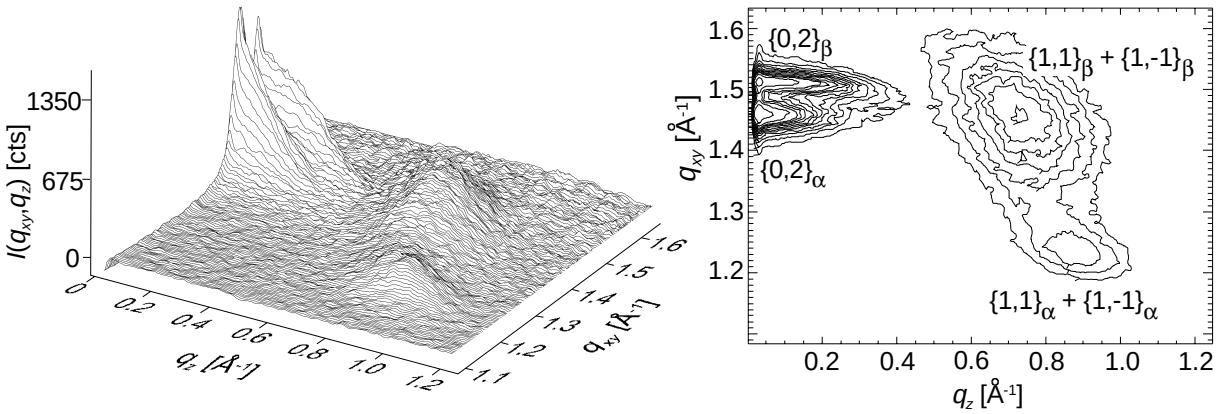

Figure 26. GIXD pattern $I(q_{xy}, q_z)$ measured for the monolayer of **2b** as surface plot (left) and contour plot (right, contours are lines of equal diffracted intensity) at a nominal molecular area of 50 Å^2.

Compression of the monolayer of **2b** leads to a phase transition: The oblique β-phase undergoes a transition to a rectangular phase of very similar dimensions (Figure 26). The monolayer remains dimorphic with both the α and the β phase being rectangular. The α-phase remains unchanged. The two phases would, most likely, coalesce into one phase upon further compression, as observed for **2a**. The observation of these phase transitions allows an interesting conclusion about the packing preferences of molecules **2a** and **2b**: In both cases the self-assembled oblique phase has a higher packing density (deduced from the area per chain in the unit cell in 5.1., Tables 1 and 2) than the rectangular phase. The rectangular phase, on the other hand, is the phase that is stable in the compressed monolayer. This can be interpreted in the following way: The oblique β-phase is preferred in terms of packing density and occurs naturally during self-assembly in 2-D, and supposedly, also in 3-D crystallization. The less dense packing mode, the rectangular α-phase, can be more appropriately described as a mesophase.[113,114]

Compound **3**: The influence of the position and number of the hydrophilic OH-groups was investigated by studying the monolayer of compound **3**. **3** is complementary to **2b**, since its 1,3-bis(ethynylene)benzene unit is hydrophilic, whereas the chain ends are hydrophobic (Figure 8). The GIXD pattern is presented in Figure 27 as two-dimensional surface and contour plots of the scattered intensity $I(q_{xz}, q_z)$ as a function of the horizontal q_{xz} and the vertical q_z components of the scattering vector.

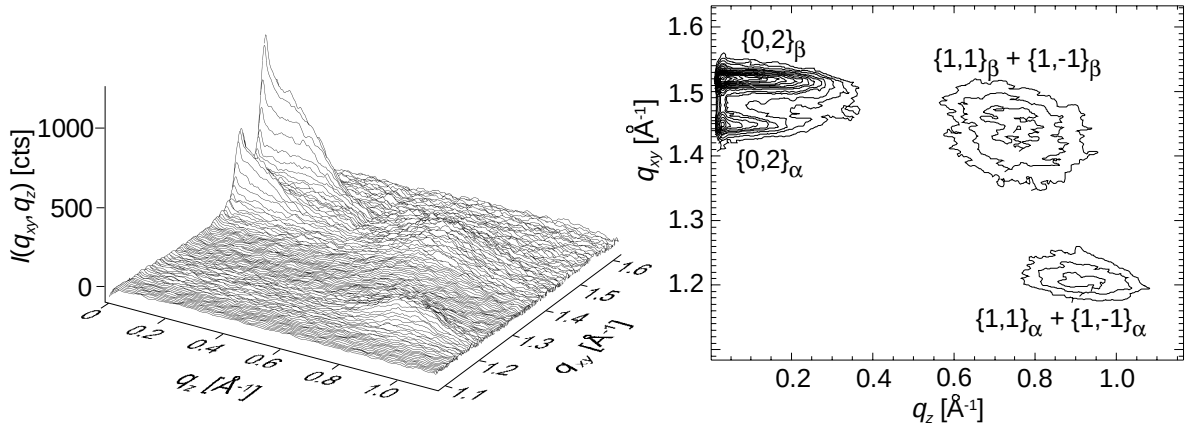

Figure 27. GIXD pattern $I(q_{xy}, q_z)$ measured for the monolayer of **3** as surface plot (left) and contour plot (right, contours are lines of equal diffracted intensity) at a nominal molecular area of 100 Å^2.

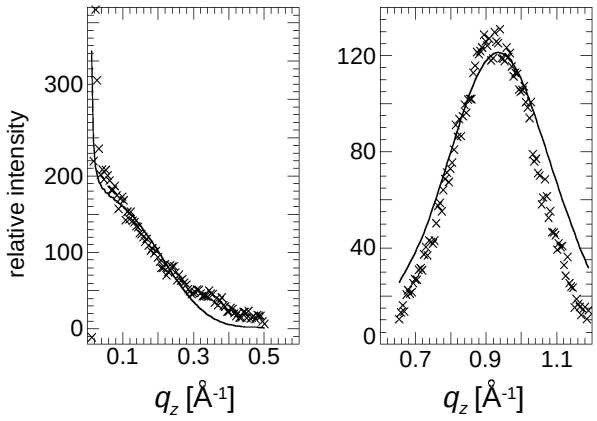

Figure 28a. Measured (crosses) and fitted (full lines) Bragg rod intensity profiles of the crystalline α-phase in the self-assembled monolayer of molecules **3** at a nominal molecular area of 100 Å^2.

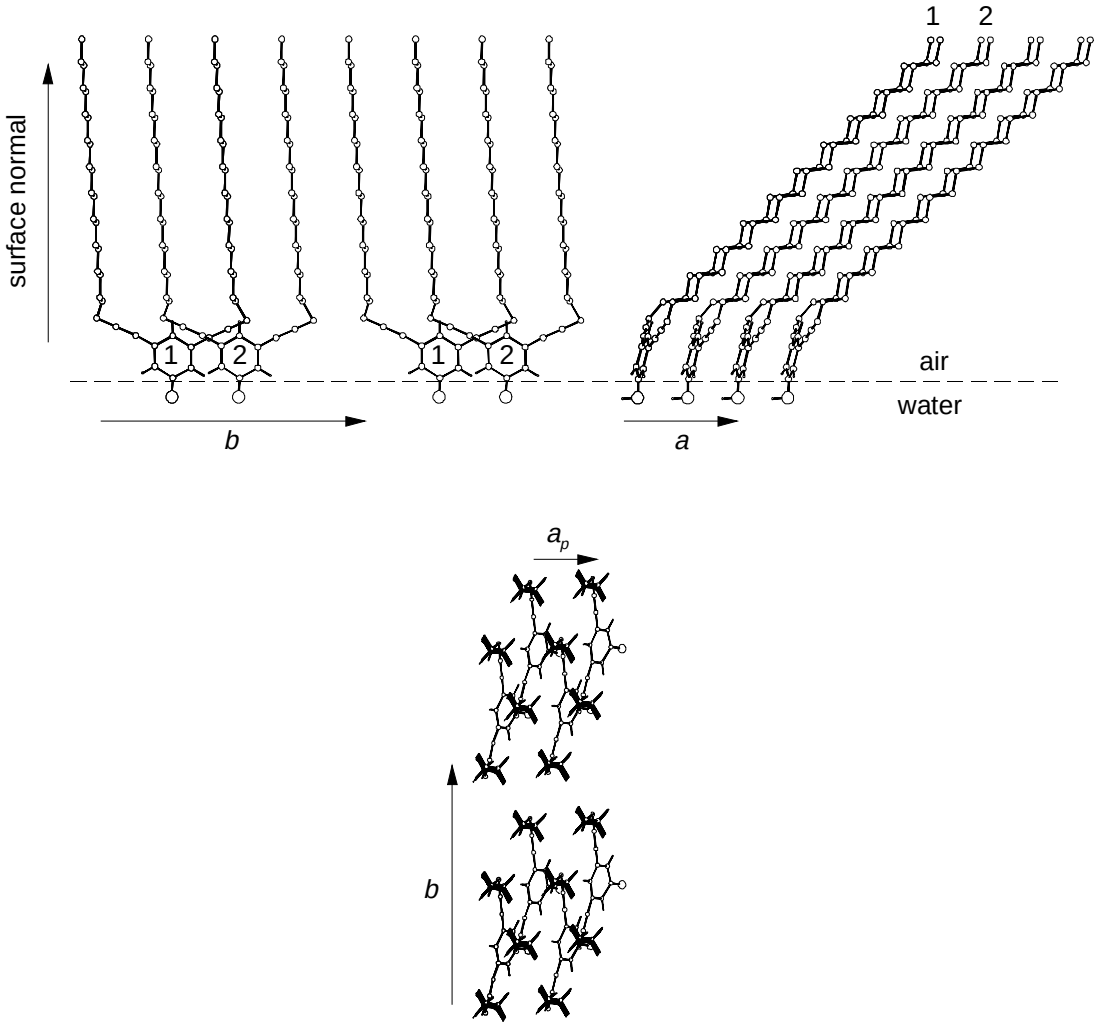

Figure 28b. Atomic coordinate molecular model of molecules **3** in the self-assembled crystalline α-phase viewed along: (top, left) the *a* axis, (top, right) the *b* axis and (bottom) the chain axis.

A crystalline monolayer is formed already at a nominal molecular area of 100 Å^2, which corresponds to a surface coverage of 40%. Figure 27 displays four Bragg peaks which are interpreted in terms of two crystalline phases, α and β. The diffraction peaks are assigned {*h*,*k*} Miller indices (5.1., Table 3) yielding two rectangular subcells which, according to their area, each contain two alkyl chains. The main difference between the two crystalline phases α and β is in their molecular tilt angle from the surface normal, of 43° and 31° respectively, in the direction of the a_s axis, as determined by the q_z-maxima of the Bragg rod intensity profiles. The length of the b_s axis, 8.7 Å for the α-phase, corresponds approximately to the distance between the ends of the two triple bonds in the 1,3-bis(ethynylene)benzene unit (Scheme 1), which separates the two chains of the molecule. X-ray structure factor calculations were again performed using an atomic coordinate molecular model constructed with the Cerius^2 computer program. As the crystalline phases are both rectangular and differ only in their molecular tilt angle, an atomic coordinate model was created only for the crystalline α-phase. The best fit between the measured and calculated Bragg rod intensity profiles (Figure 28a) was obtained for molecules tilted by 45° along the *a* direction in the packing arrangement shown in Figure 28b. As previously observed for **2a**, including the spacer unit (Figure 7) into the atomic coordinate model had no visible effect on the shapes of the Bragg rod profiles. Again it is assumed, that the absolute orientation of the molecule is fixed by the affinity of the hydrophilic OH-groups to the water surface.

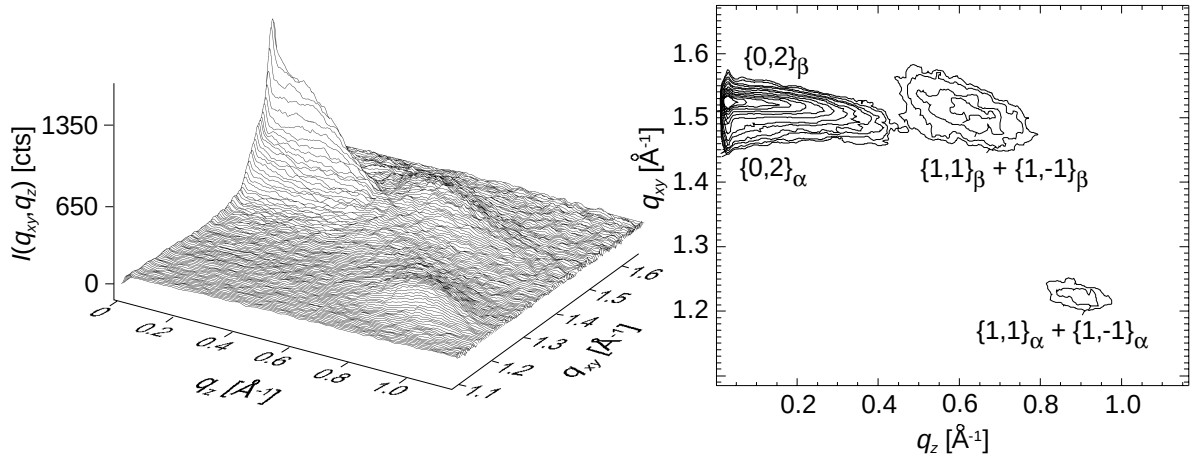

Figure 29. GIXD pattern $I(q_{xy}, q_z)$ measured for the monolayer of **3** as surface plot (left) and contour plot (right, contours are lines of equal diffracted intensity) at a nominal molecular area of 50 Å^2.

The GIXD pattern obtained from the monolayer compressed to a nominal molecular area of 50 Å^2 (Figure 29) shows that the {0,2} Bragg peaks of the α and β crystalline phases coalesce, yet the system remains dimorphic retaining essentially the same packing arrangements.

Compound **4**: The question arose whether a molecule centered by the 1,3-bis(ethynylene)benzene unit, such as molecules **1**-**3**, but which lacks hydrophilic groups, would still self-assemble into crystalline monolayers at the air-water interface. Indeed, such molecules **4** self-assembled into a crystalline structure at low surface coverage (70 Å^2 per molecule i.e. 55% coverage) at the air-water interface, according to the GIXD pattern (Figure 30). Only one crystalline phase is formed. The derived subcell dimensions, a_s = 5.01 Å, b_s = 7.57 Å, γ= 90 °, are indicative of a herring-bone packing of vertically aligned alkyl chains.[115] The crystalline film thickness, determined from the *FWHM*(q_z) of the Bragg rod intensity profiles, is about 29 Å indicative of a monolayer of folded molecules. One may construct the two-dimensional crystalline packing of molecules **4** in three possible ways shown schematically in Figure 31a-c. These suggested packings are based on the assumption that the length of the b_s axis is too short to be bridged by the 1,3-bis(ethynylene)benzene unit. The two chains of one molecule are placed at the lattice points (0,0) and (1,1) separated by 9.1 Å, a distance corresponding to the span of the 1,3-bis(ethynylene)benzene unit (Figure 31a).

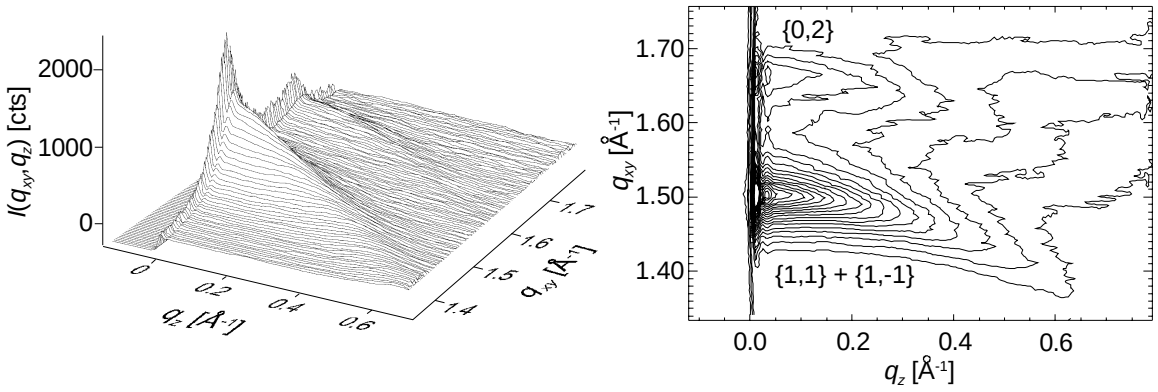

Figure 30. GIXD pattern $I(q_{xy}, q_z)$ measured for the monolayer of **4** as surface plot (left) and contour plot (right, contours are lines of equal diffracted intensity) at a nominal molecular area of 70 Å^2.

This packing arrangement would, in all likelihood, lead to spatial hindrance between the rigid spacer unit and chains of adjacent molecules. Such poor contacts may be circumvented in the arrangement shown in Figure 31b where the two chains of a molecule are placed at positions (0,0) and (1.5,0.5). The intramolecular chain-chain distance is 8.4 Å, comparable to the intramolecular chain-chain distance found in the crystalline monolayers of **1**-**3**. In principle, one may consider the formation of an interdigitated arrangement (Figure 31c) in order to avoid the poor contacts of Figure 31a, but packing is less probable since it would embody a rougher film-water interface.

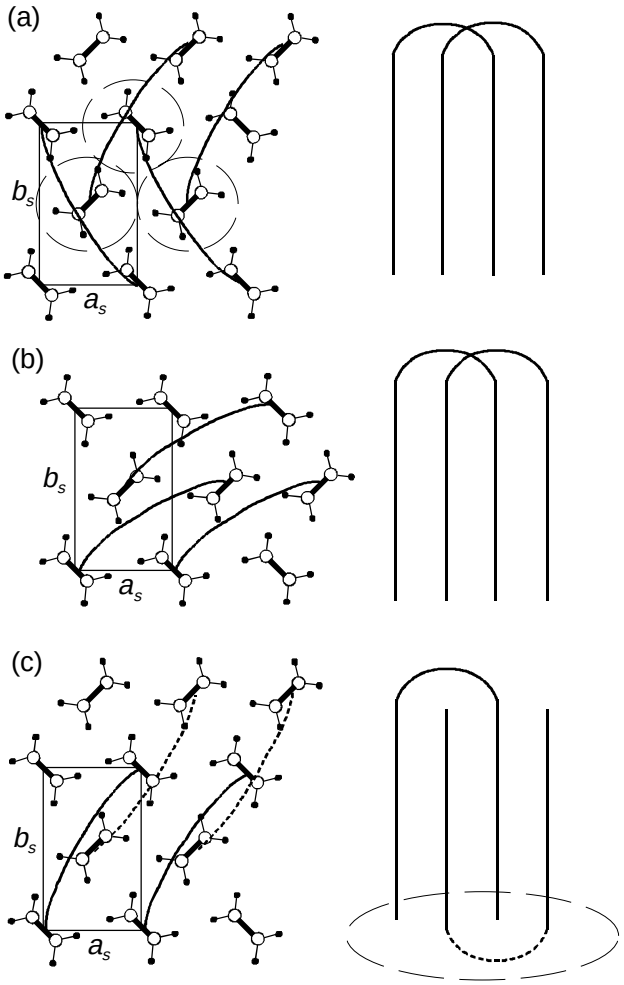

Figure 31. The three possible ways to arrange molecules **4** in the measured unit cell. Packing (b) seems to be the most sensible. The regions of unfavorable spatial hinderances in (a) are highlighted by dashed circles. The dashed line in (c) markes the rough monolayer-water interface, that is energetically unfavorable.

Specular X-ray reflectivity measurements of the film at the air-water interface provided additional information on the average film thickness. The calculated reflectivity curve in Figure 32 is based on a two-box model, the first box containing the alkyl chains and the second the spacer units. The parameters are shown in 5.2. In the fitting procedure, the number of electrons in each box, calculated from the molecular structure of **4**, the area occupied by the molecule, determined from the GIXD data, and the surface coverage of the monolayer, calculated from the number of molecules spread on the water surface, were kept fixed (5.2.). The length of the two boxes and the surface roughness were refined to

the values given in Table 3 yielding an average thickness of the film of about 32 Å, which is close to the thickness of the crystalline part of the monolayer determined by GIXD. On the grounds of all the above results one can dismiss any arrangement in which one of the chains of **4** is closely packed normal to the water surface and the other is disordered, with the molecule unfolded.

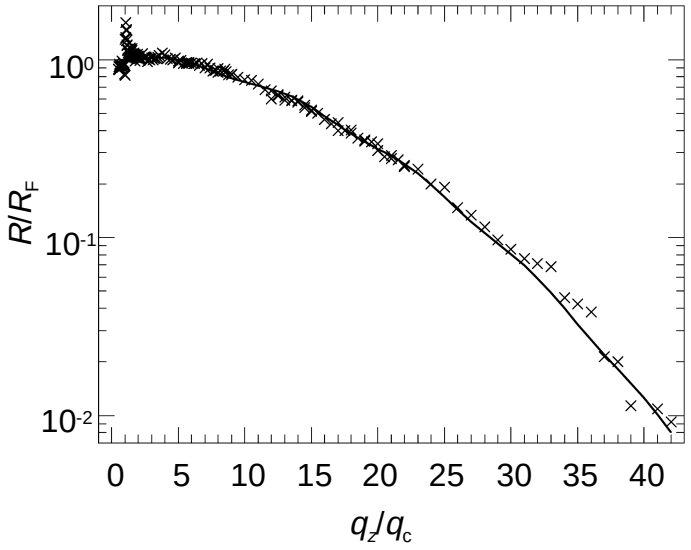

Figure 32. Measured (x) and fitted (line) X-ray reflectivity curve for a self-assembled monolayer of molecules **4** at the air-water interface.

Compound **5**: To give an experimental illustration of a molecular fold promoted by a moiety other than the 1,3-bis(ethynylene)benzene unit, compound **5** was investigated. This molecule is structurally derived from **3** but lacks the two triple bonds attached to the benzene ring. Consequently intramolecular van-der-Waals contacts between the chains should occur during the self-assembly into two-dimensional crystallites at the air-water interface. If the molecular design concept of this work is correct, the two-dimensional crystallization behavior of molecule **5**, as an example for a conventional two-chain amphiphile, should be different from that of **3**. The benzene ring of **5** separates the stems of its two alkane chains by approximately 5 Å, a value which is close to the distance between nearest-neighbor chains in *n*-alkane crystals.[51]

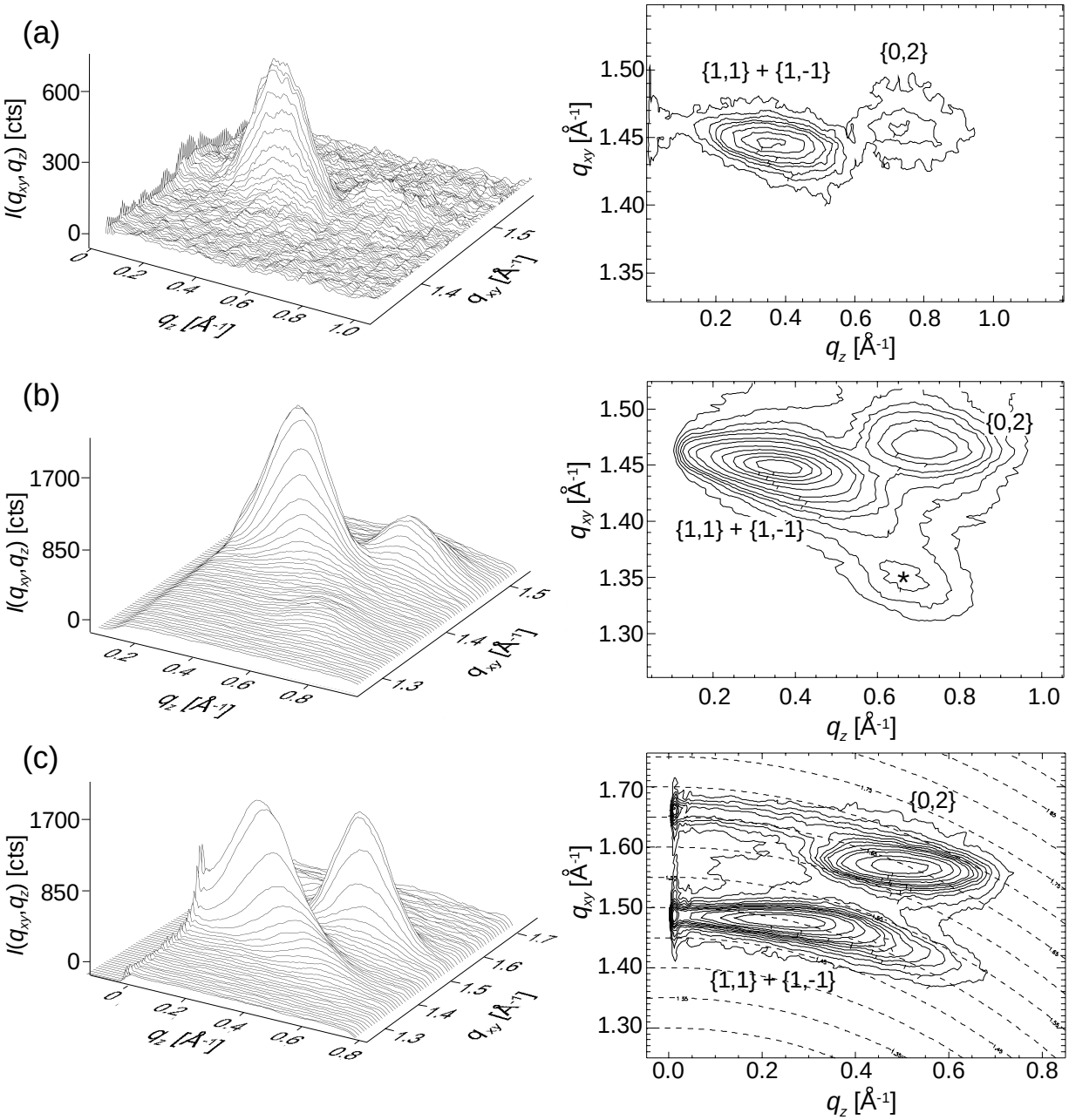

Figure 33. GIXD pattern $I(q_{xy}, q_z)$ measured for the monolayer of **5** as surface plot (left) and contour plot (right, contours are lines of equal diffracted intensity) at nominal molecular areas of: (a) 70, (b) 50 and (c) 38 Å^2.

The GIXD pattern measured at a nominal molecular area of 70 Å^2 (Figure 33a) shows the formation of a self-assembled crystalline monolayer at about 62% surface coverage. The two Bragg peaks are interpreted in terms of a rectangular unit cell (5.1., Table 4) with the molecular chains tilted by about 26° with respect to the surface normal. In contrast to all the systems described above, in this crystalline monolayer the molecules are tilted in the direction of the unit cell *b* axis, as

determined from the q_z-maxima of the two Bragg rod intensity profiles (cf. Figure 4c, chapter 1.2.).

Upon compression of the film to 50 Å^2 per molecule the intensity of the two Bragg rods increases (Figure 33b) and a weak peak appears at q_{xy} = 1.35 Å^{-1} and q_z = 0.66 Å^{-1} which belongs to an additional crystalline phase.[116] Further compression to 38 Å^2 per molecule yields a GIXD pattern (Figure 33c) in which the two Bragg rods belonging to the initial phase have their q_z-maxima at lower q_z values. The unit cell dimensions of this phase decrease slightly since the molecular chain tilt is reduced by 8° (5.1., Table 4). The GIXD pattern in Figure 33c shows additional Bragg peaks at q_{xy} = 1.49 Å^{-1} and 1.66 Å^{-1}, q_z = 0 Å^{-1} which are skewed along lines of $q_{total} = (q_{xy}^2 + q_z^2)^{1/2}$ = constant. These peaks yield a rectangular unit cell of dimensions 5.1 Å x 7.6 Å corresponding to a herring-bone packing of vertically aligned alkyl chains. The skewing behavior may be interpreted in terms of monolayer bending which occurs on compression of the film.[112]

The packing arrangement of the self-assembled dominant crystalline phase observed for molecule **5** is now discussed. The unit cell dimensions of this phase projected down the molecular chain axis, a_p and b_p, are given by $a_p = a$ and $b_p = b\cos t$, where t is the chain tilt angle with respect to the surface normal. The values of a_p and b_p (5.1., Table 4) are almost the same (a_p = 5.0 Å and b_p = 7.7 Å) for the different compression states of the monolayer and are evidence for a herring-bone packing of the alkyl chains. It is interesting to note at this point, that these projected subcell dimensions and the tilt direction are very similar to the values measured for a crystalline monolayer of the single chain alcohol *n*-tricosanol.[46] For comparison, the projected unit cell dimensions of the crystalline phases of **1**-**3** (for example, $a_p = a_s\cos t$ = 4.8 Å and $b_p = b$ = 8.7 Å for the α-phase of **3** in which the chain tilt is along the *a* direction) are clearly different from those observed for the herring-bone motif.

X-ray structure factor calculations using atomic coordinate models created in Cerius^2 with the help of the above derived unit cell parameters were performed for the dominant phase in Figure 33b. The model contained chains of 20 CH_2-groups tilted by 27º from the surface normal along the *b* direction. It yielded the calculated Bragg rod intensity profiles shown in Figure 34a.

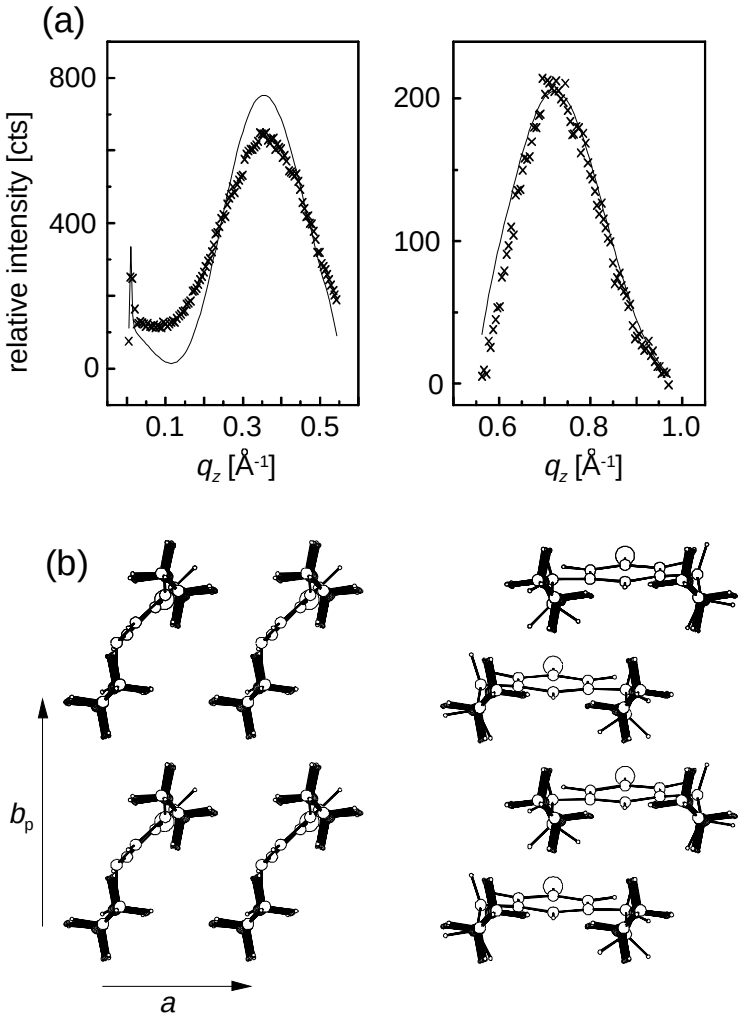

Figure 34. (a): Fitted (crosses) and measured (full line) $I(q_z)$ data for the dominant phase in the crystalline monolayer of **5** at 50 Å^2/molecule. These fits were obtained by including chains of 20 CH_2 groups length in the calculations. The chains are tilted along the *b* direction and packed in the herring-bone motif. The two CH_2 groups (per chain) at the benzene ring are disordered (b): Atomic coordinate molecular model of the chains (viewed along the chain axis) describing the packing arrangement of the molecules **5** in the dominant crystalline phase. There are two possible ways to place the benzene ring as a spacer between adjacent chains.

However, there is an ambiguity whether the chain linkage is oriented along the *a* axis (Figure 34b, right) or along the unit cell diagonal 0.5(***a*** + ***b***) (Figure 34b, left). The arrangement in (Figure 34b, right) is strongly favored since the dimensions of the linkage are unaffected by the change in the molecular tilt angle *t* which occurs upon film compression (see 5.1., Table 4). A positional disorder in this molecular packing arrangement is caused by the fact that adjacent molecules along the *b* direction may be randomly offset by ±0.5*a*.

Compound **6**: Finally, an oligomer was investigated which can be described as being built up of two inverted U-shaped molecules similar to **2b** linked by the 1,3-bis(ethynylene)benzene spacer unit. This molecule was designed to fold three times into an M-shape as promoted by the affinity of the two hydrophilic OH end groups to the water (Figure 8).

Molecules **6** self-assemble on water at a surface coverage as low as 30% (nominal molecular area of 260 Å^2). The GIXD pattern for a nominal molecular area of 200 Å^2 (Figure 35) displays two broad peaks corresponding to a centered, rectangular subcell of dimensions a_s = 5.0 Å, b_s = 8.7 Å. The molecules are tilted along the a_s axis by 25° with respect to the surface normal. These cell dimensions and the tilt direction of the chains appear now to be fingerprint evidence for one packing mode of amphiphilic molecules containing the 1,3-bis(ethynylene)benzene unit as a spacer and being aligned in ribbons parallel to the b_s axis. In this arrangement the chains of one molecule are separated by an average distance of about 8.7 Å. Consequently, b_s is a subcell dimension and must be multiplied by four to give the true unit cell repeat as $b = 4b_s$ = 34.8 Å. Along the *a* axis the unit cell repeat is $a = a_s$ = 5.0 Å. The projected dimensions are $a_p = a_s\cos t$ = 4.5 Å, $b_p = b_s$ and projected area per chain $\frac{1}{2}a_pb_p$ = 19.6 Å^2. As this unit cell contains two molecules each having four chains, the {0,2} and {1,1} + {1,-1} Bragg peaks must be

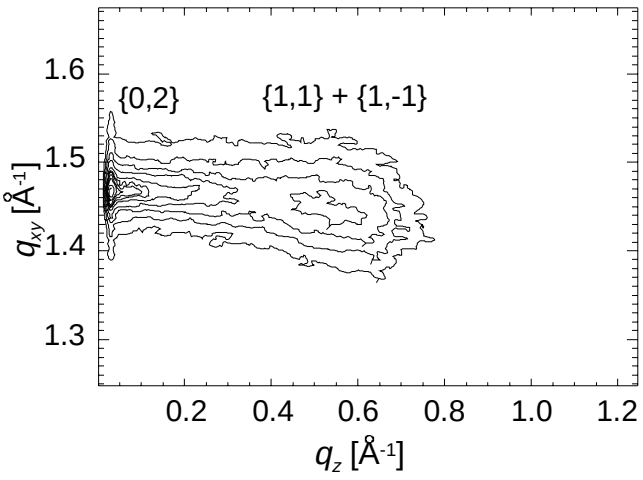

Figure 35. Conplot of the diffracted intensity $I(q_{xy}, q_z)$ of a crystalline monolayer of compound **6** at a nominal molecular area of 200 Å^2.

re-assigned Miller indices as {0,8} and {1,4} + {1,-4} respectively. The two Bragg peaks in the GIXD pattern (Figure 35) partially overlap and thus the corresponding Bragg rods were deconvoluted into two separate profiles (Figure 36a) in order to perform X-ray structure factor calculations. The crystalline film thickness of about 14 Å, as determined from the *FWHM*(q_z) of the two Bragg rods (Figure 36b), indicates that chains of a length of 12 to 13 CH_2-groups contribute to the diffraction signal.

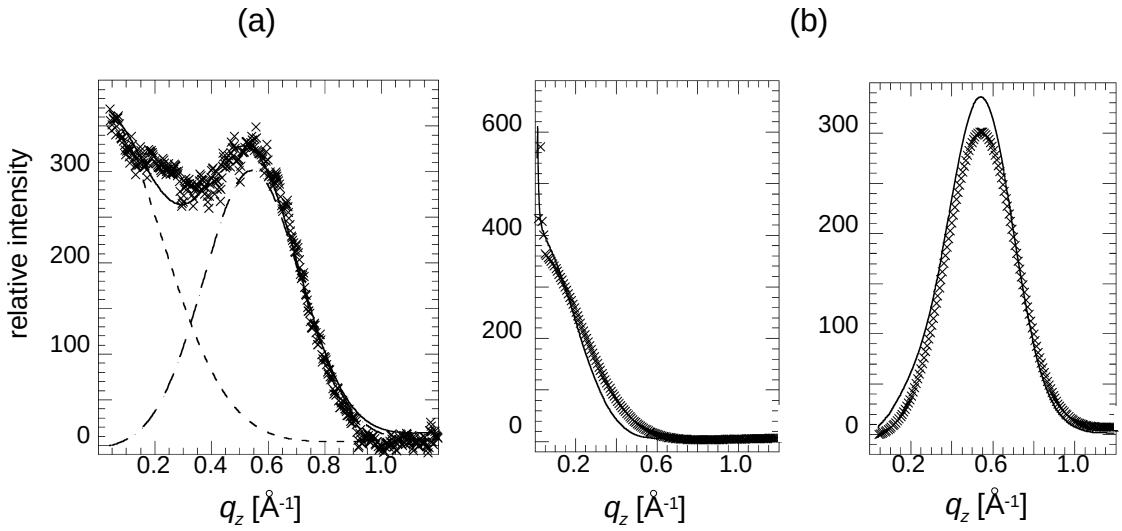

Figure 36. (a): Deconvolution of the diffraction signal into two separate Bragg rods. (b) Measured (crosses) and fitted (full lines) Bragg rod intensity profiles for the monolayer of **6** at 200 Å^2 per molecule.

The X-ray structure factor calculations, using an atomic coordinate molecular model, yielded a good fit to the measured Bragg rods when chains of only 12 CH_2-groups were considered (Figure 36b). This result is interpreted as indicating crystalline registry of only the central 12 CH_2-groups of the chains of the molecule **6**. The remaining parts of **6**, most likely the regions close to the folds, are not in registry and therefore do not contribute to the diffraction signal. The fitting procedure of the model data to the measured data is explained in more detail in 5.4. Figure 37a shows the packing arrangement of the chains of 12 CH_2-groups superimposed on the molecular model of **6** in a three-times folded conformation viewed along the *a* axis. In analogy to the monolayers of the molecules **1 2a**, **2b**, **3**, molecules **6** are arranged in ribbons along the *b* axis (Figure 37b). The absence of reflections corresponding to the repeat spacings 0.5*b* and *b* indicates crystalline disorder, involving molecular

ribbons parallel to *b* which may be randomly offset in steps of ±0.25*b*. The crystalline coherence length along the *a* axis from $L_{1,4}$ = 60 Å corresponds to about 24 molecular ribbons. In the *b* direction one finds $L_{0,8}$ = 70 Å, which corresponds to two molecules (2*b* = 69.7 Å) in registry. The GIXD pattern of this crystalline monolayer remains unchanged upon film compression to a nominal molecular area of 80 $Å^2$ (complete surface coverage).

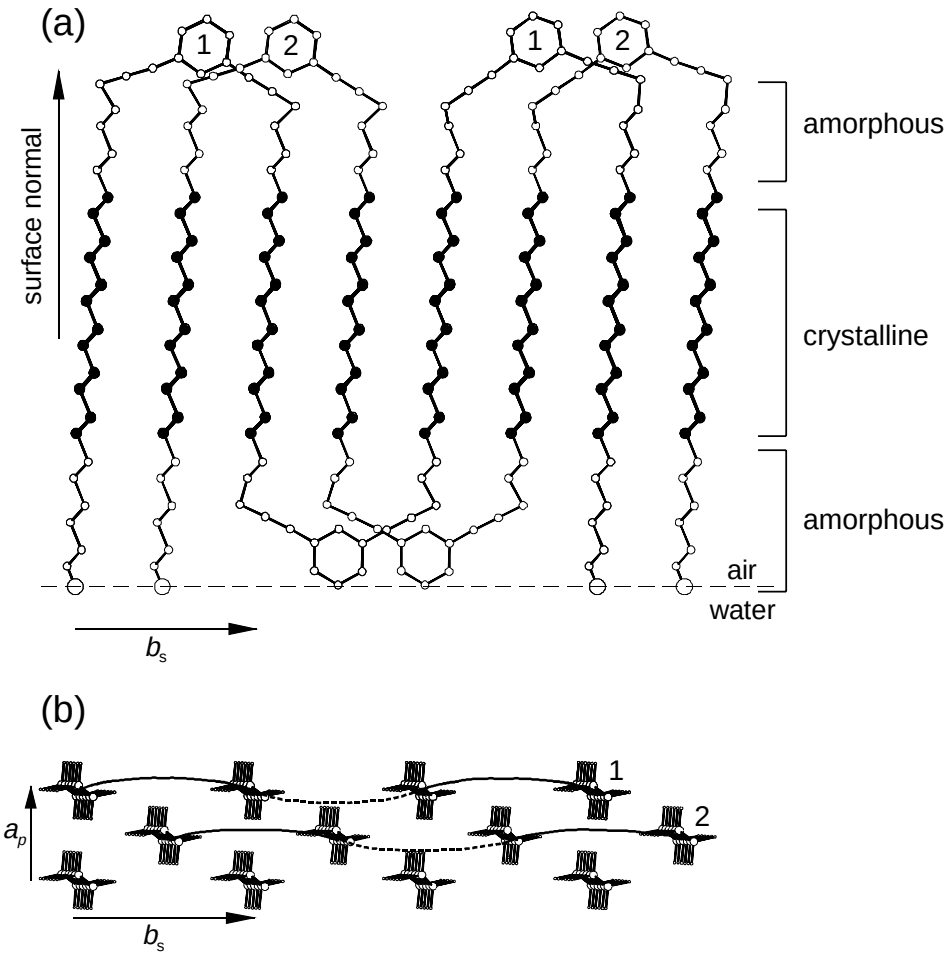

Figure 37. (a): Molecules **6** in the self-assembled monolayer in an M-conformation overlayed with the atomic coordinate molecular model of the central crystalline part (view along *a* axis). The molecules are arranged in ribbons along the *b* axis. Only the central, crystalline part of **6** (chains of 12 CH_2 groups length) contributes to the diffraction signal. (b): view along the chain axis of the atomic coordinate molecular model. The undulating shape of the molecule is scetched as a wavy line.

2.3.3. AFM studies of the self-assembled monolayers of molecules 2a and 6

Although the surface sensitive X-ray techniques already proved that the Langmuir layers of all compounds discussed in this work are crystalline monolayers, additional AFM studies are interesting as they can reveal unregularities in the film structure and the build-up of amorphous material on top of the crystalline monolayer. In order to carry out AFM studies three compounds, **1**, **2a**, and **6**, were selected. **1** was selected as it is the shortest-chain compound and does not self-assemble on the water surface into a crystalline monolayer. **2a** does self-assemble into a crystalline monolayer and, in the ideal case, a film of monomolecular height should be seen by AFM on the mica. Finally, although the *Π-A* isotherm of compound **6** already indicated a self-assembly of such molecules into a three-times folded conformation, the overall height of the self-assembled film would be an indirect prove of the molecular conformation of **6** within this film.

Compound **1** was transferred onto hydrophilic mica by applying the Langmuir - Blodgett technique. It is the only example for which the Langmuir - Blodgett technique worked very well for the transfer. This may be due to the fact that, as determined by GIXD, molecules **1** do not form a crystalline monolayer. As a consequence, AFM images of the transferred films could not be recorded because the films were destroyed by the AFM tip (tapping mode). No useful could be extracted. For all the other molecules (**2**-**6**) the Langmuir - Blodgett technique did not work. This can be explained by the fact that these molecules do form crystalline monolayers. As the LB-transfer involves a 90° orientational change during the transfer one would expect a kind of “recrystallization” to be required when the film is pulled out with the substrate. This will hinder or, as in this case, prevent the transfer onto the solid substrate.

Molecules **2a**, as an example for all molecules crystallizing in a U-shape, were transferred onto hydrophilic mica by the horizontal deposition technique at a nominal molecular area of 50 $Å^2$ (self-assembled state). The 50μm scan (Figure 38a) shows a stable film with defects. The film height is about 25 Å which corresponds approximately to a monolayer of **2a**. The defects are holes in the monolayer.

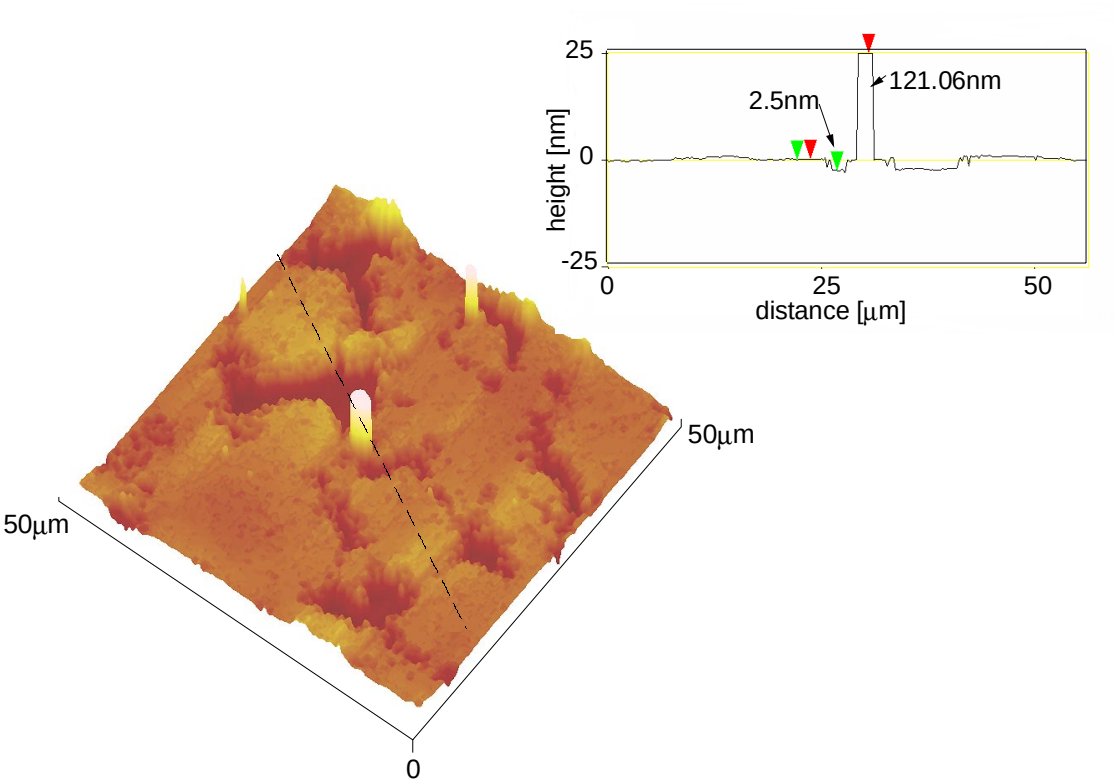

Figure 38a. 50µm-AFM scan of the self-assembled monolayer of molecules **2a** transferred onto mica by the horizontal deposition technique at a nominal molecular area of 50 Å^2. The dashed line corresponds to the scan of the AFM tip.

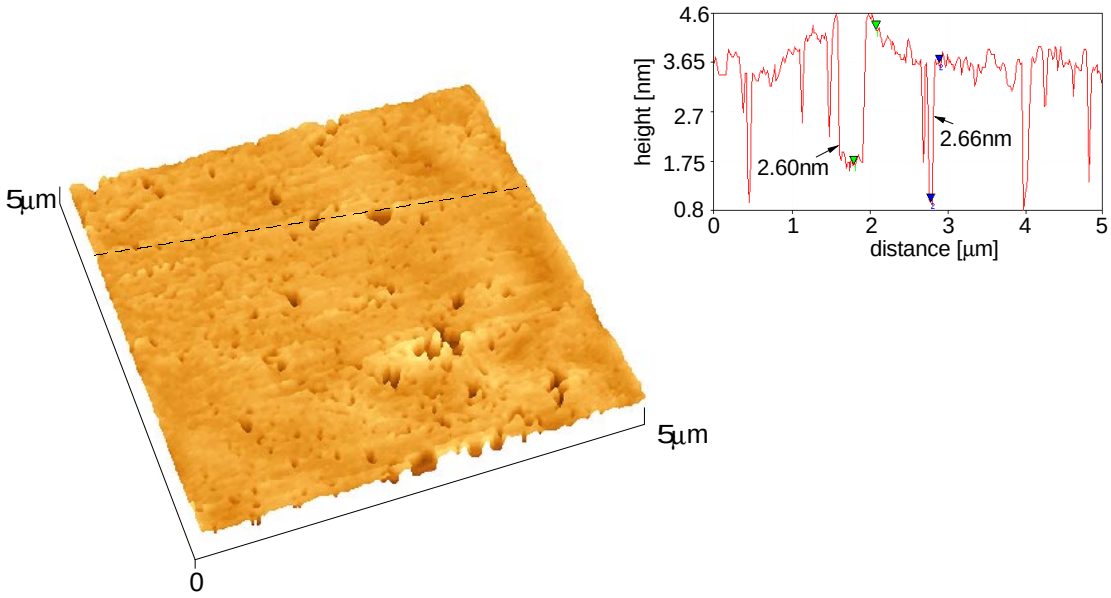

Figure 38b. 5µm-AFM scan of the self-assembled monolayer of molecules **2a** transferred onto mica by the horizontal deposition technique at a nominal molecular area of 50 Å^2. The dashed line corresponds to the scan of the AFM tip.

The huge “piles” of material (over 1000 Å !) in the middle and upper right of Figure 38a are, most likely, three-dimensional crystalline assemblies of **2a**. This effect is called “relaxation” of the monolayer and is frequently observed when monolayers are kept at constant surface pressure.[117] It is due to the higher surface energy of a two-dimensional crystal in comparison to a three-dimensional crystal. The 5µm scan (Figure 38b) did not yield any further information. The thickness in this case (between 26 and 27 Å) again corresponded to a monomolecular film of **2a** featuring hole defects and low surface roughness.

Self-assembled films of molecules **6** were transferred onto hydrophilic mica by the horizontal deposition technique in order to find indirect prove of the molecular conformation of this molecule.

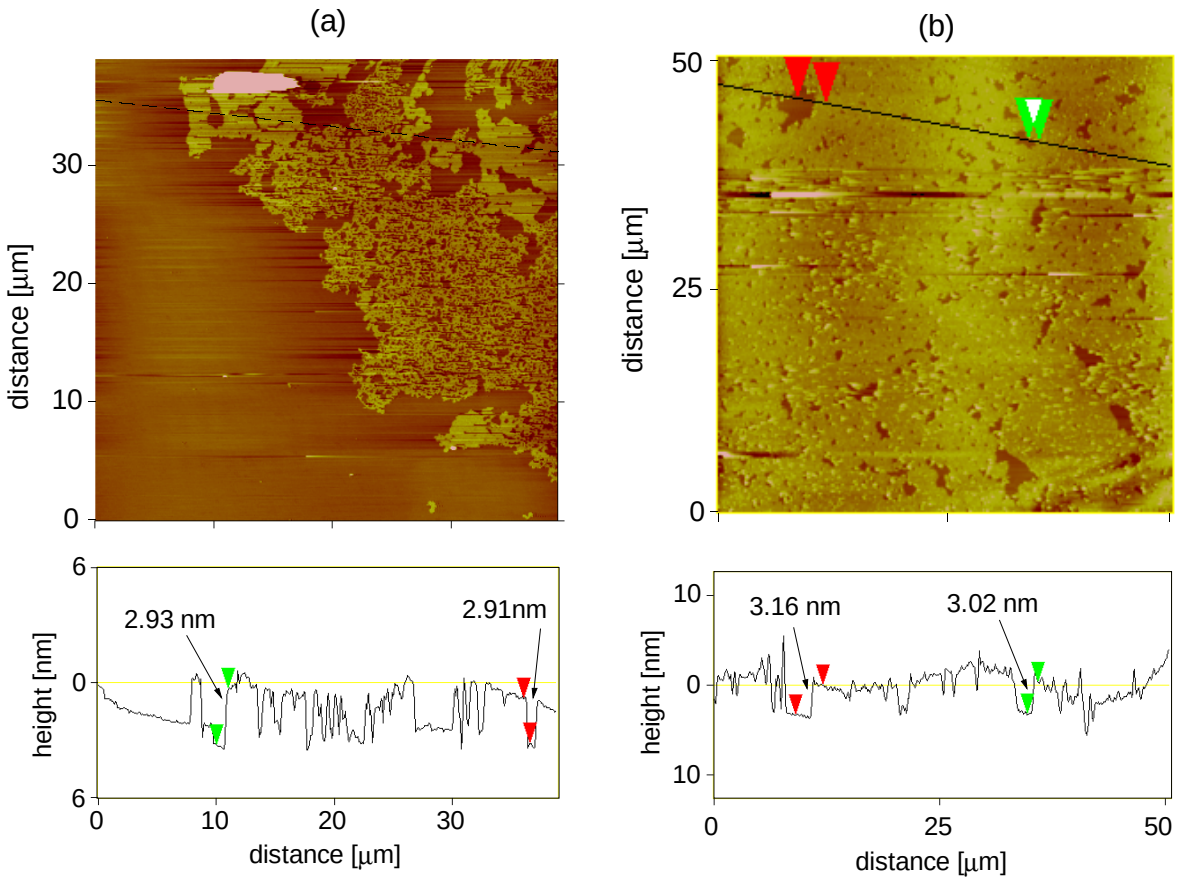

Figure 39. 50µm-AFM scan of the self-assembled monolayer of molecules **6** transferred onto mica by the horizontal deposition technique at a nominal molecular area of: (a) 200 Å^2 and (b) 80 Å^2. The dashed line corresponds to the scan of the AFM tip.

The 50μm scan at 200 Å^2 per molecule shows the crystalline self-assembly (proven by GIXD) of molecules **6** into isolated crystalline islands (Figure 39a). The islands themselves have a height of about 29 Å which corresponds to a monolayer of molecules **6** in the three-times folded conformation depicted in Figure 37. At 80 Å^2 per molecule the crystalline islands are brought closer together (Figure 39b) while the film thickness remains unchanged (~ 30 Å). The huge "lumps" of material in the upper half of both figures are due to the relaxation process described above. A 2μm scan at 80 Å^2 (Figure 40) revealed different domain morphologies and a surface roughness of 6-7 Å which is interpreted as a result of the amorphous, soft surface of the monolayer of **6** as shown in Figure 37.

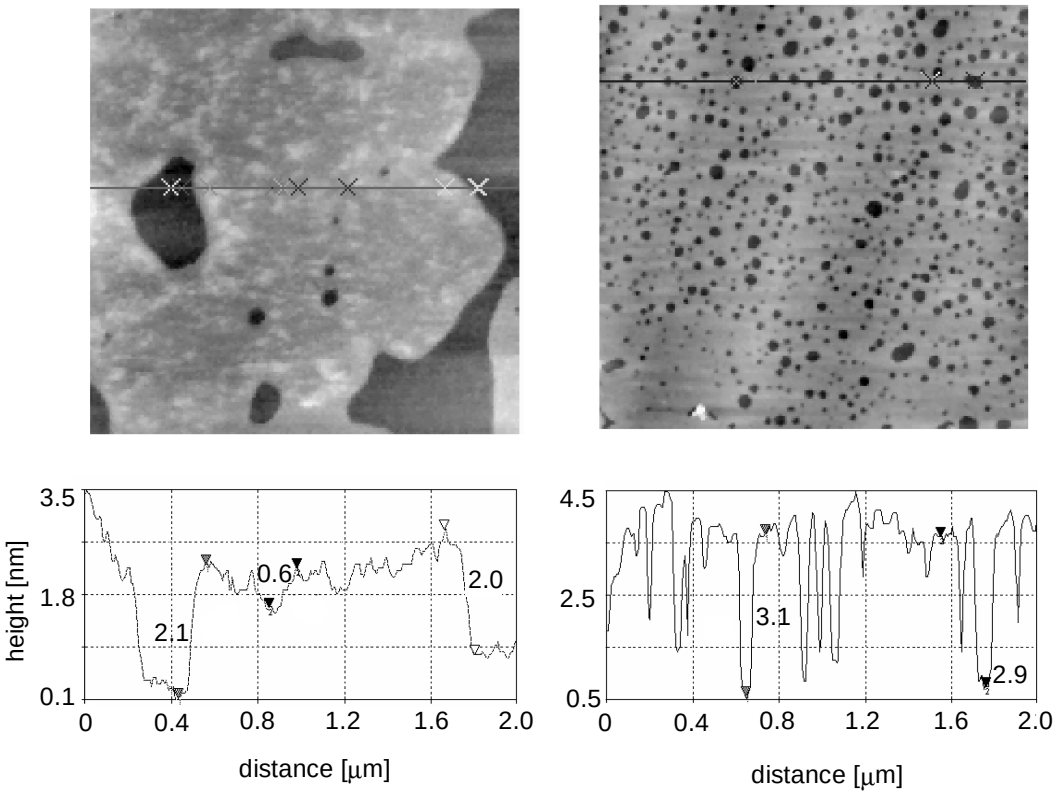

Figure 40. 2μm-AFM scan of the self-assembled monolayer of molecules **6** transferred onto mica by the horizontal deposition technique at a nominal molecular area of 80 Å^2. The line corresponds to the scan of the AFM tip.

2.4. Single crystal analysis of compound 1

The analysis of the crystalline packing arrangement of compounds **1**-**6** in monolayers at the air water interface yielded very detailed information about the molecular orientation that these molecules prefer to adopt in a crystalline assembly. However, no information could be extracted about the supramolecular structure in these packing arrangements. The position and orientation of the rigid spacer unit could not be determined. A solid prove of the supramolecular structure of the molecules can only be obtained by growing larger crystals of the compounds in order to perform single crystal X-ray structure analysis. If such a crystal structure can then be related to the packing arrangements found in the monolayers, the GIXD results of chapter 2.3.2. would stand on more solid ground.

For this purpose it was attempted to grow single crystals of compounds **1**-**4** and **6** under several conditions, mainly from solution. Most attempts failed as they lead to polycrystalline precipitation. In some cases thin, needle-like crystals could be obtained but those needles were bent and therefore useless for structure analysis. However, the attempt to crystallize **1**, the compound with the shortest chains, was eventually successful. Small, waxy crystals were obtained from a toluene solution of **1** on slow evaporation. The crystal used for structure determination was plate-like and of about 500 μm size. Although the quality of the crystal was not very good its structure could be solved.

The crystal structure belongs to the triclinic space group P-1. The unit cell dimensions are a = 9.4 Å, b = 10.3 Å, c = 34.8 Å, α = 96.9°, β = 90.9° and γ = 113.1°. The structure is a centrosymmetric bilayer arrangement with two independent molecules related by a pseudo-translation symmetry within each layer. The molecules are not interdigitating but arranged in ribbons head-to-head and tail-to-tail. The terminal OH-groups are partially disordered and the OH-groups of adjacent molecular ribbons are separated by a distance which allows hydrogen bonding to occur between the ribbons as well as between the layers. The structure is shown in Figure 41 viewed along the *a* axis and along the *b* axis. For clarity the H-atoms are omitted.

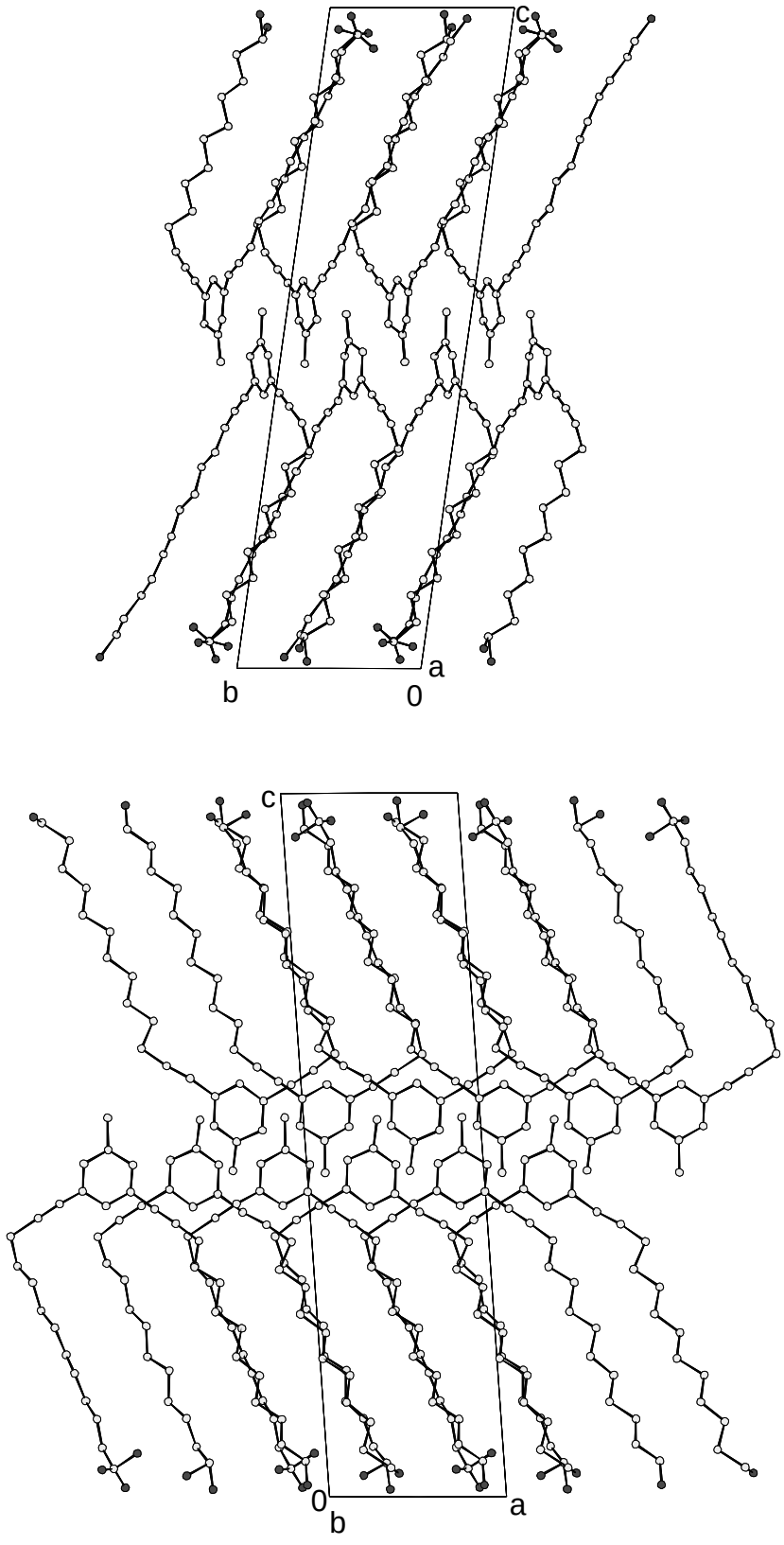

Figure 41. Packing arrangement of molecules **1** in a single crystal. top: view along *a* axis, bottom: view along *b* axis.

The molecules crystallize in a folded conformation which is stabilized by adjacent molecules through intermolecular van-der-Waals interaction. This packing arrangement is in fair agreement with the structures proposed for molecules **1** in the crystalline monolayer on the ground of very few GIXD data (see chapter 2.3.2.). It can also be related to the monolayer packings of molecules **2**-**4** and **6**. Although the length of the chains in molecule **1** is only about half of the chain lengths in molecules **2**-**4** and **6**, it can be assumed that the 3-D packing arrangements of **2**-**4** and **6** will be very similar to the crystalline packing of **1**. The single crystal structure of **1** can therefore be regarded as a model for the crystalline packing arrangements of aliphatic chain oligomers containing the 1,3-bis(ethynylene)benzene unit as a rigid spacer, which obviuosly acts as a folding unit not only in monolayers at the air-water interface, but also in bulk crystallization.

In order to relate the 3-D crystal structure of **1** to the crystalline packings of the self-assembled monolayers of **1**-**4** and **6** at the air-water interface one needs to look at the structure of one molecular layer in detail.

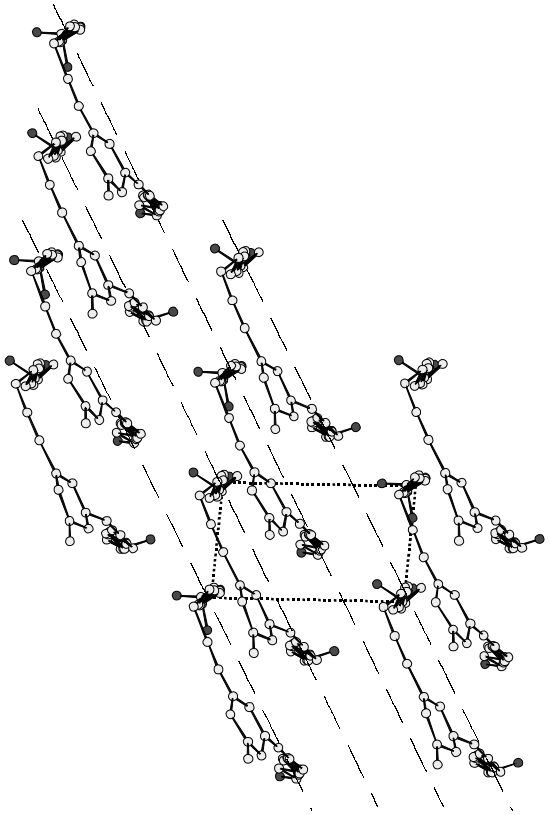

Figure 42. View along the chain axis of one molecular layer. The “herring-bone” subcell is represented by the dotted line. The adjacent molecular ribbons are outlined by dashed lines.

For this purpose the powder diffraction pattern of the above crystals structure was calculated in CERIUS[2] using the given atomic coordinates. Three very strong reflections were discerned in the calculated powder diffraction pattern in the region of 2θ = 18-23° arising from the in-layer (two-dimensional) subcell of the hydrocarbon chains. Using these values the subcell dimensions a_p = 4.95 Å, b_p = 7.52 Å, and γ = 94.9° were calculated. They describe the subcell outlined in Figure 42. These parameters are in fair agreement with the unit cell dimensions of the herring-bone packing motif found typically in crystals of *n*-alkanes (a = 4.97 Å, *b* = 7.45 Å, and γ = 90°).[51]

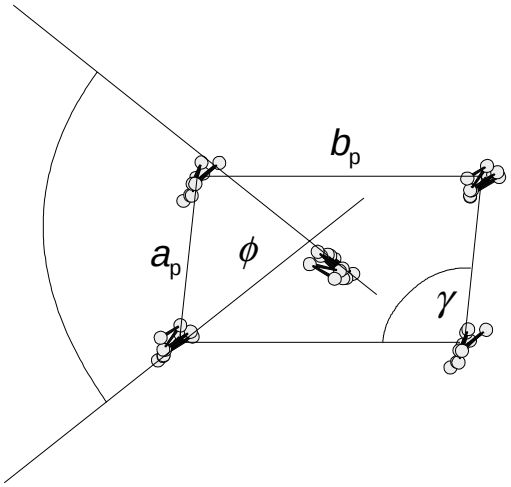

Figure 43. The oblique subcell of one molecular layer clearly shows the similarity of the packing arrangement of the chains of **1** to the "herring-bone" packing motif in *n*-alkanes. For clarity, the spacer units and the H-and O-atoms are omitted.

Ideally, the angle ϕ between the backbone of the chains should be 90°. In this case ϕ was graphically determined (Figure 43) to be ϕ = 76°. Furthermore, the subcell is slightly oblique (γ = 94.9° instead of 90°). This deviation from the herring-bone packing characteristics are most likely imposed by the presence of the 1,3-bis(ethynylene)benzene unit in the oligomer **1**.

Having solved the single crystal structure of **1** one may want to compare this three-dimensional crystalline packing with the crystalline structures determined in the monolayers of molecules containing the 1,3-bis(ethynylene)benzene unit as a rigid spacer. At this stage it is pointed out that the crystalline packings within the monolayers were obtained by fitting the intensity values $I(q_z)$ of a model structure to

the measured $I(q_z)$ profiles. The basis of these models were in any case hydrocarbon chains which were subsequently arranged in the measured unit cell. The linkage by the 1,3-bis(ethynylene)benzene unit (cf. Figures 22b, 23b, 28b, and 37b) was arbitrarily chosen on the grounds of the best geometrical fit into the model. In the case of **2a**, **2b**, **3**, and **6** the linkage is along the *b* axis forming the ribbon structure along *b*. If one now wants to compare the packing in the single crystal of **1** to these monolayer packings one should calculate the dimensions of a kind of "alternative" subcell whose *b* direction coincides with the ribbon direction formed by the U-shaped molecules **1**. This subcell is not a classical subcell because the chains within this cell are not simply related by translation. The dimensions of this "alternative" subcell can be easily derived from the above shown "herring-bone" subcell (Figure 44).

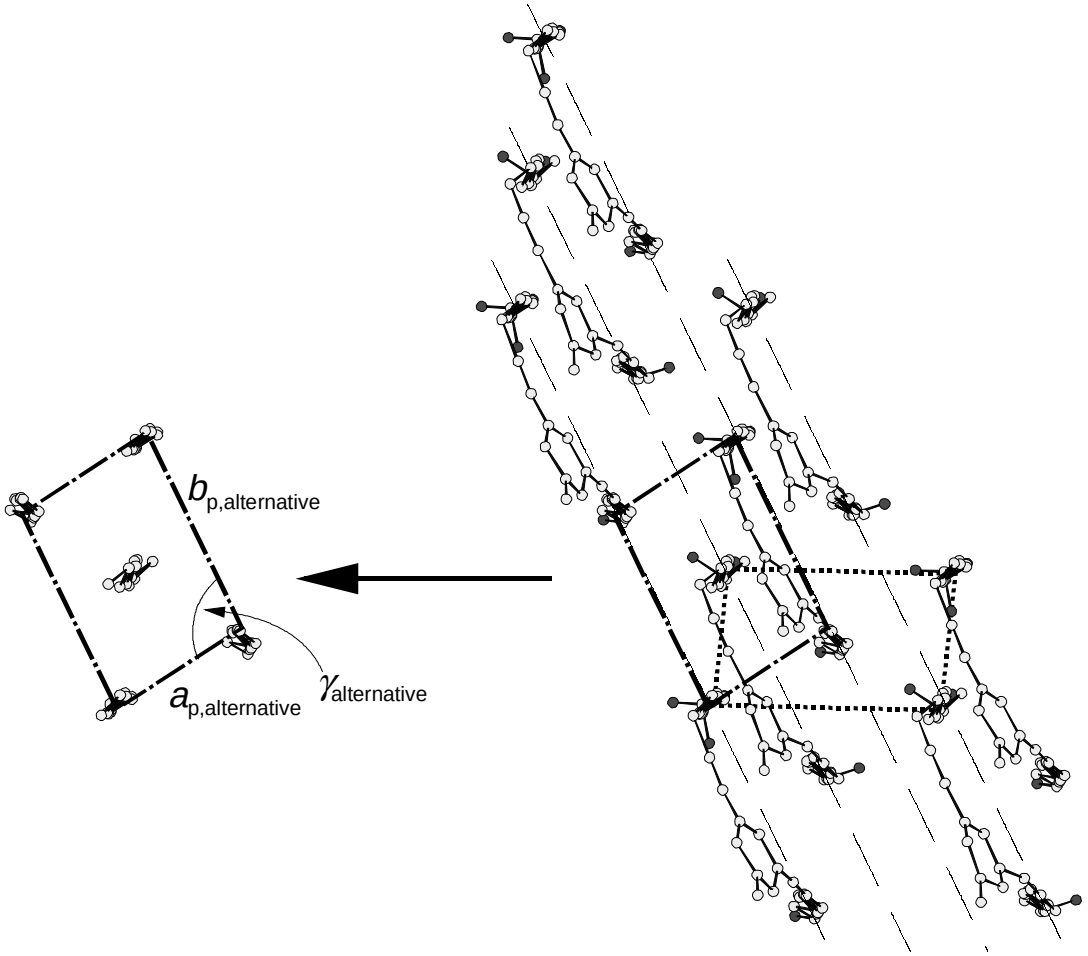

Figure 44. The "alternative" subcell of one molecular layer of **1** in the single crystal. The *b* direction coincides with the direction of the molecular ribbons. The dimensions of this subcell should be similar to those of the subcells describing the packings in the crystalline monolayers of **2a**, **2b**, **3**, and **6** (cf. Figures 22b, 23b, 28b, and 37b and 5.1., Tables 1-3) because the molecular ribbons also coincide with the crystalline *b* direction.

The dimensions of the “alternative” subcell were calculated as $a_{p,alternative}$ = 4.67 Å, $b_{p,alternative}$ = 8.03 Å, $\gamma_{alternative}$ = 98.9° and projected area per chain A_p = 18.5 Å^2. These dimensions are very similar to the projected unit cell dimensions of the subcells of the crystalline monolayers of molecules **2a**, **2b**, **3**, and **6** (cf. Figures 22b, 23b, 28b, and 37b and 5.1., Tables 1-3). In fact, they are comparable to the projected subcell dimensions of the oblique β-phases in the monolayers of **2a** and **2b** with projected areas per chain of approximately 18 Å^2.

The projected subcell dimensions of the crystalline monolayer of **1** itself (a_p = 5.1 Å and b_p = 8.4 Å) are not comparable to the dimensions of the subcell in Figure 44. The reason for this may be that the subcell dimensions of the monolayer packing arrangement of **1** were determined from a strongly compressed monolayer. 3-D crystallization is not constrained by such pressure forces. Hence, if a 3-D crystal structure is compared to the packing in a crystalline monolayer of the same, or a similar, molecule it should be compared to a crystalline structure spontaneously formed by self-assembly. This conclusion is also in agreement with another observation: On compression of the monolayers of molecules **2a** and **2b** the oblique β-phases are transformed into less densely packed, rectangular phases.

3. Summary

A series of oligomers, **1**-**4** and **6** (Figure 8), has been synthesized all having in common that their linear alkyl chains are linked by the relatively rigid 1,3-bis(ethynylene)benzene. The latter separates the stems of the two attached alkyl chains by about 9Å and thus excludes intramolecular chain-to-chain interaction during crystallization. For comparison, the conventional two-chain amphiphile **5** was prepared. In **5** a benzene ring separates the stems of the attached alkyl chains by about 5Å, a distance that allows intramolecular chain-to-chain interaction during crystallization.

It was shown by grazing incidence X-ray diffraction (GIXD) that oligomers **2**-**4** and **6** spontaneously self-organize at the air-water interface into crystalline monolayers. The molecules are arranged in ribbons and adopt a folded conformation forming a regular array of functional groups at the monolayer surface. In this way, three distinct molecular shapes of the type inverted U (**2a**, **2b**), U (**3**) and M (**6**) could be obtained depending on the number of 1,3-bis(ethynylene)benzene units and on the number and position of the hydrophilic groups in the molecule. The alkyl chains crystallize in a pseudo-herringbone packing arrangement[54] with fingerprint subcell dimensions projected along the alkyl chain axis of a_p = 4.3 - 4.7 Å, b_p = 8.3 - 8.7 Å, and $\gamma \approx 90°$. This spontaneous self-organization did not occur in the case of oligomer **1** whose chains are approximately half as long as in **2**-**4** and **6**. Oligomer **1** formed a crystalline monolayer at the air-water interface only on the application of additional surface pressure. The self-organized crystalline monolayer of the conventional two-chain amphiphile **5** is very similar to the crystalline self-aggregates of tricosanol at the air-water interface. In that **5** differs markedly from all oligomers containing the 1,3-bis(ethynylene)benzene unit. It does not form the ribbon structure observed for **2**-**4** and **6**, but rather behaves like a single chain alcohol of comparable chain length.

The crystalline monolayers of **2a** and **6** were transferred onto hydrophilic mica and characterized by AFM. The thickness of the transferred films corresponds to a monolayer of inverted U-shaped molecules in the case of **2a**, and to a monolayer of M-shaped molecules in the case of **6**.

Single crystal structure analysis of oligomer **1** showed that the folded (U-) conformation of alkyl chains intersected by the 1,3-bis(ethynylene)benzene unit is also adopted in bulk crystals. The structure is a layer structure and the individual molecules are, as in the crystalline monolayers of oligomers **2a**, **2b**, **3**, and **6**, arranged in ribbons. The subcell dimensions of the chain packing are very similar to the projected subcell dimensions of the crystalline monolayers of oligomers **2a**, **2b**, **3**, and **6**.

Characterization of oligomers **1**-**6** by differential scanning calorimetry (DSC) revealed an interesting behavior of the oligomers. One can divide them into three groups: (a) The short oligomer **1**, which does not crystallize from the melt in the time scale of the DSC measurement, (b) the oligomers **2**-**5**, which crystallize from the melt forming one crystalline phase (**2b**, **3**, and **4**) or two crystalline phases (**2a** and **5**), and (c) the oligomer **6**, which behaves very much like a flexible, linear macromolecule. All oligomers were also crystallized from solution on slow evaporation of the solvent. For all oligomers the melting temperatures and enthalpies measured in this case were higher than the corresponding values for same compounds crystallized from the melt.

4. Experimental part

4.1. Synthesis

All reactions were carried out under argon. For column chromatography Merck silica gel (40 – 63 μm) was used. The abbreviation PE stands for petroleum ether with a boiling range of 30-40°C. Diethyl ether and THF were freshly distilled from sodium/benzophenone. 1,3-Dimethyl-3,4,5,6-tetrahydro-2-pyrimidone (DMPU) was dried over CaH_2. NMR spectra were recorded on a BRUKER AMX 300 at room temperature in $CDCl_3$, unless stated otherwise. The spectra of the THP-protected compounds **2a** and **14** were recorded in CD_2Cl_2 because $CDCl_3$ is prone to HCl formation which destroys the acid labile THP ether. The carbon multiplicity was determined with the DEPT experiment. Prior to the elemental analysis and monolayer investigations every sample was recrystallized from CH_2Cl_2 in order to remove dust particles or grease. Compound **7b** was kindly given by Dr. S. Höger.

4.1.1. Synthesis of the target molecules 1, 2a, 2b, 3, 4, 5 and 6 (Figure 8)

Synthesis of compounds 1, 2a, 2b, 3, 4, and 10a:[118] To a degassed solution of 3,5-diiodobenzene **7** and 1-alkyne **8** (2.1 mol equivalents) in THF (10 mL per mmol **7**) and piperidine (5 mL per mmol **7**) were added CuI (2 mol%) and $Pd(PPh_3)_2Cl_2$ (1 mol%) at rt. After stirring for 16 h, the suspension was poured into diethyl ether and the organic phase was washed with 2N HCl. The combined aqueous phases were extracted with diethyl ether. The combined organic phases were washed with water, dried ($MgSO_4$), and the solvent was removed. Column chromatography (PE) followed by recrystallization in CH_2Cl_2 gave **4** (1.60 g, 78%) as a colorless solid.

Desilylation of crude **9a**-**d** was carried out in THF using a 1M solution of *n*-Bu_4NF in THF (1 molar equivalent relating to **8**; 1 h at rt). After removal of the solvent in vacuo the residue was purified by column chromatography. The impurities were eluted with PE/diethyl ether 5/2 v/v. Subsequent elution with diethyl ether yielded **1** (0.46 g, 82%), **2a** (0.88 g, 79%), **2b** (0.19 g, 85%) and **9a** (3.05 g, 79%) as colorless solids.

Crude **9e** was deprotected by stirring for 1 h in dioxane, MeOH, toluene sulfonic acid monohydrate (0.4 g, 2.1 mmol) at rt. Chromatography with PE/CH_2Cl_2 2:1 v/v resulted in **3** (0.92 g, 80%) as a colorless solid.

1: ^{1}H NMR: δ = 1.15 - 1.48 (m, 28H), 1.48 - 1.63 (m, 8H), 2.24 (s, 3H), 2.35 (t, *J* = 7.0 Hz, 4H), 3.61 (t, *J* = 6.7 Hz, 4H), 7.08 (d, *J* = 1.4 Hz, 2H), 7.21 (t, *J* = 1.4 Hz, 1H);
^{13}C NMR: δ = 19.4 (CH_2), 20.9 (CH_3), 25.7 and 28.7 - 29.7 (seven signals, CH_2), 32.8 and 63.1 (2 CH_2), 80.1, 90.4 and 124.0 (3 C), 131.3 and 131.7 (2 CH), 137.8 (C);
$C_{33}H_{52}O$ (480.779): calcd. C 82.44, H 10.90; found C 82.03, H 10.60.

2a: ^{1}H NMR: δ = 1.15 - 2.00 (m, 92H), 2.37 (t, *J* = 7.1 Hz, 4H), 3.57 - 3.63 (m, 5H), 3.83 (d of t, *J* = 9.1 Hz, *J* = 3.1 Hz, 1H), 5.36 (t, *J* = 3.1 Hz, 1H), 6.96 (d, *J* = 1.3 Hz, 2H), 7.01 (t, *J* = 1.3 Hz, 1H);
^{13}C NMR: δ = 19.1, 19.8, 25.7, 26.3 and 29.3-30.8 (twentyfour signals, CH_2), 33.5, 62.6 and 63.4 (3 CH_2), 80.2 and 91.4 (2 C), 97.1 and 119.6 (2 CH), 125.7 (C), 128.5 (CH), 157.3 (C);
$C_{61}H_{106}O_4$ (903.519): calcd. C 81.09, H 11.83; found C 80.92, H 11.64.

2b: ^{1}H NMR (35 °C): δ = 1.15 - 1.48 (m, 76H), 1.48 - 1.63 (m, 8H), 2.36 (t, *J* = 7.0 Hz, 4H), 3.62 (t, *J* = 6.6 Hz, 4H), 7.13 - 7.18 (m, 1H), 7.24 - 7.27 (m, 2H), 7.40 (m, 1H);[119]
^{13}C NMR (35 °C): δ = 19.4 and 25.7 (2 CH_2), 28.7 - 29.7 (nineteen signals, CH_2), 32.8 and 63.1 (2 CH_2), 80.0, 90.9 and 124.2 (3 C), 128.1, 130.5 and 134.6 (3 CH);
$C_{56}H_{98}O_2$ (803.400): calcd. C 83.72, H 12.30; found C 83.51, H 12.20.

3: ^{1}H NMR: δ = 0.86 (t, *J* = 6.7 Hz, 6H), 1.15 - 1.48 (m, 76H), 1.48 - 1.63 (m, 4H), 2.35 (t, *J* = 7.0 Hz, 4H), 4.67 (very broad s, 1H), 6.74 (d, *J* = 1.3 Hz, 2H), 7.00 (t, *J* = 1.3 Hz, 1H);
^{13}C NMR: δ = 14.1 (CH_3), 19.4 and 22.7 (2 CH_2) and 28.7 - 29.7 (nineteen signals, CH_2), 79.7 (C), 91.0 (C), 117.8 (CH), 125.4 (C), 127.7 (CH), 155.0 (COH);
$C_{54}H_{94}O$ (759.346): calcd. C 85.41, H 12.48; found C 85.06, H 12.57.

4: ^{1}H NMR: δ = 0.86 (t, *J* = 6.7 Hz, 6H), 1.15 - 1.48 (m, 76H), 1.56 (m, 4H), 2.24 (s, 3H), 2.35 (t, *J* = 7.0 Hz, 4H), 7.09 (br. s, 2H), 7.21 (br. s, 1H);

^{13}C NMR: δ = 14.1 (CH_3), 19.4 (CH_2), 21.0 (CH_3), 22.7 (CH_2), 28.8 - 29.7 (eighteen signals, (CH_2)), 31.9 (CH_2), 80.1, 90.4 and 124.0 (3 C), 131.4 and 131.7 (2 CH), 137.8 (C);
$C_{55}H_{96}$ (757.373): C 87.22, H 12.78; found C 87.20, H 12.54.

10a: ^{1}H NMR (35°C): δ = 1.15 - 1.48 (m, 60H), 1.48 - 1.63 (m, 8H), 2.37 (t, *J* = 7.0 Hz, 4H), 3.62 (t, *J* = 6.6 Hz, 4H), 7.13 - 7.18 (m, 1H), 7.24 - 7.27 (m, 2H), 7.40 (m, 1H);[119]
^{13}C NMR (35 °C): δ = 19.4 and 25.8 (2 CH_2), 28.7 - 29.7 (fifteen signals, CH_2), 32.9 and 63.1 (2 CH_2), 80.0, 90.9 and 124.3 (3 C), 128.1, 130.5 and 134.6 (3 CH);
$C_{48}H_{82}O_2$ (691.184): calcd. C 83.41, H 11.96; found C 83.35, H 12.02.

Synthesis of compound 6: To a solution of triphenylphosphine (3.37 g, 12.9 mmol) in CH_2Cl_2 (30 mL) was added Br_2 (0.66 mL, 12.9 mmol) at 0 °C. After stirring for 30 min at rt imidazole (0.92 g, 13.5 mmol) and **10a** (3.07 g, 4.4 mmol) were added. The reaction mixture was stirred for 4 h at rt. It was hydrolyzed with water and the organic phase was washed with saturated aqueous $Na_2S_2O_3$, dried ($MgSO_4$) and concentrated in vacuo. Chromatography (PE/diethyl ether 2/1 v/v) of the residue gave **10b** as a colorless solid (2.81 g, 78 %).

To a solution of trimethylsilylacetylene (0.74 g, 7.53 mmol) in THF (20 mL) was slowly added 1.6 M *n*-BuLi in *n*-Hexan (4.32 mL, 6.91 mmol) at -80 °C. After addition of DMPU (20 mL) and **10b** (2.57 g, 3.14 mmol) the temperature was allowed to rise slowly to rt. Stirring for 16 h at rt, aqueous work-up and drying ($MgSO_4$), deprotection in THF using *n*-Bu_4NF (5.5 mL, 1M solution in THF), removal of the solvent in vacuo and subsequent column chromatography (PE/dichloromethane 7/1 v/v) gave **10c** (1.62 g, 80 %) as a colorless solid.

Following the procedure for the aryl-alkynyl coupling reaction described for compounds **1**, **2a**, **2b**, **3**, **4**, and **10a**, the coupling of 1,3-diiodobenzene **7a** (3.90 g, 11.8 mmol) with **8c** (5.00 g, 11.8 mmol) gave, after column chromatography (PE/diethyl ether 5/1 v/v) **11** (5.54 g, 75 %) as a colorless solid.

Following the procedure for the aryl-alkynyl coupling reaction described for compounds **1**, **2a**, **2b**, **3**, **4**, and **10a**, the coupling of **10c** (0.35 g, 0.5 mmol) with **11** (0.67 g, 1.0 mmol) gave, after chromatography (PE, PE:CH_2Cl_2 = 70:9 v/v, PE:diethyl ether = 5:2 v/v) the silylated compound **6** (0.6 g, 67%). 0.28 g of this material were desilylated in THF using *n*-$BuNF_4$ (0.5 mL, 1M solution in THF). Removal of the solvent followed by chromatography (diethyl ether) yielded **6** (0.19 g, 68 %) as a colorless solid.

10b: ^{1}H NMR: δ = 1.15 - 1.48 (m, 60H), 1.57 (m, 4H), 1.83 (m, 4H), 2.36 (t, *J* = 7.0 Hz, 4H), 3.39 (t, *J* = 6.9 Hz, 4H), 7.13 - 7.18 (m, 1H), 7.24 - 7.27 (m, 2H), 7.40 (m, 1H);[119]
^{13}C NMR: δ = 19.4 and 28.2 (2 CH_2), 28.7 - 29.7 (fifteen signals, CH_2), 32.9 and 34.0 (2 CH_2), 80.0, 90.9 and 124.2 (3 C), 128.1, 130.5 and 134.6 (3 CH);
$C_{48}H_{80}Br_2$ (816.968): calcd. C 70.57, H 9.87; found C 70.21, H 9.98.

10c: ^{1}H NMR: δ = 1.15 - 1.48 (m, 60H), 1.48 - 1.63 (m, 8H), 1.92 (t, *J* = 2.6 Hz, 2H), 2.16 (d of t, J_d = 2.6 Hz, J_t = 7.0 Hz, 4H), 2.36 (t, *J* = 7.0 Hz, 4H), 7.13 - 7.18 (m, 1H), 7.24 - 7.27 (m, 2H), 7.40 (m, 1H);[119]
^{13}C NMR: δ = 18.4, 19.4 and 28.5 (3 CH_2), 28.7 - 29.7 (sixteen signals, CH_2), 68.0 (CH),[120] 80.0 (C), 84.8 (C),[120] 90.8 (C), 124.2 (C), 128.1, 130.5 and 134.6 (3 CH);
$C_{52}H_{82}$ (707.228): calcd. C 88.31, H 11.69; found C 88.41, H 11.71.

11: ^{1}H NMR: δ = 0.03 (s, 6H), 0.88 (s, 9H), 1.15 - 1.63 (m, 42H), 2.36 (t, *J* = 7.0 Hz, 2H), 3.58 (t, *J* = 6.6 Hz, 2H), 6.98 (t, *J* = 7.8 Hz, 1H), 7.31 (t of d, J_t = 1.6 Hz, J_d = 7.8 Hz, 1H), 7.56 (t of d, J_t = 1.6 Hz, J_d = 7.8 Hz, 1H), 7.73 (t, *J* = 1.6 Hz, 1H);
^{13}C NMR: δ = -5.3 (CH_3Si), 18.4 (C), 19.4 and 25.8 (2 CH_2), 26.0 (CH_3), 28.6 - 29.7 (nineteen signals, CH_2), 32.9 and 63.3 (2 CH_2), 79.0 and 92.1 (2 C), 93.6 (CI), 126.3 (C), 129.6, 130.7, 136.5 and 140.2 (4 CH);
$C_{37}H_{65}OISi$ (680.917): calcd. C 65.27, H 9.62; found C 65.38, H 9.62.

6: ^{1}H NMR (35 °C): δ = 1.15 - 1.35 (m, 138H), 1.48 - 1.63 (m, 16H), 2.36 (t, *J* = 7.0 Hz, 12H), 3.62 (t, *J* = 6.6 Hz, 4H), 7.13 - 7.18 (m, 1H), 7.24 - 7.27 (m, 2H), 7.40 (m, 1H);[119]

^{13}C NMR (35 °C): δ = 19.4 and 25.8 (2 CH_2), 28.7 - 29.7 (twenty signals, CH_2), 63.1 (CH_2), 80.0, 90.9 and 124.3 (3 C), 128.1, 130.5 and 134.6 (3 CH);
$C_{114}H_{182}O_2$ (1584.710): C 86.40, H 11.58; found C 86.07, H 11.54.

Synthesis of compound 5:[121] To Mg (0.34 g, 14.1 mmol) in diethyl ether (30 mL) was added slowly docosyl bromide (4.58 g, 11.8 mmol). After refluxing for 16 h, docosyl magnesium bromide **13** was added to a solution of **12** (1.25 g, 4.5 mmol) and Ni(dppp)Cl_2 (0.025 g, 0.045 mmol) in diethyl ether (20 mL). After refluxing for 5 days the reaction mixture was poured onto ice. The organic phase was washed with 2N HCl. The aqueous phase was extracted with diethyl ether. The combined organic phases were washed with saturated aqueous Na_2CO_3 and dried ($MgSO_4$) giving crude, O-silylated **5**. Deprotection of the crude product in THF using *n*-BuNF_4 (2.5 mL, 1M solution in THF) for 2 h at rt and subsequent column chromatography eluting first with PE/dichloromethane 7/1 v/v, then with PE/diethyl ether 1/1 v/v, yielded compound **5** (1.80 g, 56 %) as a colorless solid.

5: ^{1}H NMR: δ = 0.87 (t, *J* = 6.7 Hz, 6H), 1.15 - 1.40 (m, 76H), 1.50 - 1.65 (m, 4H), 2.50 (t, *J* = 7.7 Hz, 4H), 4.48 (s, 1H), 6.45 (broadened d, *J* = 1.1 Hz, 2H), 6.56 (broadened t, 1H);
^{13}C NMR: δ = 14.1 (CH_3), 22.7 (CH_2), 29.4 - 29.7 (seventeen signals, CH_2), 31.3, 31.9 and 35.9 (3 CH_2), 112.5 and 121.3 (2 CH), 144.6 and 155.4 (2 C);
$C_{50}H_{94}O$ (711.302): calcd. C 84.43, H 13.32; found C 84.30, H 13.40.

Compound **12** was obtained by silylation of 3,5-dichlorephenol.[101]

4.1.2. Synthesis of the monodisperse chains

Synthesis of compound 14:[122] To propynol (30.00 g, 0.54 mol) in diethyl ether (100 mL) were added TsOH monohydrate (5.14 g, 27 mmol). 3,4-Di-hydro-2H-pyran were then slowly added to the solution and the mixture was stirred for 2 h at rt. Subsequent treatment with 2N NaOH, washing with water and drying ($MgSO_4$) yielded crude **14**. Fractional distillation using a membrane pump yielded **14** as a clear, colorless liquid (26.8 g, 35 %).

14: ^{1}H NMR: δ = 1.40 - 1.90 (m, 6H), 2.45 (t, ^{4}J = 2.5 Hz, 1H), 3.48 (m, 1H), 3.79 (m, 1H), 4.18 (dd, ^{4}J = 2.4 Hz, ^{2}J = 5.8 Hz, 1H), 4.26 (dd, ^{4}J = 2.4 Hz, ^{2}J = 5.7 Hz, 1H), 4.76 (t, J = 3.2, 1H);
^{13}C NMR: δ = 19.5, 25.8, 30.7, 54.2 and 62.3 (5 CH_2), 74.0 (CH), 80.4 (C), 97.3 (CH).

Synthesis of compound 16a:[99] To a solution of **14** (7.62 g, 54.00 mmol) in THF (150 mL) at -80 °C *n*-BuLi (30.93 mL of 1.6 M solution in *n*-hexane, 49.49 mmol) was slowly added and the mixture was stirred for 15 minutes. After addition of DMPU (150 mL) and octadecyl bromide (**15a**, 15.00 g, 45 mmol) the temperature was allowed to rise slowly to rt. Stirring for 16 h at rt, aqueous work-up and drying ($MgSO_4$), deprotection in dioxane (100 mL) using $TsOH \cdot H_2O$ (2 g, 10.5 mmol), 2 drops of 2N HCl and MeOH (30 mL), aqueous work-up, removal of the solvent in vacuo and subsequent column chromatography (PE/diethyl ether 1/1 v/v) gave **16a** (10.5 g, 76 %) as a slightly yellowish, crystalline solid.

16a: ^{1}H NMR: δ = 0.86 (t, J = 6.7 Hz, 3H), 1.15 - 1.40 (m, 30H), 1.48 (m, 2H), 2.19 (t of t, ^{5}J = 2.2 Hz, ^{3}J = 7.0 Hz, 2H), 4.23 (t, J = 2.2 Hz, 2H);
^{13}C NMR: δ = 14.1 (CH_3), 18.7 and 22.7 (2 CH_2), 28.6 - 29.7 (fourteen signals, CH_2), 31.9 and 51.5 (2 CH_2), 78.3 and 86.7 (2 C);
$C_{21}H_{40}O$ (308.55): calcd. C 81.75, H 13.07; found C 81.46, H 13.28.

Synthesis of compound 17a:[100] To freshly distilled (from CaH_2) 1,3-diamino propane (100 mL), Lithium (1.18 g, 169 mmol) was added in small, freshly cut pieces at rt. The solution, which turned deep blue after stirring for 5 minutes, was heated to 70 °C leading, after 30 minutes, to discoloration and a white precipitation. While cooling to rt KO^{t}Bu (12.66 g, 113 mmol) was added and the solution was stirred at rt for 20 minutes. In two portions **16a** (8.7 g, 28.2 mmol) was added followed by stirring for 16 h at 45 °C. The mixture was then poured onto water/ice (200 mL) and the resulting beige precipitate was filtered off and washed with 2N HCl and water. The press cake was dissolved in boiling EtOH and allowed to crystallize overnight at 5 °C. The precipitate was filtered off and yielded, after drying and chromatography (PE/diethyl ether 1/1 v/v), **17a** (7.52 g, 86 %) as a slightly yellowish, crystalline solid.

17a: ^{1}H NMR: δ = 1.15 - 1.40 (m, 30H), 1.51 (m, 4H), 1.92 (t, *J* = 2.7 Hz, 1H), 2.16 (d of t, J_d = 2.6 Hz, J_t = 7.0 Hz, 2H), 3.62 (t, *J* = 6.6 Hz, 2H);
^{13}C NMR: δ = 18.4 and 25.7 (2 CH_2), 28.5 - 29.7 (fifteen signals, CH_2), 32.8 and 63.1 (2 CH_2), 68.0 (CH),[120] 84.8 (C);[120]
$C_{21}H_{40}O$ (308.55): calcd. C 81.75, H 13.07; found C 82.06, H 12.87.

Synthesis of compound 16b:[99] To a solution of **14** (7.62 g, 54.00 mmol) in THF (150 mL) at -80 °C *n*-BuLi (30.93 mL of 1.6 M solution in *n*-hexane, 49.49 mmol) was slowly added and the mixture was stirred for 15 minutes. After addition of DMPU (150 mL) and docosyl bromide (**15b**, 17.53 g, 45 mmol) the temperature was allowed to rise slowly to rt. Stirring for 16 h at rt, aqueous work-up and drying ($MgSO_4$), deprotection in dioxane (100 mL) using $TsOH \cdot H_2O$ (2 g, 10.5 mmol), 2 drops of 2N HCl and MeOH (30 mL), removal of the solvent in vacuo and subsequent column chromatography (PE/diethyl ether 1/1 v/v) gave **16b** (13.2 g, 81 %) as a slightly yellowish, crystalline solid.

16b: ^{1}H NMR: δ = 0.86 (t, *J* = 6.7 Hz, 3H), 1.15 - 1.40 (m, 38H), 1.48 (m, 2H), 2.19 (t of t, ^{5}J = 2.2 Hz, ^{3}J = 7.0 Hz, 2H), 4.23 (t, *J* = 2.1 Hz, 2H);
^{13}C NMR: δ = 14.1 (CH_3), 18.7 and 22.7 (2 CH_2), 28.6 - 29.7 (eighteen signals, CH_2), 31.9 and 51.5 (2 CH_2), 78.3 and 86.7 (2 C);
$C_{25}H_{48}O$ (364.66): calcd. C 82.34, H 13.27; found C 82.26, H 13.25.

Synthesis of compound 17b:[100] To freshly distilled (from CaH_2) 1,3-diamino propane (110 mL) Lithium (1.49 g, 214 mmol) was added in small, freshly cut pieces at rt. The solution, which turned deep blue after stirring for 5 minutes, was heated to 70 °C leading, after 30 minutes, to discoloration and a white precipitation. While cooling to rt KO^{t}Bu (16.16 g, 144 mmol) was added and the solution was stirred at rt for 20 minutes. In two portions **16b** (13.1 g, 36 mmol) was added followed by stirring for 16 h at 45 °C. The mixture was then poured onto water/ice (300 mL) and the resulting beige precipitate was filtered off and washed with 2N HCl and water. The press cake was dissolved in boiling EtOH and allowed to crystallize overnight at 5 °C. The precipitate was filtered off and yielded, after drying and chromatography (PE/diethyl ether 1/1 v/v), **17b** (8.4 g, 64 %) as a slightly yellowish, crystalline solid.

17b: ^{1}H NMR: δ = 1.15 - 1.40 (m, 38H), 1.51 (m, 4H), 1.92 (t, J = 2.6 Hz, 1H), 2.16 (d of t, J_d = 2.6 Hz, J_t = 7.1 Hz, 2H), 3.62 (t, J = 6.6 Hz, 2H);
^{13}C NMR: δ = 18.4 and 25.7 (2 CH_2), 28.5 - 29.7 (nineteen signals, CH_2), 32.8 and 63.1 (2 CH_2), 68.0 (CH),[120] 84.8 (C);[120]
$C_{25}H_{48}O$ (364.66): calcd. C 82.34, H 13.27; found C 82.36, H 13.19.

O-silylation of 17a and 17b:[101] To a solution of TBDMS-chloride (1.2 mol equivalents) and imidazole (2.5 mol equivalents) in DMF (1 mL per mmol **17**) at 45 °C the α,ω-alkynol **17** (1 mol equivalent) was added. After stirring for 16 h, the solvent was removed under reduced pressure (membrane pump) and the remaining yellow residue was purified by column chromatography (PE:diethyl ether 1:1 v/v) yielding **8a** (5.80 g, 78%) and **8c** (3.63 g, 92%) as yellowish solids.

8a: ^{1}H NMR: δ = 0.02 (s, 6H), 0.87 (s, 9H), 1.15 - 1.40 (m, 30H), 1.49 (m, 4H), 1.91 (t, J = 2.7 Hz, 1H), 2.16 (d of t, J_d = 2.6 Hz, J_t = 7.0 Hz, 2H), 3.57 (t, J = 6.6 Hz, 2H);
^{13}C NMR: δ = -5.26 (CH_3), 18.37, 18.41 and 25.8 (3 CH_2), 26.0 (CH_3), 28.5 - 29.7 (fourteen signals, CH_2), 32.9 and 63.3 (2 CH_2), 68.0 (CH),[120] 84.8 (C).[120]

8c: ^{1}H NMR: δ = 0.02 (s, 6H), 0.87 (s, 9H), 1.15 - 1.40 (m, 38H), 1.49 (m, 4H), 1.91 (t, J = 2.6 Hz, 1H), 2.16 (d of t, J_d = 2.6 Hz, J_t = 7.0 Hz, 2H), 3.57 (t, J = 6.6 Hz, 2H);
^{13}C NMR: δ = -5.26 (CH_3), 18.37, 18.41 and 25.8 (3 CH_2), 26.0 (CH_3), 28.5 - 29.7 (eighteen signals, CH_2), 32.9 and 63.3 (2 CH_2), 68.0 (CH),[120] 84.8 (C).[120]

Synthesis of compound 8d: To a solution of TMS-acetylene (2.90 g, 29.5 mmol) in THF (100 mL) at -80 °C *n*-BuLi (20.3 mL of 1.6 M solution in *n*-hexane, 32.4 mmol) was slowly added and the mixture was stirred at -80 °C for 15 minutes. After addition of DMPU (100 mL) and docosyl bromide (**15b**, 9.57 g, 24.6 mmol) the temperature was allowed to rise slowly to rt. Stirring for 16 h at rt, aqueous work-up and drying ($MgSO_4$), deprotection in THF (100 mL) using *n*-$BuNF_4$ (30 mL, 1M solution in THF), removal of the solvent in vacuo and subsequent column chromatography (PE) gave **8d** (6.6 g, 80 %) as a colorless, waxy solid.

8d: ^{1}H NMR: δ = 0.86 (t, J = 6.7 Hz, 3H) 1.15 - 1.40 (m, 38H), 1.51 (m, 2H), 1.91 (t, J = 2.7 Hz, 1H), 2.16 (d of t, J_d = 2.7 Hz, J_t = 7.1 Hz, 2H);

^{13}C NMR: δ = 14.1 (CH_3), 18.4 and 22.7 (2 CH_2), 28.5 - 29.7 (eighteen signals, CH_2), 31.9 (CH_2), 68.0 (CH),[120] 84.8 (C);[120]
$C_{24}H_{46}$ (334.63): calcd. C 86.14, H 13.86; found C 86.17, H 13.87.

The O-trimethylsilyl-tridec-12-yn-1-ol **8b** was synthesized and characterized by Jürgen Thiel following a procedure described by A. Godt.[102]

4.1.3. Synthesis of the 3,5-diiodobenzene derivatives 7b and 7c

The crude diiodophenol **21** was synthesized as described.[104]

O-protection of 21: To a solution of crude **21** (3.30 g, 9.54 mmol) in CH_2Cl_2 (50 mL) were added DHP (3.48 g, 38.17 mmol) and TsOH·H_2O (0.1 g, 0.48 mmol). After stirring overnight at rt the solvent was removed in vacuo and subsequent chromatography (PE/CH_2Cl_2 70/9 v/v) gave **7c** (1.62 g, 40 %) as a white, crystalline solid.

7c: $C_{11}H_{12}I_2O_2$ (430.02): calcd. C 30.72, H 2.81; found C 30.52, H 2.60;
T_m = 57 °C.

The 3,5-diiodotoluene **7b** was synthesized by Sonja Kunert following as described.[103]

7b: $C_7H_6I_2$ (343.92): calcd. C 24.45, H 1.76; found C 24.48, H 1.62.

4.2. Thermal analysis

Thermogravimetry (TGA) was carried out under nitrogen atmosphere using a METTLER-TOLEDO TGA 50 thermobalance. The heating rate was 10 K/min.

Differential scanning calorimetry (DSC) was carried out under nitrogen using a METTLER-TOLEDO DSC TA 3000 calorimeter. The standard heating rate was 10 K/min, unless indicated otherwise.

4.3. *Π-A* isotherms

The surface pressure - area (*Π-A*) isotherms were measured using a computer controlled Lauda film balance placed in a laminar hood. The sample solutions in $CHCl_3$ (2.5 - 6.0 x 10^{-4} M) were spread on the water subphase at 20 °C and the system was allowed to equilibrate for 30 minutes at 5°C. Compound **2a** was spread from a CH_2Cl_2 solution due to the acid lability of the THP ether. The water used had been purified by a Millipore purification system to give a resistance of 18 MΩcm.

4.4. AFM measurements

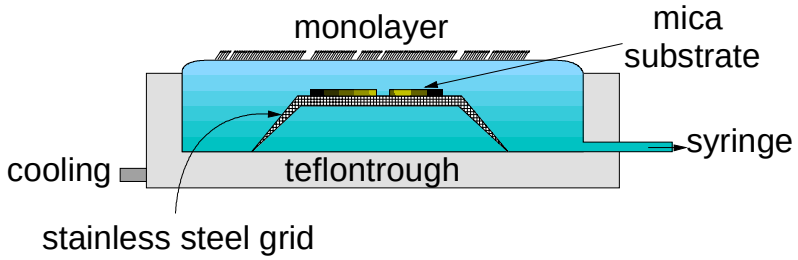

Figure 45. Langmuir trough used for horizontal deposition of the Langmuir films onto freshly cleaved mica substrates.

For AFM measurements the monolayers were transferred onto freshly cleaved mica by the horizontal deposition technique. The mica pieces (1 x 1 cm) were placed on a stainless steel mesh inside a specially designed teflon trough (Figure 45).[123] The trough was filled with water and the sample solutions were spread on the water surface at 20 °C. After equilibrating the system for 30 minutes at 5 °C the resulting

Langmuir monolayers were deposited on the mica by slowly removing the water via a motor-driven syringe. After drying the samples in air the AFM measurements were carried out using a Topometrix TMX 2010 stage with integrated Si_3N_4 pyramidal tips on cantilevers, with force constants between 0.03-0.40 N/m. The applied contact force during imaging exceeded the equilibrium force by 2-5 nN.

4.5. GIXD measurements

Grazing incidence X-ray diffraction (GIXD), a surface sensitive, in-situ analytical method for Langmuir monolayers, is described in detail elsewhere.[31] The GIXD experiments were carried out at the beamline BW1 using the liquid surface diffractometer (Figure 46) at Hasylab synchrotron source, DESY, Hamburg. The sample solutions (2.5 – 6.0 x 10^{-4} M) were spread on the water subphase at 20 °C.

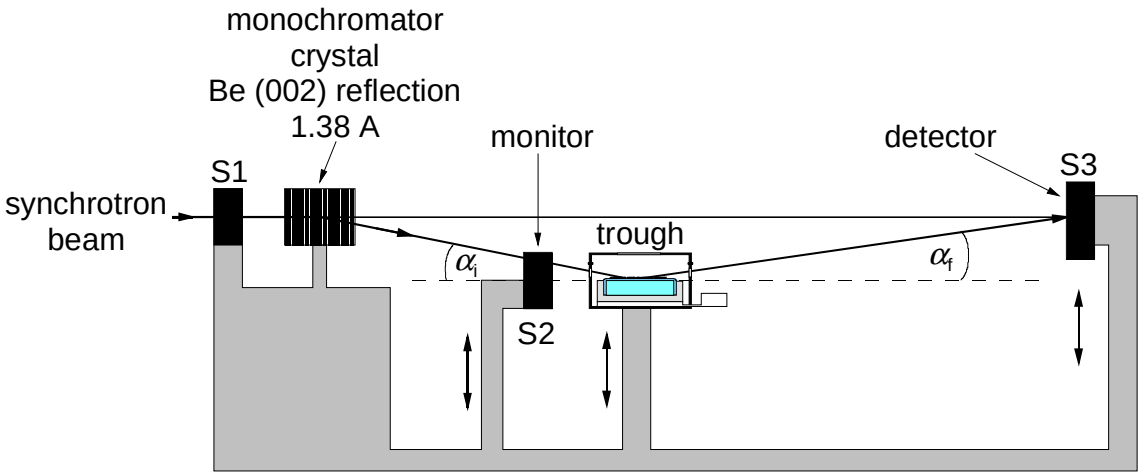

Figure 46. Special GIXD setup at the HASYLAB, DESY; Hamburg. The monochromatic synchrotron beam is striking the air-water interface at an incident angle of $\alpha_i = 0.85\alpha_c = 0.12°$. The diffracted signal is detected by a position sensitive detector (PSD).

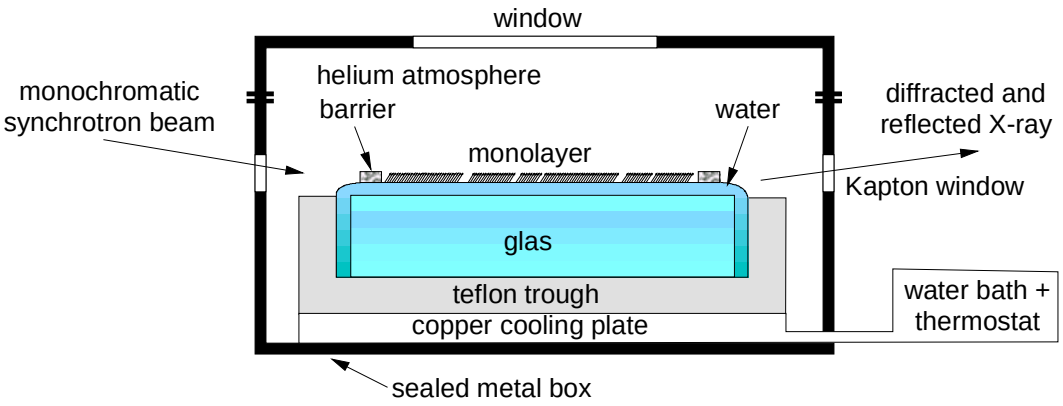

Figure 47. The Langmuir trough of the GIXD setup in Figure 46. The whole trough is surrounded by a metal box which is airtight. After spreading the sample solution, the metal box is closed and flushed with Helium. The monolayer is equilibrated for about 1 hour at 5 °C. GIXD can then be measured and the surface pressure can be adjusted by common barriers.

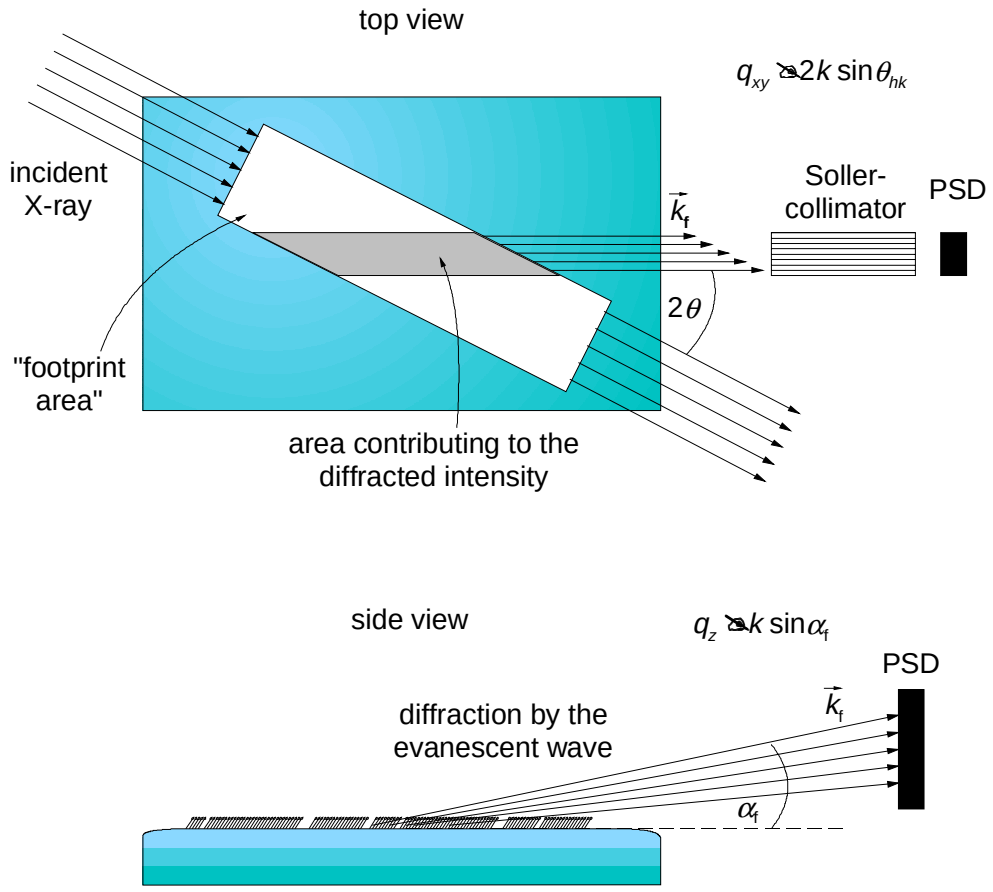

Figure 48. Top and side view of the GIXD scattering geometry at the air-water interface.

The trough (Figure 47), mounted on the diffractometer and equipped with a Wilhelmy balance, was sealed, flushed with Helium and equilibrated at 5 °C for 1 hour. A monochromatic X-ray beam was adjusted to strike the water surface at an incident angle $\alpha_i \approx 0.85\alpha_c$ (where α_c is the critical angle for total external reflection of X-rays for the air-water interface). The dimensions of the footprint of the incoming X-ray beam on the water surface were approximately 2x50 or 5x50 mm^2. The measurements were performed by scanning over a range along the horizontal component of the X-ray scattering vector, $q_{xy} \approx (4\pi/\lambda)\sin(2\theta_{xy}/2)$, $2\theta_{xy}$ being the angle between the projections onto the horizontal plane of the incident and the diffracted beams. The scattered intensity was detected by a position-sensitive detector (PSD) which resolves the vertical component of the X-ray scattering vector, $q_z \approx (2\pi/\lambda)\sin\alpha_f$, (where α_f is the vertical angle between the diffracted beam and the horizon), in the q_z-range 0.00 to 1.40 $Å^{-1}$. The scattering geometry is shown in Figure 48.

The diffraction data may be presented in three ways: (i) the GIXD pattern as a two-dimensional intensity distribution $I(q_{xy}, q_z)$ in a surface or contour plot; (ii) the GIXD pattern $I(q_{xy})$ obtained by integrating over the whole q_z window of the PSD, which yields the Bragg peaks; (iii) the Bragg rod intensity profiles, which are the scattered intensity $I(q_z)$ recorded in channels along the PSD integrated across the q_{xy} range of each Bragg peak. Several different types of information were extracted from the measured GIXD pattern. The $2\theta_{xy}$ (or q_{xy}) positions of the Bragg peaks are used for the calculation of the lattice repeat distances $d = 2\pi/q_{xy}$ and assigning them {h,k} Miller indices yields the unit cell parameters a and b. The vertical full width at half maximum, $FWHM(q_z)$, of the Bragg rod intensity profiles gives an estimate of the thickness $d \approx 0.9(2\pi/FWHM(q_z))$ of the crystalline film on the water surface. The horizontal full width at half maximum of the Bragg peaks $FWHM(q_{xy})$ yields the crystalline coherence lengths $L_{hk} \approx 0.9(2\pi/FWHM(q_{xy}))$.

For long, linear molecules (or for the more complicated molecules which consist mainly of long, straight, parallel hydrocarbon segments), to a first approximation, the tilt angle t of the molecular axis with respect to the normal to the interface, and the horizontal azimuthal direction of the tilt, can be determined[108] from the set of equations: $\cos\psi_{hk}\tan t = q_{z,max}/|(\boldsymbol{q}_{hk})|$, where, for each ($h$,$k$) Bragg rod, ψ_{hk} is the azimuthal angle between the molecular tilt direction projected onto the xy plane and the reciprocal lattice vector $\boldsymbol{q}_{hk}$ and $q_{z,max}$ is the peak position along the Bragg rod.

For more quantitative purposes, the intensity at each q_z value in a Bragg rod intensity profile is given by the square of the molecular structure factor $F_{hk}(q_z)$. Thus, X-ray structure factor calculations were performed using atomic coordinate models to yield $I(q_z)$ values which fit the measured Bragg rod intensity profiles.[49]

4.6. Specular X-ray reflectivity[31]

Specular X-ray reflectivity measurements of a film at the air-water interface may be inverted to give the vertical density-profile across the interface, laterally averaged over all of the film, not just the crystalline part of it. The information gained includes the thickness and the surface roughness of the film. The measurements were carried out at the same liquid surface diffractometer as used for the GIXD experiments. The X-ray reflectivity was performed on the film of molecule **3** at a nominal molecular area of 50 Å^2 by scanning the incident beam angle α_i (equal to the reflected beam angle α_f) from $0.5\alpha_c$ to $42\alpha_c$. The reflected radiation was measured by a NaI scintillation counter. The measured reflectivity is presented in the form of normalized X-ray reflectivity R/R_F (R_F is the Fresnel reflectivity calculated for a perfect, sharp interface) as a function of the normalized vertical scattering vector q_z/q_c, where $q_z = (4\pi/\lambda)\sin\alpha_f$ and q_c is the scattering vector at the critical angle of incidence α_c, $q_c = (4\pi/\lambda)\sin\alpha_c$.

4.7. X-ray structure analysis of the single crystal of 1

The sample (**1**) was crystallized from toluene on slow evaporation. The diffractometer used was Cad 4 and the wavelength was Cu Kα = 1.5418 Å. The determination of the cell was carried out on the basis of the least squares calculating the angles of 25 reflexes with $\theta > 20°$. Of the measured 5605 reflexes only 2120 were classified as “observed” on the basis $I > 3\sigma(I)$. Empirical absorption correction did not have a marked effect. The structure was solved by direct methods using ShelXS. Full matrix least squares was used for refinement with carbons and oxygens having anisotropic temperature factors. Hydrogens were in the riding mode with isotropic temperature factors. The final R values were R = 11.69 % and $R_{weighted}$ = 10.74 %.

5. Appendix

5.1. Crystallographic data extracted from the GIXD measurements on the monolayers of compounds 2a, 2b, 3 and 5

Table 1. Assignment of the GIXD data measured for the monolayer of compounds **2a**, calculated unit cell parameters and crystalline coherence lengths $L_{h,k}$.

	α-phase rectangular subcell		β-phase oblique subcell	
{*h*, *k*} Miller index for subcell	q_{xy} [Å^{-1}]	$q_{z,max}$ [Å^{-1}]	q_{xy} [Å^{-1}]	$q_{z,max}$ [Å^{-1}]
{0,2}$_\alpha$	1.445	0.00		
{1,1} + {1,-1}$_\alpha$	1.245	0.87		
{1,-1}$_\beta$			1.510	0.15
{0,1}$_\beta$			1.545	0.63
{1,0}$_\beta$			1.420	0.77
a_s [Å]	6.20		5.06 ($a_{s,\ oblique}$)	
b_s [Å]	8.70		4.65 ($b_{s,\ oblique}$)	
γ_s [°]	90		118.9	
molecular tilt angle *t* [°]	41 (along *a*)		29.5 (along $a_{pseudo\text{-}rectangular}$)	
area per chain [Å^2]	27.0		20.9	
projected area per chain [Å^2]	20.4		18.0	
L [Å]	$L_{1,0}$ = 100, $L_{0,1}$ = 180		$L_{1,0}$ = 80, $L_{0,1}$ = 50, $L_{1,-1}$ = 150	
a; (a_p) [Å]	6.20; (4.68)		4.95[a]; (4.30)	
b [Å]	17.40		16.73[a]	
γ [°]	90		95.5[a]	

[a] For the oblique β-phase, a_s and b_s, were converted into the pseudo-rectangular unit cell dimensions *a* and *b* calculating $\boldsymbol{a} = (\boldsymbol{a_s} + \boldsymbol{b_s})$ and $\boldsymbol{b} = 2(\boldsymbol{b_s} - \boldsymbol{a_s})$.[94]

Table 2. Assignment of the GIXD data measured for the monolayer of compound **2b**, calculated unit cell parameters and crystalline coherence lengths $L_{h,k}$.

	α-phase rectangular subcell		β-phase oblique subcell	
{*h*, *k*} Miller index for subcell	q_{xy} [Å^{-1}]	$q_{z,\max}$ [Å^{-1}]	q_{xy} [Å^{-1}]	$q_{z,\max}$ [Å^{-1}]
$\{0,2\}_{\alpha}$	1.440	0.00		
$\{1,1\} + \{1,-1\}_{\alpha}$	1.220	0.90		
$\{1,-1\}_{\beta}$			1.505	0.07
$\{0,1\}_{\beta}$			1.480	0.76
$\{1,0\}_{\beta}$			1.385	0.82
a_s [Å]	6.38		5.08 ($a_{s,\text{ oblique}}$)	
b_s [Å]	8.73		4.75 ($b_{s,\text{ oblique}}$)	
γ_s [°]	90		116.7	
molecular tilt angle *t* [°]	42 (along *a*)		33 (along $a_{\text{pseudo-rectangular}}$)	
area per chain [Å^2]	27.9		21.5	
projected area per chain [Å^2]	20.7		18.0	
L [Å]	$L_{1,0}$ = 100, $L_{0,1}$ = 200		$L_{1,0}$ = 70, $L_{0,1}$ = 40, $L_{1,-1}$ = 160	
a; (a_p) [Å]	6.38; (4.74)		5.16[a]; (4.33)	
b [Å]	17.46		16.74[a]	
γ [°]	90		94.3[a]	

[a] For the oblique β-phase, a_s and b_s, were converted into the pseudo-rectangular unit cell dimensions *a* and *b* calculating $\boldsymbol{a} = (\boldsymbol{a_s} + \boldsymbol{b_s})$ and $\boldsymbol{b} = 2(\boldsymbol{b_s} - \boldsymbol{a_s})$.[94]

Table 3. Assignment of the GIXD data measured for the monolayer of compound **3**, calculated unit cell parameters and crystalline coherence lengths $L_{h,k}$.

	α-phase		β-phase	
{*h*, *k*} Miller index for subcell	q_{xy} [Å^{-1}]	$q_{z,max}$ [Å^{-1}]	q_{xy} [Å^{-1}]	$q_{z,max}$ [Å^{-1}]
{0,2}	1.445	0	1.516	0
{1,1} + {1,-1}	1.205	0.90	1.445	0.73
a_s; (a_p) [Å]	6.52; (4.77)		5.11; (4.39)	
$b_s = b_p$ [Å]	8.70		8.29	
γ [°]	90		90	
molecular tilt angle *t* [°]	43 (along *a*)		30.7 (along *a*)	
area per chain[a] [Å^2]	28.4		21.2	
projected area per chain[b] [Å^2]	20.7		18.2	
L [Å]	$L_{1,0}$ = 110, $L_{0,1}$ = 200		$L_{1,0}$ = 70, $L_{0,1}$ = 180	
$a = a_s$ [Å]	6.52		5.11	
$b = 2b_s$ [Å]	17.40		16.58	

[a] area per chain = $0.5a_sb_s$.
[b] projected area per chain = $0.5a_pb_p = 0.5a_sb_s\cos t$, where $a_p = a_s\cos t$.

Table 4. Assignment of the GIXD data measured for the monolayer of compound **5** and calculated unit cell parameters of the crystalline α-phase.

{*h*, *k*} Miller index for subcell	70 Å^2 per molecule		50 Å^2 per molecule		38 Å^2 per molecule	
	q_{xy} [Å^{-1}]	$q_{z,max}$ [Å^{-1}]	q_{xy} [Å^{-1}]	$q_{z,max}$ [Å^{-1}]	q_{xy} [Å^{-1}]	$q_{z,max}$ [Å^{-1}]
{0,2}	1.455	0.74	1.466	0.72	1.570	0.50
{1,1} + {1,-1}	1.445	0.35	1.448	0.36	1.480	0.25
a (a_p) [Å]	5.03 (5.03)		5.03 (5.03)		5.00 (5.00)	
b (b_p) [Å]	8.64 (7.76)		8.57 (7.70)		8.00 (7.61)	
γ [°]	90		90		90	
molecular tilt angle *t* [º]	26 (along *b*)		26 (along *b*)		18 (along *b*)	
area per chain [Å^2]	21.73		21.55		20.00	
projected area per chain [Å^2]	19.52		19.37		19.05	

5.2. Fitted parameters[a] of the two-box model of electron density corresponding to the calculated reflectivity curve for the monolayer of molecules 4

compound	no. of boxes	*%cov*	*A* [Å^2]	ρ_1/ρ_W	L_1 [Å]	ρ_2/ρ_W	L_2 [Å]	L_T [Å]	σ[Å]
4	2	80	39.5	1.02	26.3	1.01	5.5	31.8	3.0

[a] *%cov* is the surface coverage of the monolayer. *A* is the area occupied by one molecule. ρ_W = 0.334 e/Å^3 is the electron density of the water subphase and ρ_1 (N_1 = 354) and ρ_2 (N_2 = 72, with *N* being the number of electrons) are the electron densities of boxes 1 and 2, respectively, given by $\rho_j = N_j /AL_j$ where L_1, L_2 are the lengths of the corresponding boxes. The total length is $L_T = L_1 + L_2$. σ is the surface roughness parameter.

5.3. Derivation of the pseudo-rectangular subcell

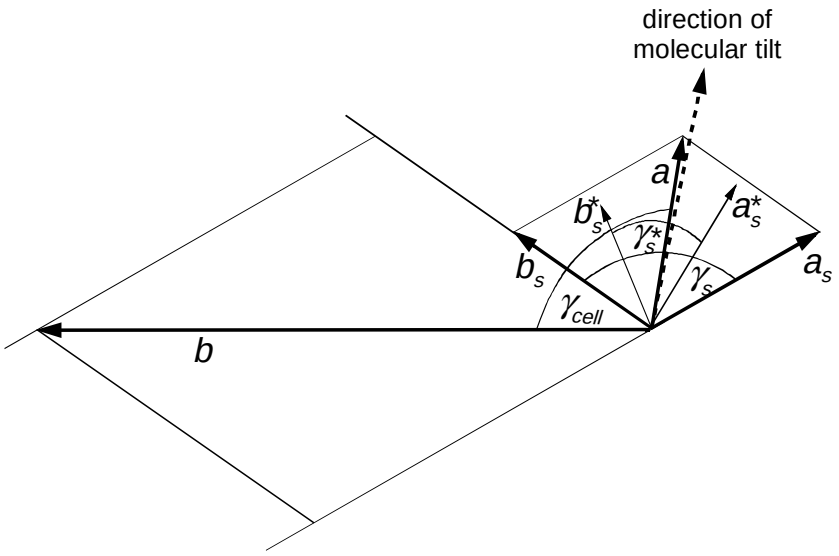

q_{xy}	q_z	{h k}			$d_{hk}^* = q_{hk}/2\pi$
1.505	0.07	{1 -1}	a_s = 5.08 Å		0.2395281
1.480	0.76	{0 1}	b_s = 4.75 Å		0.2355493
1.385	0.82	{1 0}	γ_s^* = 63.275°	$\cos\gamma_s^* = \frac{d_{01}^{*2} - d_{1\,-1}^{*2} + d_{10}^{*2}}{2 d_{01}^* d_{10}^*}$	0.2204296
			γ_s = 116.725°		

$\boldsymbol{a} = |\boldsymbol{a_s} + \boldsymbol{b_s}| = 5.16$ Å

$\boldsymbol{b} = |2(\boldsymbol{b_s} - \boldsymbol{a_s})| = 2 \times 8.37$ Å $= 16.74$ Å

$\sphericalangle(\boldsymbol{a_s}, \boldsymbol{a_s} + \boldsymbol{b_s}) = 55.27°$

$\tan t \cos\psi_{1\,-1} = 0.07/1.505$

$\tan t \cos\psi_{01} = 0.76/1.480$, $(\psi_{01} = \gamma_s^* - \psi_{10})$

$\tan t \cos\psi_{10} = 0.82/1.385$

$\tan t \cos\psi_{10} = 0.5920578$

$\tan t \cos(\gamma_s^* - \psi_{10}) = 0.5135135$

$$\frac{\cos\psi_{10}}{\cos(\gamma_s^* - \psi_{10})} = 1.1529549$$

for $\psi_{10} = 25°$ $\quad \frac{\cos\psi_{10}}{\cos(63.275° - 25°)} = 1.15446$

$\sphericalangle(\boldsymbol{a}, \boldsymbol{a_s}) = 55.27°$

$\sphericalangle(\boldsymbol{a_s^*}, \boldsymbol{a_s}) = 26.725°$

$\sphericalangle(\boldsymbol{a}, \boldsymbol{a_s^*}) = 55.27° - 26.725° = 28.545°$

$\sphericalangle(\boldsymbol{t}, \boldsymbol{a_s^*}) = 25°$

$\sphericalangle(\boldsymbol{t}, \boldsymbol{a}) = 3.545°$

$\tan t = 0.65326$

$t = 33.155°$

5.4. The fitting program and the Bragg rod fitting procedure on one example

5.4.1. The fitting program

The fitting program, BRUXUZ, for Bragg rods obtained from GIXD measurements in this work was written by Franck Leveiller and Didier Jacquemain at the Weizmann Institute of Science, Rehovot, Israel. The program calculates, using an atomic coordinate molecular model, Bragg rod intensity profiles, $I_{hk}(q_z)$, from two-dimensional films composed of amphiphilic molecules (for maximally 10 peaks consisting of one or several combined reflections) and compares them to the observed $I_{hk}(q_z)$ data. This program may generally be used to elucidate and to refine the two-dimensional crystalline structures of amphiphilic molecules at the air-water interface.[49,69,124] In monolayer systems, the number of distinct Bragg reflections is generally low and the Bragg rods themselves may not show much intensity variation along the profile. Thus, from the few data available only a few parameters can be meaningfully fitted. For this reason a rigid body refinement of the two-dimensional structure is performed, in other words, one uses molecules in a fixed molecular conformation. The molecular orientation is then refined varying the three Eulerian angles (ω, t and ϕ).[125] Positional refinement involves only little translation along the x and y directions, depending on the crystal symmetry.[49,126] For a given molecular model, BRUXUZ provides output files of the fitted $I_{hk}(q_z)$ profiles as well as of the corresponding packing arrangement. To help refining the structure, BRUXUZ also generates a reliability index map (R_W map) of the fit of the observed to the calculated $I_{hk}(q_z)$ data by applying successive rotations and translations to the molecules in the unit cell (i.e. varying the parameters ω, t, ϕ, Δx and Δy).

In the program, the variation of the intensity $I_{hk}(q_z)$ along the Bragg rod as a function of q_z is calculated using equation (1):

$$I_{hk}(q_z) = \mathrm{K} \times L \times P \times A_{ABCD} \times A_{\mathrm{cell}}^{-2} \times V(q_z) \times \left|F_{hk}(q_z)\right|^2 \times DW_{hk}(q_z) \qquad (1)$$

The observed $I_{hk}(q_z)$ data is a sum over those (h,k) reflections whose Bragg rods coincide at a particular horizontal 2θ angle (or q_{xy} position). In equation (1) the

most important contribution comes from the molecular structure factor amplitude $F_{hk}(q_z)^2$. The structure factor F_{hk} is given by:

$$F_{hk}(q_z) = \sum_j f_j e^{i \mathbf{q}_{hk} \cdot \mathbf{r}_j} e^{i q_z z_j} \qquad (2)$$

The sum is over atoms j in the unit cell of dimensions a, b. The j^{th} atom has the scattering factor f_j and is located at the lateral vector position $\mathbf{r_j} = x_j\mathbf{a} + y_j\mathbf{b}$ and at the vertical position z_j (in Å). Anomalous dispersion causes the scattering factor to be complex and it can only be presented by

$$f_{0,anomalous} = f_0 + f' + \mathrm{i}f'' \qquad (3)$$

where f_0 is the normal scattering factor, f' is a real correction term (usually negative), and f'' is the imaginary component.

The Debye-Waller factor is given by $DW_{hk}(q_z) = \exp -(q_{hk}^2 U_{xy} + q_z^2 U_z)$, where U_{xy} and U_z are the mean square displacements in each horizontal direction x, y and along the vertical direction z, respectively. They account for the thermal motion of the atoms[127,128] in the molecule, as well as for possible ripples on the water surface, which lead to roughness of the interface.[41,42,129]

The grazing geometry factor $V(q_z)$ describes the interference of rays diffracted upwards with rays, which are diffracted down and subsequently reflected back upwards by the monolayer-water interface.[36] $V(q_z)$ differs from unity only when $q_z = q_c/2$ and, in this case, contributes to a sharp peak. Explicitly, the grazing geometry factor $V(q_z)$ is a function of $n = 2q_z/q_c$, where $q_c = (4\pi/\lambda)\sin\alpha_c = 0.021764$ Å^{-1}:

$$V(n) = 2n \qquad \text{for } 0 < n < 1$$

and

$$V(n) = 2n/[n + (n^2 - 1)^{1/2}] \qquad \text{for } n > 1$$

In equation (1) the corrections for the crossed beam area ($A_{ABCD} \propto 1/\sin(2\theta_{hk})$), Lorentz factor ($L \propto 1/\sin(2\theta_{hk})$) and polarization factor ($P = \cos^2 q_{hk}$) have been inserted. A_{cell} is the area of the unit cell. The factor K is normally a constant for any

given set of measurements and mainly depends on the crystallite size, beam intensity, and a number of fundamental constants. It scales the calculated to the observed intensity. Due to the sharpness of the peak at the vicinity $q_z = q_c/2$ there are large uncertainties concerning intensities measured close to this q_z value. Thus, only intensities recorded for $q_z \geq 0.023$ Å^{-1} are used in the calculation of K.

A measure of the correctness of the model structure may be calculated, as for three-dimensional crystal structures, from the weighted reliability index R_{weighted} of the fit of the observed to the calculated Bragg rod data:

$$R_{\text{weighted}} = \frac{\sum_{hk\,q_z} w \left| I_0(q_z) - I_{\text{calc}}(q_z) \right|}{\sum_{hk\,q_z} w\, I_0(q_z)} \qquad (5)$$

where I_0 and I_{calc} are the observed and the calculated intensities and $w = 1/\sigma(I_0)$, where $\sigma(I_0)$ is the estimated standard deviation of I_0. The summation is over all the observed intensities of all the measured *hk* Bragg rod profiles.

5.4.2. Fitting of the calculated Bragg rod intensity profiles to the measured, deconvoluted profiles (cf. Figure 36) for the monolayer of 6 at a nominal molecular area of 200 Å^2

The starting point of the fitting procedure is the construction of a molecular model of an aliphatic chain containing 17 CH_2 groups in the CERIUS^2 computer program. This chain is minimized in its energy and is the basis of the molecular model. The Eulerian angles were specified according to the conventions of Goldstein[125] but with ω, t, and ϕ standing for the angles φ, θ, and ψ, respectively. ω is the rotation angle of the molecule about the vertical axis, t is, as defined previously, the tilt angle of the chain from the vertical, and ϕ is the rotation angle of the chain about its long axis or, in other words, the rotation angle of the backbone of the chain. Starting from $\omega = t = \phi = 0$, the three angles are optimized for the given model. The best fit for this model is the one with the lowest R_w value. The first step was the selection of the symmetry operation for the two chains in the subcell. Relating the two chains by translation gave the best R_w value.

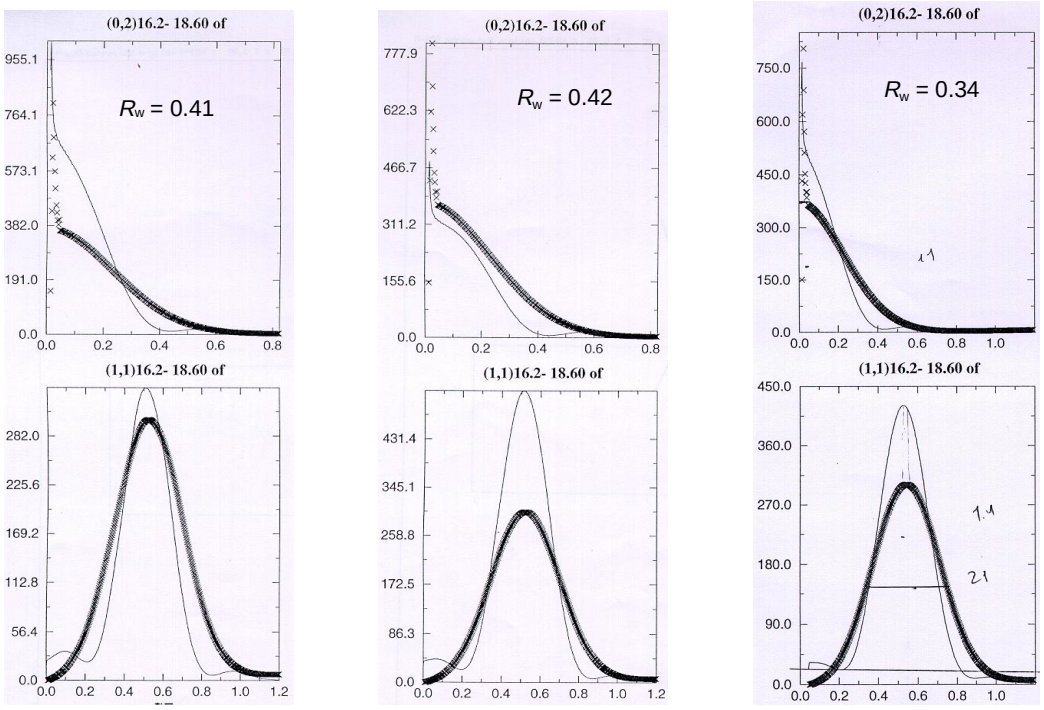

17 CH_2 per chain — *b*-glide ⊥ to *a* — x y z; 0.5-x, 0.5+y, z

17 CH_2 per chain — *a*-glide ⊥ to *b* — x y z; 0.5+x, 0.5-y, z

17 CH_2 per chain — translation — x y z; 0.5+x, 0.5+y, z

After having found that the two chains in the subcell are related by translation one now had to consider the fact that the full widths at half maximum (*FWHM*) of the measured $I(q_z)$ profiles are larger than the *FWHM* of the fitted Bragg rods. This indicates that the thickness of the crystalline part is smaller than assumed, i.e. less than 17 CH_2 groups are contributing to the diffraction signal. Despite this observation, in the following step the remaining parts of molecule **6** were constructed, minimized in their energy and edited to the initial model of the chains. The result was still a reasonable fit but the peak positions were slightly altered. Yet, there was no change in the fit of the *FWHM*. In order to improve this fit, selected parts of the model of the complete molecule **6** were gradually given zero occupancy, as described in the text below each graph **A** - **G**.

The best and final fit (graph **I**) was eventually obtained from a model of molecule **6** with only the central 12 CH_2 groups of the chains of **6** contributing to the diffraction signal. The calculated $I(q_z)$ profiles fitted the measured data very well (R_w = 0.15). The molecular packing according to this fit is shown in a view along the chain axis. It is this atomic coordinate molecular model, that is superimposed on the model of molecule **6** in Figure 37 in chapter 2.3.2. Continuing the procedure and considering only chains of 11 CH_2 groups (graph **G**) results in a worse fit of the calculated data.

In principle, one may now go back to the beginning of the fitting procedure and question, whether relating the two chains in the subcell by glide symmetry would also give a good fit of the calculated data. Doing so results in a worse fit and even in a shift in the peak position of the calculated data, as one can clearly see in graph **H**.

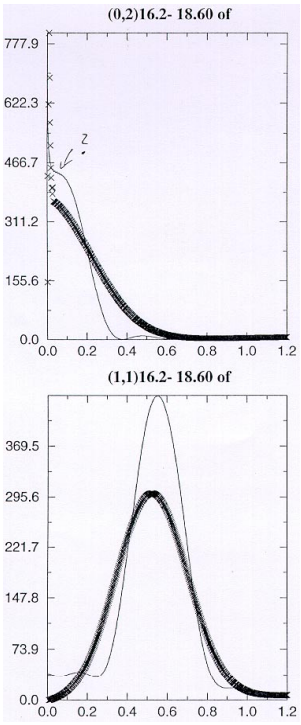

complete molecule **6**

A

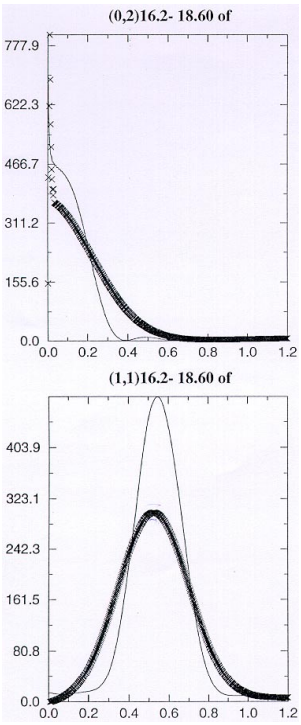

molecule **6** without:
2 top spacer units

B

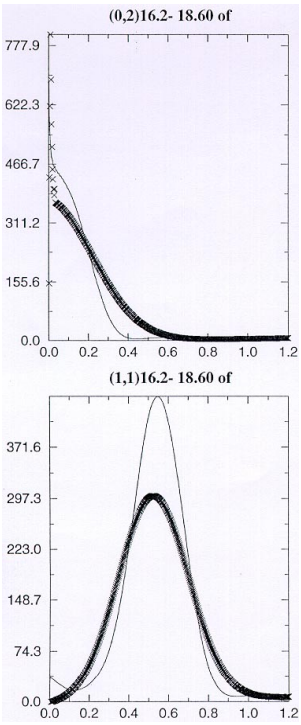

molecule **6** without:
2 top spacer units
2x$(CH_2)_4$ from bottom

C

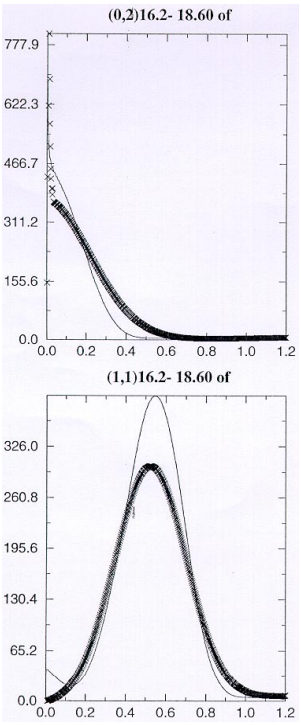

molecule **6** without:
2 top spacer units
2x$(CH_2)_4$ from bottom
4x$(CH_2)_3$ from top

D

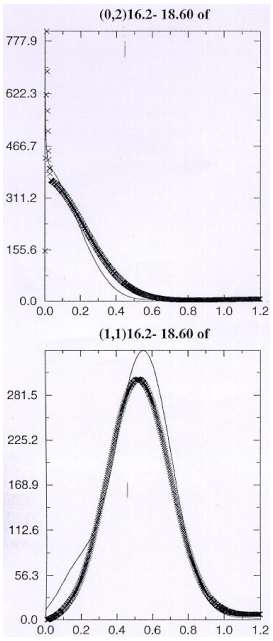

molecule **6** without:
2 top spacer units
4x$(CH_2)_6$ from top

E

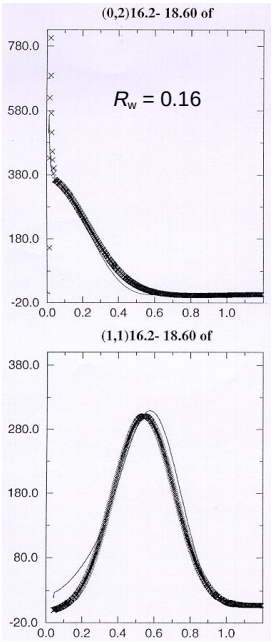

molecule **6** without:
2 top spacer units
2x$(CH_2)_4$ from bottom
4x$(CH_2)_6$ from top

i.e. 13 CH_2 per chain

F

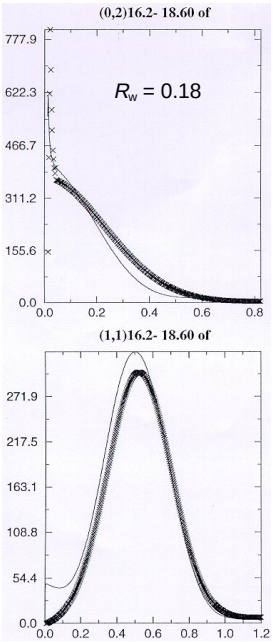

molecule **6** without:
2 top spacer units
2x$(CH_2)_4$ from bottom
4x$(CH_2)_2$ from bottom
4x$(CH_2)_6$ from top

i.e. 11 CH_2 per chain

G

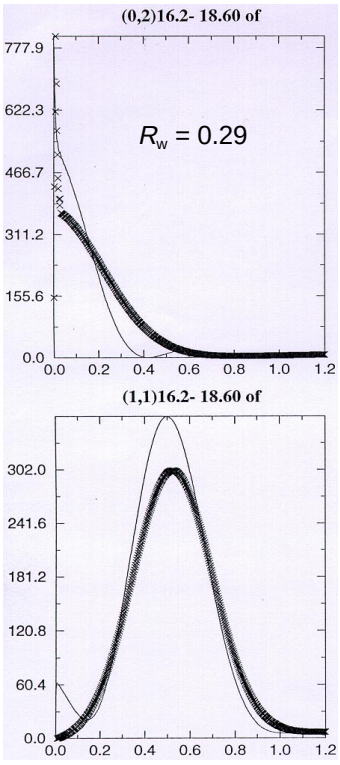

a-glide ⊥ to *b*
12 CH_2 per chain

H

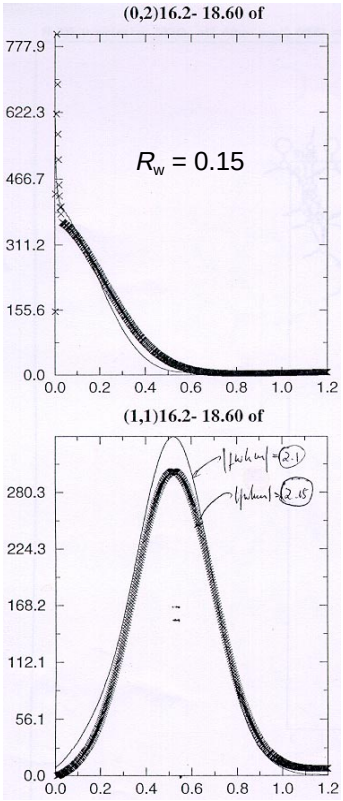

translation
12 CH_2 per chain

FINAL FIT !

I

t = 25° along *a* axis

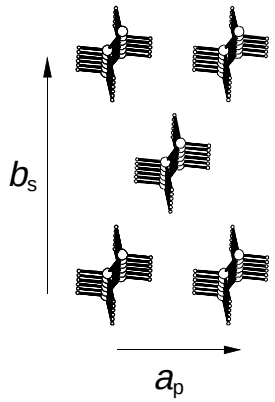

atomic coordinate molecular model of the crystalline part of the self-assembled monolayer of **6** viewed along the chain axis

5.5. Data of the single crystal structure analysis of compound 1

The structure is triclinic and the space group is P-1. The unit cell parameters are a = 9.4 Å, b = 10.3 Å, c = 34.8 Å, α = 96.9°, β = 90.9° and γ = 113.1°.

Table 1. Atomic coordinates, isotropic temperature factor and occupancy for the single crystal structure of compound **1** (Figure 41).

atom	*x*/*a*	*y*/*b*	*z*/*c*	*U*(iso)	occupancy
C(1)	0.384(3)	-0.357(3)	0.4953(6)	0.0797	
C(3)	0.216(2)	-0.455(2)	0.4375(6)	0.0692	
C(5)	0.488(2)	-0.357(2)	0.4303(5)	0.0358	
C(8)	0.054(2)	-0.524(2)	0.4145(4)	0.0182	
C(9)	-0.078(2)	-0.587(2)	0.3939(5)	0.0223	
C(21)	0.621(3)	-0.343(3)	0.4050(7)	0.0980	
C(22)	0.749(2)	-0.300(3)	0.3875(7)	0.0962	
C(20)	0.334(2)	-0.341(2)	0.0485(4)	0.0500	
O(2)	1.403(2)	0.063(2)	0.0334(5)	0.0982	
O(101)	0.345(3)	-0.374(3)	0.0105(7)	0.060(6)	0.5000
O(102)	0.200(3)	-0.326(3)	0.0297(7)	0.060(6)	0.5000
C(2)	0.234(3)	-0.443(2)	0.4792(5)	0.0661	
C(4)	0.342(2)	-0.426(2)	0.4124(4)	0.0304	
C(6)	0.505(2)	-0.348(2)	0.4725(5)	0.0631	
H(21)	0.148(3)	-0.483(2)	0.4942(5)	0.0835	
H(41)	0.326(2)	-0.452(2)	0.3850(4)	0.0440	
H(61)	0.605(2)	-0.323(2)	0.4841(5)	0.0863	
C(7)	0.417(2)	-0.323(2)	0.5366(4)	0.0332	
H(71)	0.525(2)	-0.269(2)	0.5423(4)	0.0526	
H(72)	0.385(2)	-0.408(2)	0.5482(4)	0.0526	
H(73)	0.362(2)	-0.267(2)	0.5465(4)	0.0526	
C(10)	-0.206(2)	-0.650(2)	0.3701(5)	0.0782	
H(101)	-0.280(2)	-0.723(2)	0.3820(5)	0.0797	
H(102)	-0.246(2)	-0.581(2)	0.3656(5)	0.0797	
C(11)	-0.166(2)	-0.707(2)	0.3324(3)	0.0500	
H(111)	-0.107(2)	-0.761(2)	0.3375(3)	0.0188	
H(112)	-0.259(2)	-0.767(2)	0.3177(3)	0.0188	
C(12)	-0.071(2)	-0.590(2)	0.3091(4)	0.0248	
H(121)	0.030(2)	-0.541(2)	0.3215(4)	0.0389	
H(122)	-0.121(2)	-0.526(2)	0.3083(4)	0.0389	
C(13)	-0.056(2)	-0.650(2)	0.2670(4)	0.0238	
H(131)	-0.009(2)	-0.717(2)	0.2680(4)	0.0288	
H(132)	-0.156(2)	-0.698(2)	0.2545(4)	0.0288	
C(14)	0.032(2)	-0.539(2)	0.2433(5)	0.0470	
H(141)	0.138(2)	-0.508(2)	0.2520(5)	0.0599	
H(142)	0.001(2)	-0.461(2)	0.2478(5)	0.0599	
C(15)	0.026(2)	-0.585(2)	0.1993(5)	0.0723	
H(151)	0.045(2)	-0.670(2)	0.1944(5)	0.0768	
H(152)	-0.075(2)	-0.603(2)	0.1893(5)	0.0768	
C(16)	0.145(3)	-0.461(3)	0.1797(6)	0.0919	
H(161)	0.247(3)	-0.440(3)	0.1900(6)	0.1199	

H(162)	0.125(3)	-0.376(3)	0.1835(6)	0.1199	
C(17)	0.128(3)	-0.519(3)	0.1358(6)	0.0870	
H(171)	0.155(3)	-0.600(3)	0.1325(6)	0.0984	
H(172)	0.024(3)	-0.548(3)	0.1267(6)	0.0984	
C(18)	0.221(2)	-0.413(2)	0.1117(5)	0.0603	
H(181)	0.313(2)	-0.355(2)	0.1272(5)	0.0900	
H(182)	0.168(2)	-0.356(2)	0.1056(5)	0.0900	
C(19)	0.268(2)	-0.471(2)	0.0714(6)	0.0741	
H(191)	0.347(2)	-0.503(2)	0.0761(6)	0.0756	
H(192)	0.181(2)	-0.547(2)	0.0578(6)	0.0756	
C(23)	0.884(3)	-0.248(3)	0.3625(7)	0.1406	
H(231)	0.928(3)	-0.316(3)	0.3560(7)	0.1739	
H(232)	0.961(3)	-0.161(3)	0.3747(7)	0.1739	
C(24)	0.806(3)	-0.223(3)	0.3228(6)	0.0835	
H(241)	0.725(3)	-0.309(3)	0.3111(6)	0.1024	
H(242)	0.767(3)	-0.151(3)	0.3286(6)	0.1024	
C(25)	0.948(2)	-0.172(2)	0.2977(5)	0.0441	
H(251)	1.032(2)	-0.097(2)	0.3125(5)	0.0554	
H(252)	0.976(2)	-0.251(2)	0.2901(5)	0.0554	
C(26)	0.907(3)	-0.118(3)	0.2593(6)	0.0838	
H(261)	0.902(3)	-0.028(3)	0.2659(6)	0.0956	
H(262)	0.811(3)	-0.185(3)	0.2470(6)	0.0956	
C(27)	1.044(2)	-0.095(2)	0.2331(5)	0.0387	
H(271)	1.140(2)	-0.032(2)	0.2464(5)	0.0458	
H(272)	1.046(2)	-0.187(2)	0.2261(5)	0.0458	
C(28)	1.015(3)	-0.042(3)	0.1965(6)	0.1024	
H(281)	0.989(3)	0.038(3)	0.2038(6)	0.1184	
H(282)	0.932(3)	-0.114(3)	0.1804(6)	0.1184	
C(29)	1.161(3)	0.003(3)	0.1721(7)	0.1070	
H(291)	1.242(3)	0.080(3)	0.1875(7)	0.1583	
H(292)	1.191(3)	-0.075(3)	0.1664(7)	0.1583	
C(30)	1.133(3)	0.055(3)	0.1339(6)	0.0843	
H(301)	1.119(3)	0.142(3)	0.1400(6)	0.1114	
H(302)	1.041(3)	-0.017(3)	0.1209(6)	0.1114	
C(31)	1.263(3)	0.085(4)	0.1065(7)	0.1270	
H(311)	1.349(3)	0.170(4)	0.1162(7)	0.1744	
H(312)	1.292(3)	0.006(4)	0.1043(7)	0.1744	
C(32)	1.212(3)	0.098(3)	0.0671(7)	0.1192	
H(321)	1.147(3)	0.006(3)	0.0539(7)	0.1290	
H(322)	1.155(3)	0.157(3)	0.0702(7)	0.1290	
C(33)	1.361(3)	0.172(3)	0.0417(9)	0.1123	
H(331)	1.437(3)	0.254(3)	0.0566(9)	0.1784	
H(332)	1.334(3)	0.196(3)	0.0180(9)	0.1784	
C(41)	-0.112(2)	0.118(2)	0.4934(4)	0.0224	
C(43)	-0.002(2)	0.120(2)	0.4340(5)	0.0409	
C(45)	-0.273(1)	0.035(2)	0.4349(4)	0.0119	
C(48)	0.126(2)	0.165(2)	0.4093(4)	0.0305	
C(49)	0.239(2)	0.209(2)	0.3893(4)	0.0293	
C(61)	-0.409(2)	-0.019(2)	0.4161(5)	0.0782	
C(62)	-0.536(1)	-0.084(2)	0.3964(5)	0.0418	
C(73)	-0.206(4)	0.168(4)	0.040(1)	0.1468	
O(11)	0.879(2)	0.752(2)	0.0169(5)	0.1237	
O(121)	-0.271(7)	0.230(6)	0.039(2)	0.10(1)	0.3300
O(122)	-0.070(6)	0.263(5)	0.062(1)	0.10(1)	0.3300
O(123)	-0.145(6)	0.119(6)	0.013(1)	0.10(1)	0.3300
C(42)	0.021(2)	0.167(2)	0.4724(4)	0.0500	

C(44)	-0.147(2)	0.065(2)	0.4144(5)	0.0623
C(46)	-0.256(2)	0.071(2)	0.4737(5)	0.0307
H(421)	0.121(2)	0.222(2)	0.4848(4)	0.0359
H(441)	-0.156(2)	0.042(2)	0.3870(5)	0.1022
H(461)	-0.344(2)	0.060(2)	0.4879(5)	0.0642
C(47)	-0.102(3)	0.134(3)	0.5390(5)	0.1022
H(471)	-0.204(3)	0.098(3)	0.5479(5)	0.1110
H(472)	-0.050(3)	0.232(3)	0.5493(5)	0.1110
H(473)	-0.047(3)	0.082(3)	0.5476(5)	0.1110
C(50)	0.361(1)	0.248(2)	0.3639(4)	0.0500
H(501)	0.442(1)	0.332(2)	0.3767(4)	0.0239
H(502)	0.396(1)	0.173(2)	0.3596(4)	0.0239
C(51)	0.328(2)	0.283(2)	0.3266(5)	0.0420
H(511)	0.275(2)	0.345(2)	0.3302(5)	0.0604
H(512)	0.263(2)	0.196(2)	0.3111(5)	0.0604
C(52)	0.465(3)	0.347(3)	0.3046(7)	0.1027
H(521)	0.522(3)	0.440(3)	0.3178(7)	0.1388
H(522)	0.526(3)	0.292(3)	0.3048(7)	0.1388
C(53)	0.428(2)	0.363(2)	0.2631(5)	0.0437
H(531)	0.361(2)	0.412(2)	0.2630(5)	0.0653
H(532)	0.377(2)	0.269(2)	0.2495(5)	0.0653
C(54)	0.569(3)	0.428(3)	0.2396(6)	0.1140
H(541)	0.622(3)	0.522(3)	0.2533(6)	0.1211
H(542)	0.636(3)	0.379(3)	0.2387(6)	0.1211
C(55)	0.529(2)	0.456(2)	0.1994(5)	0.0509
H(551)	0.493(2)	0.531(2)	0.2004(5)	0.0844
H(552)	0.447(2)	0.368(2)	0.1898(5)	0.0844
C(56)	0.653(2)	0.487(2)	0.1730(5)	0.0598
H(561)	0.744(2)	0.561(2)	0.1857(5)	0.0830
H(562)	0.671(2)	0.402(2)	0.1669(5)	0.0830
C(57)	0.621(2)	0.530(2)	0.1352(5)	0.0631
H(571)	0.593(2)	0.609(2)	0.1409(5)	0.0860
H(572)	0.537(2)	0.453(2)	0.1207(5)	0.0860
C(58)	0.760(2)	0.574(2)	0.1104(5)	0.0381
H(581)	0.849(2)	0.634(2)	0.1270(5)	0.0628
H(582)	0.773(2)	0.490(2)	0.1000(5)	0.0628
C(59)	0.748(2)	0.651(2)	0.0747(4)	0.0286
H(591)	0.746(2)	0.740(2)	0.0847(4)	0.0389
H(592)	0.655(2)	0.595(2)	0.0590(4)	0.0389
C(60)	0.878(2)	0.678(3)	0.0508(5)	0.0161
H(601)	0.969(2)	0.736(3)	0.0667(5)	0.0768
H(602)	0.881(2)	0.588(3)	0.0418(5)	0.0768
C(63)	-0.697(2)	-0.166(2)	0.3706(4)	0.0365
H(631)	-0.766(2)	-0.239(2)	0.3838(4)	0.0650
H(632)	-0.742(2)	-0.099(2)	0.3671(4)	0.0650
C(64)	-0.670(3)	-0.228(3)	0.3283(6)	0.1235
H(641)	-0.767(3)	-0.290(3)	0.3150(6)	0.1583
H(642)	-0.608(3)	-0.280(3)	0.3314(6)	0.1583
C(65)	-0.591(3)	-0.108(3)	0.3051(6)	0.0950
H(651)	-0.657(3)	-0.061(3)	0.3009(6)	0.1378
H(652)	-0.499(3)	-0.043(3)	0.3196(6)	0.1378
C(66)	-0.557(4)	-0.163(3)	0.2650(7)	0.1219
H(661)	-0.645(4)	-0.239(3)	0.2520(7)	0.1803
H(662)	-0.477(4)	-0.195(3)	0.2687(7)	0.1803
C(67)	-0.484(3)	-0.032(3)	0.2410(5)	0.0800
H(671)	-0.568(3)	-0.007(3)	0.2343(5)	0.1053

H(672)	-0.404(3)	0.049(3)	0.2551(5)	0.1053
C(68)	-0.432(2)	-0.089(2)	0.2026(4)	0.0416
H(681)	-0.509(2)	-0.177(2)	0.1901(4)	0.0609
H(682)	-0.341(2)	-0.103(2)	0.2089(4)	0.0609
C(69)	-0.390(2)	0.028(2)	0.1760(4)	0.0124
H(691)	-0.481(2)	0.045(2)	0.1714(4)	0.0512
H(692)	-0.310(2)	0.114(2)	0.1884(4)	0.0512
C(70)	-0.341(2)	-0.020(2)	0.1363(4)	0.0468
H(701)	-0.424(2)	-0.098(2)	0.1223(4)	0.0701
H(702)	-0.258(2)	-0.048(2)	0.1412(4)	0.0701
C(71)	-0.281(3)	0.111(2)	0.1110(5)	0.0787
H(711)	-0.355(3)	0.153(2)	0.1113(5)	0.0914
H(712)	-0.184(3)	0.181(2)	0.1218(5)	0.0914
C(72)	-0.264(2)	0.063(2)	0.0702(5)	0.0547
H(721)	-0.363(2)	-0.006(2)	0.0605(5)	0.0611
H(722)	-0.194(2)	0.017(2)	0.0713(5)	0.0611

Table 2. Anisotropic temperature factors.

atom	U(11)	U(22)	U(33)	U(23)	U(13)	U(12)
C(1)	0.12(3)	0.08(3)	0.08(2)	-0.01(2)	-0.01(2)	0.06(2)
C(3)	0.03(2)	0.08(2)	0.16(3)	0.05(2)	0.03(2)	0.03(2)
C(5)	0.10(2)	0.06(2)	0.03(1)	0.03(1)	0.03(1)	0.06(2)
C(8)	0.03(1)	0.03(1)	0.04(1)	0.02(1)	0.02(1)	0.02(1)
C(9)	0.06(2)	0.06(2)	0.05(1)	0.03(1)	0.04(1)	0.06(2)
C(21)	0.10(3)	0.08(2)	0.14(2)	-0.03(2)	-0.02(2)	0.04(2)
C(22)	0.11(3)	0.07(3)	0.13(2)	-0.02(2)	-0.03(2)	0.04(3)
C(20)	0.02(1)	0.07(1)	0.00(1)	0.02(1)	0.003(8)	-0.01(1)
O(2)	0.12(2)	0.14(2)	0.09(1)	0.03(1)	0.06(1)	0.06(2)
C(2)	0.11(3)	0.07(2)	0.05(2)	0.01(2)	0.01(2)	0.05(2)
C(4)	0.02(1)	0.04(2)	0.03(1)	0.00(1)	-0.01(1)	-0.01(1)
C(6)	0.06(2)	0.04(2)	0.10(2)	-0.01(1)	-0.01(2)	0.01(2)
C(7)	0.05(1)	0.06(2)	0.03(1)	0.01(1)	-0.00(1)	0.04(1)
C(10)	0.05(2)	0.09(2)	0.10(2)	0.01(2)	-0.01(1)	0.02(2)
C(11)	0.04(1)	0.04(1)	0.014(6)	-0.019(7)	-0.011(6)	-0.002(9)
C(12)	0.03(1)	0.04(1)	0.03(1)	-0.00(1)	0.012(9)	0.03(1)
C(13)	0.01(1)	0.04(1)	0.03(1)	0.00(1)	0.00(1)	-0.01(1)
C(14)	0.03(2)	0.04(2)	0.07(1)	0.00(1)	-0.01(1)	0.00(1)
C(15)	0.09(2)	0.09(2)	0.07(2)	0.01(2)	0.01(1)	0.05(2)
C(16)	0.12(3)	0.08(3)	0.08(2)	0.01(2)	0.04(2)	0.04(2)
C(17)	0.13(2)	0.17(3)	0.07(2)	0.06(2)	0.06(2)	0.08(2)
C(18)	0.06(2)	0.07(2)	0.06(2)	-0.00(1)	-0.02(1)	0.03(1)
C(19)	0.07(2)	0.08(2)	0.08(2)	0.02(2)	-0.00(1)	0.04(2)
C(23)	0.14(2)	0.16(3)	0.15(3)	0.03(3)	0.06(2)	0.07(2)
C(24)	0.06(2)	0.13(3)	0.09(2)	0.01(2)	0.03(2)	0.03(2)
C(25)	0.04(1)	0.05(2)	0.04(1)	-0.01(1)	0.00(1)	0.01(1)
C(26)	0.10(2)	0.16(3)	0.09(2)	0.07(2)	0.04(2)	0.08(2)
C(27)	0.03(1)	0.05(2)	0.04(1)	0.01(1)	-0.00(1)	-0.02(1)
C(28)	0.13(3)	0.20(4)	0.07(2)	0.04(2)	0.04(2)	0.10(3)
C(29)	0.11(3)	0.12(3)	0.09(2)	0.02(2)	-0.02(2)	0.03(2)

C(30)	0.10(2)	0.13(3)	0.07(2)	0.05(2)	0.03(2)	0.07(2)
C(31)	0.21(4)	0.18(4)	0.05(2)	0.02(2)	0.04(2)	0.05(3)
C(32)	0.13(3)	0.14(3)	0.09(2)	0.00(2)	0.02(2)	0.06(3)
C(33)	0.10(3)	0.09(3)	0.17(3)	-0.03(2)	0.01(2)	0.03(2)
C(41)	0.04(1)	0.04(1)	0.02(1)	0.01(1)	0.01(1)	0.03(1)
C(43)	0.02(1)	0.03(1)	0.11(2)	0.01(1)	0.01(1)	0.01(1)
C(45)	0.05(1)	0.02(1)	0.00(1)	-0.002(9)	-0.002(9)	0.02(1)
C(48)	0.02(1)	0.04(1)	0.05(1)	0.04(1)	-0.00(1)	0.01(1)
C(49)	0.03(1)	0.03(1)	0.04(1)	0.00(1)	-0.00(1)	0.02(1)
C(61)	0.08(2)	0.10(2)	0.06(2)	0.01(2)	0.01(1)	0.04(2)
C(62)	0.02(1)	0.07(2)	0.06(1)	0.01(1)	-0.01(1)	0.01(1)
C(73)	0.10(3)	0.18(4)	0.17(4)	0.07(4)	-0.01(3)	-0.01(3)
O(11)	0.13(2)	0.20(2)	0.13(2)	0.11(2)	0.06(1)	0.07(2)
C(42)	0.15(2)	0.17(2)	-0.00(1)	-0.01(1)	-0.00(1)	0.05(2)
C(44)	0.11(2)	0.06(2)	0.06(2)	0.03(2)	0.04(2)	0.05(2)
C(46)	0.05(2)	0.05(2)	0.03(1)	0.03(1)	0.01(1)	0.01(1)
C(47)	0.22(3)	0.06(2)	0.09(2)	0.02(2)	0.01(2)	0.06(2)
C(50)	0.14(1)	0.15(1)	0.02(1)	0.03(1)	0.021(8)	0.02(1)
C(51)	0.04(1)	0.04(2)	0.04(1)	0.01(1)	0.01(1)	0.01(1)
C(52)	0.11(2)	0.10(3)	0.10(2)	0.04(2)	-0.01(2)	0.02(2)
C(53)	0.07(2)	0.06(2)	0.05(2)	0.01(1)	-0.01(1)	0.04(2)
C(54)	0.13(3)	0.12(3)	0.09(2)	0.03(2)	0.03(2)	0.03(2)
C(55)	0.04(2)	0.04(2)	0.07(2)	0.01(1)	0.00(1)	-0.01(1)
C(56)	0.10(2)	0.09(2)	0.06(2)	0.04(1)	0.05(2)	0.06(2)
C(57)	0.07(2)	0.05(2)	0.07(2)	-0.01(1)	0.00(1)	0.00(2)
C(58)	0.02(1)	0.07(2)	0.06(1)	0.01(1)	-0.00(1)	0.02(1)
C(59)	0.04(1)	0.02(1)	0.02(1)	-0.00(1)	0.00(1)	-0.01(1)
C(60)	0.06(2)	0.15(3)	0.02(1)	0.05(2)	0.00(1)	0.01(2)
C(63)	0.03(1)	0.04(2)	0.06(1)	0.03(1)	-0.02(1)	0.01(1)
C(64)	0.16(2)	0.11(2)	0.16(2)	0.05(2)	0.06(2)	0.08(2)
C(65)	0.12(2)	0.08(3)	0.08(2)	0.01(2)	-0.02(2)	-0.02(2)
C(66)	0.18(4)	0.11(3)	0.11(2)	0.01(2)	0.01(2)	0.08(3)
C(67)	0.12(3)	0.09(3)	0.06(2)	0.05(2)	0.01(1)	0.03(2)
C(68)	0.04(1)	0.06(2)	0.02(1)	0.01(1)	-0.00(1)	0.00(1)
C(69)	0.02(1)	0.04(1)	0.03(1)	0.02(1)	-0.004(9)	-0.03(1)
C(70)	0.05(1)	0.05(2)	0.03(1)	0.00(1)	0.00(1)	-0.01(1)
C(71)	0.12(2)	0.11(2)	0.07(2)	0.05(2)	0.05(2)	0.03(2)
C(72)	0.08(2)	0.10(2)	0.05(2)	0.02(1)	0.02(1)	0.07(2)

Table 3. Bond lengths.

atoms	length [Å]	atoms	length [Å]	atoms	length [Å]
C(1) - C(2)	1.40(2)	C(18) - C(19)	1.59(2)	C(73) - O(121)	1.05(6)
C(1) - C(6)	1.37(2)	C(23) - C(24)	1.64(3)	C(73) - O(122)	1.41(5)
C(1) - C(7)	1.43(2)	C(24) - C(25)	1.55(2)	C(73) - O(123)	1.26(5)
C(3) - C(8)	1.56(1)	C(25) - C(26)	1.60(2)	C(73) - C(72)	1.55(3)
C(3) - C(2)	1.44(2)	C(26) - C(27)	1.55(2)	O(11) - C(60)	1.47(2)
C(3) - C(4)	1.45(2)	C(27) - C(28)	1.50(2)	C(50) - C(51)	1.45(2)
C(5) - C(21)	1.51(2)	C(28) - C(29)	1.57(2)	C(51) - C(52)	1.47(2)
C(5) - C(4)	1.37(2)	C(29) - C(30)	1.54(2)	C(52) - C(53)	1.52(2)
C(5) - C(6)	1.46(2)	C(30) - C(31)	1.52(3)	C(53) - C(54)	1.54(2)
C(8) - C(9)	1.31(1)	C(31) - C(32)	1.48(3)	C(54) - C(55)	1.53(2)
C(9) - C(10)	1.33(1)	C(32) - C(33)	1.64(3)	C(55) - C(56)	1.46(2)

C(21) - C(22)	1.31(2)	C(41) - C(42)	1.41(2)	C(56) - C(57)	1.50(2)
C(22) - C(23)	1.50(2)	C(41) - C(46)	1.38(2)	C(57) - C(58)	1.53(2)
C(20) - O(101)	1.34(3)	C(41) - C(47)	1.57(2)	C(58) - C(59)	1.58(2)
C(20) - O(102)	1.48(3)	C(43) - C(48)	1.45(1)	C(59) - C(60)	1.44(2)
C(20) - C(19)	1.56(2)	C(43) - C(42)	1.35(2)	C(63) - C(64)	1.60(2)
O(2) - C(33)	1.32(3)	C(43) - C(44)	1.39(2)	C(64) - C(65)	1.50(2)
C(10) - C(11)	1.49(2)	C(45) - C(61)	1.31(1)	C(65) - C(66)	1.53(3)
C(11) - C(12)	1.51(2)	C(45) - C(44)	1.34(2)	C(66) - C(67)	1.59(3)
C(12) - C(13)	1.55(2)	C(45) - C(46)	1.35(2)	C(67) - C(68)	1.56(2)
C(13) - C(14)	1.47(2)	C(48) - C(49)	1.25(1)	C(68) - C(69)	1.54(2)
C(14) - C(15)	1.54(2)	C(49) - C(50)	1.42(1)	C(69) - C(70)	1.55(2)
C(15) - C(16)	1.57(2)	C(61) - C(62)	1.26(1)	C(70) - C(71)	1.61(2)
C(16) - C(17)	1.56(2)	C(62) - C(63)	1.61(1)	C(71) - C(72)	1.48(2)
C(17) - C(18)	1.46(2)				

Table 4. Bond angles.

atoms	angles [°]	atoms	angles [°]
C(2) - C(1) - C(6)	117.2(18)	C(46) - C(41) - C(47)	118.7(15)
C(2) - C(1) - C(7)	121.0(19)	C(48) - C(43) - C(42)	120.0(16)
C(6) - C(1) - C(7)	118.1(20)	C(48) - C(43) - C(44)	114.4(16)
C(8) - C(3) - C(2)	122.6(17)	C(42) - C(43) - C(44)	122.7(13)
C(8) - C(3) - C(4)	112.7(16)	C(61) - C(45) - C(44)	118.8(15)
C(2) - C(3) - C(4)	124.1(14)	C(61) - C(45) - C(46)	121.6(16)
C(21) - C(5) - C(4)	116.1(16)	C(44) - C(45) - C(46)	119.5(13)
C(21) - C(5) - C(6)	122.0(18)	C(43) - C(48) - C(49)	177.3(19)
C(4) - C(5) - C(6)	118.1(14)	C(48) - C(49) - C(50)	174.7(19)
C(3) - C(8) - C(9)	176.4(19)	C(45) - C(61) - C(62)	172.5(26)
C(8) - C(9) - C(10)	174.9(19)	C(61) - C(62) - C(63)	178.9(21)
C(5) - C(21) - C(22)	166.3(24)	O(121)- C(73) - O(122)	102.8(63)
C(21) - C(22) - C(23)	171.6(29)	O(121)- C(73) - O(123)	129.6(59)
O(101)- C(20) - O(102)	76.2(16)	O(122)- C(73) - O(123)	98.8(43)
O(101)- C(20) - C(19)	114.8(19)	O(121)- C(73) - C(72)	111.3(40)
O(102)- C(20) - C(19)	106.6(15)	O(122)- C(73) - C(72)	96.1(27)
C(1) - C(2) - C(3)	114.6(17)	O(123)- C(73) - C(72)	110.9(38)
C(3) - C(4) - C(5)	115.9(13)	C(41) - C(42) - C(43)	115.0(14)
C(1) - C(6) - C(5)	121.7(18)	C(43) - C(44) - C(45)	119.3(14)
C(9) - C(10) - C(11)	109.0(15)	C(41) - C(46) - C(45)	120.7(14)
C(10) - C(11) - C(12)	112.8(14)	C(49) - C(50) - C(51)	117.2(14)
C(11) - C(12) - C(13)	112.6(13)	C(50) - C(51) - C(52)	114.4(16)
C(12) - C(13) - C(14)	113.9(15)	C(51) - C(52) - C(53)	114.2(19)
C(13) - C(14) - C(15)	117.1(16)	C(52) - C(53) - C(54)	114.9(18)
C(14) - C(15) - C(16)	110.0(17)	C(53) - C(54) - C(55)	113.6(19)
C(15) - C(16) - C(17)	105.4(19)	C(54) - C(55) - C(56)	115.0(18)
C(16) - C(17) - C(18)	113.8(21)	C(55) - C(56) - C(57)	115.4(18)
C(17) - C(18) - C(19)	117.5(18)	C(56) - C(57) - C(58)	113.1(17)
C(20) - C(19) - C(18)	106.5(17)	C(57) - C(58) - C(59)	116.1(15)
C(22) - C(23) - C(24)	103.3(19)	C(58) - C(59) - C(60)	112.9(16)
C(23) - C(24) - C(25)	101.4(16)	O(11) - C(60) - C(59)	117.6(18)
C(24) - C(25) - C(26)	111.0(16)	C(62) - C(63) - C(64)	111.1(14)
C(25) - C(26) - C(27)	107.1(16)	C(63) - C(64) - C(65)	110.1(19)
C(26) - C(27) - C(28)	110.2(16)	C(64) - C(65) - C(66)	111.8(21)
C(27) - C(28) - C(29)	111.5(18)	C(65) - C(66) - C(67)	109.2(20)

C(28) - C(29) - C(30)	112.3(19)	C(66) - C(67) - C(68)	107.2(19)
C(29) - C(30) - C(31)	115.3(20)	C(67) - C(68) - C(69)	107.4(16)
C(30) - C(31) - C(32)	111.8(23)	C(68) - C(69) - C(70)	111.6(15)
C(31) - C(32) - C(33)	110.9(22)	C(69) - C(70) - C(71)	110.2(15)
O(2) - C(33) - C(32)	100.2(23)	C(70) - C(71) - C(72)	111.7(18)
C(42) - C(41) - C(46)	118.9(14)	C(73) - C(72) - C(71)	122.1(21)
C(42) - C(41) - C(47)	121.8(16)		

6. References

[1] I. Langmuir, *J. Am. Chem. Soc.* **1917**, *39*, 1848.
[2] J.D. Swalen, D.L. Allara, J.D. Andrade, E.A. Chandross, S. Garrof, J. Israelachvili, T.J. McCarthy, R. Munray, R.F. Pease, J.F. Rabolt, K.J. Wynne, H. Yu, *Langmuir* **1987**, *3*, 932.
[3] E.M. Landau, M. Levanon, L. Leiserowitz, M. Lahav, J.Sagiv, *Nature* **1985**, *318*, 353.
[4] E.M. Landau, S. Grayer-Wolf, M. Levanon, L. Leiserowitz, M. Lahav, J.Sagiv, *J. Am. Chem. Soc.* **1989**, *111*, 1436.
[5] E.M. Landau, R. Popovitz-Biro, S. Grayer-Wolf, M. Levanon, L. Leiserowitz, M. Lahav, J.Sagiv, *J. Am. Chem. Soc.* **1989**, *111*, 1436.
[6] S. Mann, B.R. Heywood, S. Rajam, J.D Birchall, *Nature* **1988**, *334*, 692.
[7] S Rajam, B.R. Heywood, J.B.A. Walker, S. Mann, R.J. Davey, J.D Birchall, *J. Chem Soc. Faraday Trans*. **1991**, *87*, 727.
[8] H. Kuhn, D. Möbius, *Angew. Chem. Int. Ed. Engl*. **1971**, *10*, 620.
[9] L.M. Blinov, N.V. Dubinin, L.V. Mikhnev, S.G. Yudin, *Thin Solid Films* **1984**, *120*, 161.
[10] I.R. Girling, P.V. Kolinski, N.A. Cade, J.D. Earls, I.R. Peterson, *Opt. Commun*. **1985**, *55*, 289.
[11] J.D. Swalen, *Thin Solid Films* **1988**, *160*, 197.
[12] W. Groh, D. Lupo, H. Sixl, *Adv. Mater*. **1989**, 366.
[13] H. Fuchs, H. Ohst, W. Prass, *Adv. Mater*. **1991**, *3*, 10.
[14] T. Morizumi, *Thin Solid Films* **1988**, *160*, 413.
[15] Y.R. Shen, *Nature* **1989**, *337*, 519.
[16] M. Buck, F. Eisert, M. Grunze, F. Trager, *Acta Neuropathologica* **1995**, *60*, 1.
[17] M. Flörsheimer, H. Salmen, M. Bösch, C. Brillert, M. Wierschem, H. Fuchs, *Adv. Mater*. **1997**, *9*, 1056.
[18] M. Bloembergen, P.S. Pershan, *Phys. Rev*. **1962**, *128*, 606.
[19] T. Rasing, G. Berkovic, Y.R. Shen, S.G. Grubb, M.W. Kim, *Chem. Phys. Lett*. **1986**, *130*, 1.
[20] R.M. Weis, H.M. McConnell, *Nature* **1984**, *310*, 47.
[21] V.T. Moy, D.J. Keller, H.E. Graub, H.M. McConnell, *J. Phys. Chem.* **1986**, *90*, 3198.
[22] M. Lösche, E. Sackmann, H. Möhwald, *Ber. Bunsenges. Phys. Chem*. **1983**, *87*, 848.
[23] C.M. Knobler, *Science* **1990**, *249*,870.
[24] B.F. Sinnamon, R.A. Dluhy, G.T. Barnes, *Colloids & Surfaces A-Physicochemical & Engineering Aspects* **1999**, *156*, 215.
[25] Y. Tabuchi, M. Rikukawa, K. Sanui, N. Ogata, *Synthetic Metals* **1999**, *102*, 1441.
[26] C. Steinem, A. Janshoff, M.S. Vollmer, M.R. Ghadiri, *Langmuir* **1999**, *15*, 3956.
[27] E. Okamura, N. Fukushima, S. Hayashi, *Langmuir* **1999**, *15*, 3589.
[28] F. Da Cruz, F. Armand, P.A. Albouy, M. Nierlich, A. Raudel-Teixier, *Langmuir* **1999**, *15*, 3653.
[29] D.L. Allara, R.G. Nuzzo, *Langmuir* **1985**, *1*, 52.
[30] J. Gun, R. Iscovici, J. Sagiv, *J. Colloid Interface Sci* **1984**, *101*, 201.
[31] J. Als-Nielsen, D. Jaquemain, K. Kjær, F. Leveiller, M. Lahav, L. Leiserowitz, *Phys. Rep.* **1994**, *246*, 251.
[32] R. W. James, *The Optical Principles of the Diffraction of X-rays*, Ox Bow, Woodbrodge, CT, USA, **1982**.
[33] M. Born, E. Wolf, *Principles of Optics*, MacMillan, New York, **1959**.
[34] W.C. Marra, P. Eisenberger, A.Y. Cho, *J. Appl. Phys*. **1979**, *50*, 6927.
[35] P. Eisenberger, W.C. Marra, *Phys. Rev. Lett*. **1981**, *46*, 1081.
[36] G. Vineyard, *Phys. Rev. B* **1982**, *26*, 4146.
[37] R. Feidenhans'l, *Surf. Sci. Rep*. **1989**, *10*, 105.
[38] J. Als-Nielsen, K. Kjær, *NATO Adv. Study Inst. Ser., Ser B* **1989**, *211*, 113.
[39] D. Jacquemain, S. Grayer-Wolf, F. Leveiller, M. Lahav, L. Leiserowitz, M. Deutsch, K. Kjær, J. Als-Nielsen, *J. Phys. Colloq*. **1989**, *C7*, 29.
[40] A. Braslau, M. Deutsch, P.S. Pershan, A.H. Weiss, J. Als-Nielsen, J. Bohr, *Phys. Rev. Lett*. **1985**, *54*, 114.

[41] A. Braslau, P.S. Pershan, G. Swislow, B.M. Ocko, J. Als-Nielsen, *Phys. Rev. A* **1988**, *38*, 2457.
[42] P.S. Pershan, *J. Phys. Colloq*. **1989**, *C7*, 1.
[43] L.G. Parrat, *Phys. Rev* **1954**, *95*, 359.
[44] K. Kjær, J. Als-Nielsen, C.A. Helm, P. Tippmann-Krayer, H. Möhwald*, J. Phys. Chem*. **1989**, *93*, 3200.
[45] F. Leveiller, C. Böhm, D. Jacquemain, H. Möhwald, L. Leiserowitz, K. Kjær, J. Als-Nielsen, *Langmuir* **1994**, *10*, 819.
[46] J.L. Wang, F. Leveiller, D. Jacquemain, K. Kjær, J. Als-Nielsen, M. Lahav, L. Leiserowitz, *J. Am Chem. Soc*. **1994**, *116*, 1192.
[47] V.M. Kaganer, E.B. Loginov, *Phys. Rev. E* **1995**, *51*, 2237.
[48] V.M. Kaganer, I.R. Peterson, R.M. Kenn, M.C. Shih, M. Durbin, P. Dutta, *J. Chem. Phys.* **1995**, *102*, 9412.
[49] F. Leveiller, D. Jacquemain, L. Leiserowitz, K. Kjær, J. Als-Nielsen, *J. Phys. Chem*. **1992**, *96*, 10380.
[50] I. Weissbuch, J. Majewski, K. Kjær, J. Als-Nielsen, M. Lahav, L. Leiserowitz, *J. Phys. Chem*. **1993**, *97*, 12858.
[51] A.I. Kitaigorodskii, *Organic Chemical Crystallography*, Consultants Bureau, New York **1961**.
[52] E. Segerman, *Acta Crystallogr*. **1965**, *19*, 789.
[53] A.I. Kitaigorodskii, *Organic Chemical Crystallography*, Consultants Bureau, New York **1961**, Figure 130b.
[54] I. Kuzmenko, V.M. Kaganer, L. Leiserowitz, *Langmuir* **1998**, *14*, 3882.
[55] J. Garnæs, N.B. Larsen, T. Bjørnholm, M. Jøgensen, K. Kjær, J. Als-Nielsen, J.F. Jørgensen, J.A. Zasadzinski, *Science* **1994**, *264*, 1301.
[56] S.W. Barton, B.N. Thomas, E.B. Flom, S.A. Rice, B. Lin, J.B. Peng, J.B. Ketterson, P. Dutta, *J. Chem. Phys*. **1988**, *89*, 2257.
[57] B. Lin, M.C. Shih, T.M. Bohanon, G.E. Ice, P. Dutta, *Phys. Rev. Lett*. **1990**, *65*, 191.
[58] T.M. Bohanon, B. Lin, M.C. Shih, G.E. Ice, P. Dutta, *Phys. Rev. B* **1990**, *41*, 4846.
[59] R.M. Kenn, C. Böhm, A.M. Bibo, I.R. Peterson, H. Möhwald, J. Als-Nielsen, K. Kjær, *J. Phys. Chem.* **1991**, *95*, 2092.
[60] P. Tippmann-Krayer, H. Möhwald, *Langmuir* **1991**, *7*, 2303.
[61] M.L. Schlossman, D.K. Schwartz, P.S. Pershan, E.H. Kawamoto, G.J. Kellogg, S. Lee, *Phys. Rev. Lett*. **1991**, *66*, 1599.
[62] M.C. Shih, T.M. Bohanon, J.M. Mikrut, P. Zschack, P. Dutta, *J. Chem. Phys*. **1992**, *96*, 1556.
[63] M.C. Shih, T.M. Bohanon, J.M. Mikrut, P. Zschack, P. Dutta, *Phys. Rev. A* **1992**, *45*, 5734.
[64] M.C. Shih, T.M. Bohanon, J.M. Mikrut, P. Zschack, P. Dutta, *J. Chem. Phys*. **1992**, *97*, 4485.
[65] M. Durbin, A. Malik, R. Ghaskadvi, P. Zschack, P. Dutta, *J. Phys. Chem*. **1994**, *98*, 1753.
[66] M.C. Shih, M. Durbin, A. Malik, P. Zschack, P. Dutta, *J. Chem. Phys*. **1994**, *101*, 9132.
[67] G. Brezesinski, E. Scalas, B. Struth, H. Möhwald, F. Bringezu, U. Gehlert, G. Weidemann, D. Vollhardt, *J. Phys. Chem*. **1995**, *99*, 8758.
[68] E. Scalas, G. Brezesinski, H. Möhwald, V.M. Kaganer, W.G. Bouwman, K. Kjær, *Thin Solid Films* **1996**, *284*, 56.
[69] D. Jacquemain, F. Leveiller, S.P. Weinbach, M. Lahav, L. Leiserowitz, K. Kjær, J. Als-Nielsen, *J. Am. Chem. Soc*. **1991**, *113*, 7684.
[70] S.P. Weinbach, D. Jacquemain, F. Leveiller, K. Kjær, J. Als-Nielsen, L. Leiserowitz, *J. Am. Chem. Soc*. **1993**, *115*, 11110.
[71] S.P. Weinbach, K. Kjær, J. Als-Nielsen, M. Lahav, L. Leiserowitz, *J. Phys. Chem*. **1993**, *97*, 5200.
[72] C. Böhm, F. Leveiller, D. Jacquemain, H. Möhwald, K. Kjær, J. Als-Nielsen, I. Weissbuch, L. Leiserowitz, *Langmuir* **1994**, *10*, 830.
[73] J. Majewski, R. Popovitz-Biro, W.G. Bouwman, K. Kjær, J. Als-Nielsen, M. Lahav, L. Leiserowitz, *Chem. Eur. J*. **1995**, *35*, 304.

[74] I. Weissbuch, G. Berkovic, R. Yam, J. Als-Nielsen, K. Kjær, , M. Lahav, L. Leiserowitz*, J. Phys. Chem*. **1995**, *99*, 6036.
[75] I. Weissbuch, M. Berfeld, W.G. Bouwman, K. Kjær, J. Als-Nielsen, M. Lahav, L. Leiserowitz, *J. Am. Chem. Soc*. **1997**, *119*, 933.
[76] V.M. Kaganer, H. Möhwald, P. Dutta, *Reviews of Modern Physics* **1999**, *71*, 779.
[77] J.A. McNew, J.M. Goodman, *Trends Biochem. Sci.* **1996**, *21*, 54-58.
[78] A. Keller, *Macromol. Symp*. **1995**, *98*, 1.
[79] G. Ungar, J. Stejny, A. Keller, I. Bidd, M.C. Whiting, *Science* **1985**, *229*, 386.
[80] T. Yamamoto, *J. Chem. Phys.* **1997**, *107*, 2653.
[81] P.R. Sundararajan, T.A. Kavassalis, *J. Chem. Soc. Faraday Trans.* **1995**, *91*, 2541.
[82] T.A. Kavassalis, P.R. Sundararajan, *Macromolecules* **1993**, *26,* 4144.
[83] S.J. Sutton, A.S. Vaughan, D.C. Basset, *Polymer* **1996**, *37*, 5735.
[84] D.C. Basset, R.H. Olley, S.J. Sutton, A.S. Vaughan, *Faraday Polymer.* **1996**, *37*, 4993.
[85] S.J. Organ, G. Ungar, A. Keller, *Macromolecules* **1989**, *22*, 1995.
[86] G. Ungar, *Polymer* **1986**, *27*, 1835.
[87] V. Hessel, H. Ringsdorf, R. Festag, J.H. Wendorff, *Macromol. Chem.*, *Rapid Commun*. **1993**, *14*, 707.
[88] G.A. Lindsay, J.D. Stenger-Smith, R.A. Henry, J.M. Hoover, R.A. Nissan, K.J. Wynne, *Macromolecules* **1992**, *25*, 6075.
[89] K.P. McGrath, M.J. Fournier, T.L. Mason, D.A. Tirrell, *J. Am. Chem. Soc.* **1992**, *114*, 727.
[90] G.L. Gaines, *Insoluble Monolayers at Liquid-Gas Interfaces*, Interscience, New York, **1966**.
[91] S.P. Weinbach, I. Weissbuch, K. Kjaer, W.G. Bouwman, J. Als-Nielsen, M. Lahav, L. Leiserowitz, *Adv. Mater.* **1995**, *7*, 857.
[92] I. Weissbuch, R. Popovitz-Biro, M. Lahav, L. Leiserowitz, *Acta Cryst.* **1995**, *51*, 115.
[93] R. Popovitz-Biro, R. Edgar, I. Weissbuch, R. Lavie, S. Cohen, K. Kjær, J. Als-Nielsen, E. Wassermann, L. Leiserowitz, M. Lahav, *Acta Polym.* **1998**, *49*, 626.
[94] I. Weissbuch, K. Lederer, A. Godt, K. Kjær, J. Als-Nielsen, P.-B. Howes, G. Wegner, M. Lahav, L. Leiserowitz, *J. Phys. Chem. B* **1998**, *102*, 6313.
[95] K. Lederer, A. Godt, P.B. Howes, K. Kjær, J. Als-Nielsen, M. Lahav, G. Wegner, L. Leiserowitz, I. Weissbuch, accepted in *Chem. Eur. J.*, November 1999.
[96] E. Erdik, *Tetrahedron* **1984**, *40*, 641.
[97] T. Nishiyama, T. Seshita, H. Shodai, K. Aoki, H. Kameyama, K. Komura, *Chemistry Letters* **1996**, *7*, 549.
[98] H. Masada, Y. Yasunishi, N. Kikuchi, *Nippon Kagaku Kaishi* **1995**, *10*, 844.
[99] Ö. Ünsal, Diploma Thesis, Johannes-Gutenberg-Universität, Mainz, **1996**.
[100] S.R. Abrams, A.C. Shaw, *Org. Synth*. **1987**, *66*, 127
[101] E. J. Corey, A. Venkateswarlu, *J. Am. Chem. Soc.* **1972**, *94*, 6190.
[102] A. Godt, unpublished.
[103] H. L. Wheeler, L. M. Liddle, *Am. Chem. J*. **1909**, *42*, 441.
[104] S. Höger, K. Bonrad, unpublished.
[105] B. Wunderlich, *Thermal Analysis*, Academic Press Inc., Harcourt Brace Jovanovich, San Diego, **1990**.
[106] B. Wunderlich, personal communication.
[107] ATHAS database, http://funnelweb.utcc.utk.edu/~athas/databank/paraffin/.
[108] K. Kjaer, *Physica B*, **1994**, *198*, 100.
[109] CERIUS^2, Molecular Modeling Software for materials research from BIOSYM/Molecular Simulations Inc., San Diego CA, USA and Cambridge, UK.
[110] The very low q_{xy} region corresponding to the {01} Bragg rod was not measured.
[111] A. W. Adamson, *Physical Chemistry of surfaces*, John Wiley & Sons, New York, **1990**, pp. 69.
[112] K. Kjaer, W.G. Bouwman, *Hasylab Annual Report* **1994**, 405.
[113] I.R. Peterson, R.M. Kenn, *Langmuir* **1994**, *10*, 4645.
[114] E. Sirota, *Langmuir* **1997**, *13*, 3849.

[115] I. Weissbuch, R. Popovitz-Biro, M. Lahav, L. Leiserowitz, K. Kjær, J. Als-Nielsen, *Advances in Chemical Physics*, Wiley, New York, **1997**, *102*, 39.
[116] This peak corresponds to a *d*-spacing of 4.7 Å. Since other new peaks were not encountered, this peak cannot be assigned.
[117] K. Meine, G. Weidemann, D. Vollhardt, G. Brezesinski, E.A. Kondrashkina, *Langmuir* **1997**, *13*, 6577.
[118] S. Takahashi, Y. Kuroyama, K. Sonogashira, N. Hagihara, *Synthesis* **1980**, 627.
[119] Spectrum of higher order; H. Friebolin, *Ein- und zweidimensionale NMR-Spektroskopie*, Verlag Chemie Weinheim, Weinheim-Basel-Cambridge-New York, **1988**, pp. 92.
[120] The carbon multiplicity of these two signals could not be unambiguously be determined on the grounds of the DEPT 135 spectrum. They were assigned according to: H.-O. Kalinowski, S. Berger, S. Braun, *^{13}C-NMR-Spektroskopie*, Georg Thieme Verlag, Stuttgart New York, **1984**, ch. 3, pp. 130.
[121] M. Kumada, K. Tamao, K. Sumitani, *Org. Synth.* **1978**, *58*, 127.
[122] A. Bongini, G. Cardillo, M. Orena, *Synthesis-Stuttgart* **1979**, *8*, 618.
[123] J. Majewski. L. Margulis, I. Weissbuch, R. Popovitz-Biro, T. Arad, Y. Talmon, M. Lahav, L. Leiserowitz, *Adv. Mater.* **1995**, *7*, 26.
[124] D. Jacquemain, S. Grayer-Wolf, F. Leveiller, M. Deutsch, K. Kjær, J. Als-Nielsen M. Lahav, L. Leiserowitz, *Angew. Chem.* **1992**, *31*, 130.
[125] H. Goldstein, *Classical Mechanics* **1980**, 2nd edition, Addison-Wesley, Cambridge MA.
[126] If the plane group has a polar axis, as for example in plane group *p*11*g*, only translation in the direction perpendicular to the polar axis would be required. If the plane group has no polar axis, then translation along both *x* and *y* axes would be required, but only if the molecule does not lie on a symmetry element.
[127] In general, molecular thermal vibrations in crystals are anisotropic, which leads to a dependence of the corresponding temperature factor on the direction of the scattering vector.[128] For a two-dimenional crystal lying in the *xy*-plane the extent of the GIXD data can, in favorable cases, allow the temperature factor *U* to be resolved into an in-plane U_{xy} and an out-of-plane U_z component. Then the Debye-Waller factor $DW_{hk}(q_z)$ in equation (1) can be written as $DW_{hk}(q_z) = \exp -(q_{hk}^2 U_{xy} + q_z^2 U_z)$. If all the observed reflections for the two-dimensional crystal are in the same q_{xy} range the exponential term $\exp -(q_{hk}^2 U_{xy})$ is approximately the same for all (hk) reflections and plays the role of a scaling factor. In such a case, the exponential term can be reduced to $\exp -(q_z^2 U_z)$.
[128] J. D. Dunitz, *X-ray Analysis and the Structure of Organic Molecules* **1979**, Ch. 1, pp. 43, Cornell University Press, Ithaca and London.
[129] J. Als-Nielsen, K. Kjær, *The Proceedings of the NATO Advanced Study Institute, Phase Transitions in Soft Condensed Matter*, Geilo, Norway, April 4-14, **1989**; T. Riste, D. Sherrington Eds.: Plenum Press, New York, **1989**, pp. 113.